Mahoney, J.J., Fitton, J.G., Wallace, P.J., et al., 2001
Proceedings of the Ocean Drilling Program, Initial Reports Volume 192

7. Site 1187[1]

Shipboard Scientific Party[2]

BACKGROUND AND OBJECTIVES

By the time we had penetrated ~50 m of the 65.4 m of basement cored at Site 1186, shipboard inductively coupled plasma–atomic emission spectrometry (ICP-AES) analyses had demonstrated that the basalt was of the widespread, remarkably homogeneous, ~122-Ma Kwaimbaita magma type found at Site 1183 and in the lower 92 m of basement at Site 1185. The bottom of the Kwaimbaita-type lava sequence has not been reached in any of the locations where such lavas have been encountered. For example, at Site 807 this sequence (Units C–G) is >100 m thick (Kroenke, Berger, Janecek, et al., 1991), and on the island of Malaita the Kwaimbaita Formation is >2.7 km thick (Tejada et al., in press). Furthermore, our rate of penetration in basement was low, and reentering (after an imminent drill-bit change) an uncased >900-m hole in chert-rich sediment was risky. These considerations led us to favor drilling a new site to provide fundamental new information about the age, composition, and mantle sources of the Ontong Java Plateau over deepening Site 1186. A site somewhere between Site 803 and Site 1185 (Figs. **F1, F2**) would be particularly useful because, unlike other sites on the main plateau, Site 803 and probably Site 1185 contain basalt that is significantly younger than 122 Ma. Also, the lava flows in the upper 125 m of basement at Site 1185 are compositionally different from any seen elsewhere on the plateau. We therefore selected Site 1187, near Site 804 (which did not reach basement) on the eastern edge of the main plateau (Fig. **F3**). Site 1187 is 194 km southeast of Site 803 and 146 km north of Site 1185.

Geophysical Background

Site 1187 is located at a water depth of ~3804 m (drill pipe measurement) on a single-channel seismic (SCS) reflection profile acquired on

F1. Predicted bathymetry of the Ontong Java Plateau, p. 15.

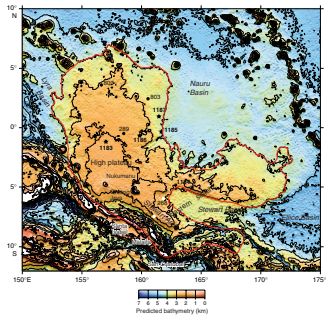

F2. Free-air gravity map of the Ontong Java Plateau region, p. 16.

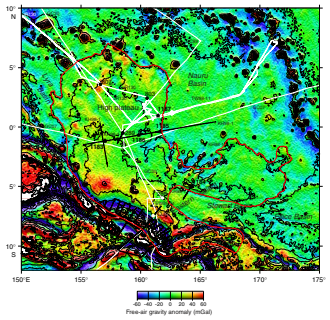

F3. Site 1187 location and site-survey data, p. 17.

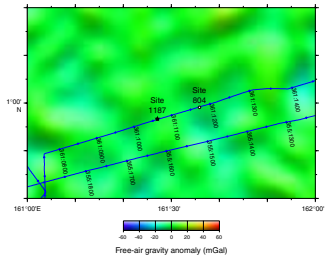

[1] **Examples of how to reference the whole or part of this volume.**
[2] **Shipboard Scientific Party addresses.**

cruise TW88-11 of the *Thomas Washington* (Figs. F2, F3, F4, F5, F6). The location is <3 km from the easternmost point where Ontong Java Plateau basement can be distinguished easily from that of the Nauru Basin. The sedimentary section, interpreted to lie between the seafloor at 5.02 s two-way traveltime (TWT) and the top of high-amplitude, discontinuous reflections at 5.43 s TWT, is characterized by parallel to subparallel reflections of low to moderate continuity. Reflection amplitudes are low to high, and frequency is high. Unconformities and variations in reflection amplitude, continuity, and configuration within the sedimentary section indicate that oceanographic and depositional conditions in the past were occasionally vigorous. The top of acoustic basement is characterized by high-amplitude, discontinuous reflections. Some medium-amplitude and discontinuous intrabasement reflections also are apparent in the seismic-reflection record.

Summary of Objectives

The main objectives at this site were to determine

1. Compositions of basement rocks in order to compare them with those of lavas at other locations where Ontong Java Plateau basement has been sampled, particularly Sites 803 and 1185 on the edge of the eastern high plateau;
2. Age of basement rocks to establish whether basement in this region is 90 Ma, 122 Ma, or some other age;
3. Physical volcanology of basement rocks and the nature of sedimentary interbeds, in order to deduce the eruptive environment (flow types, approximate water depths); and
4. The depositional environment and age of the sedimentary rocks immediately above basement.

OPERATIONS

Transit to Site 1187

We accomplished the 256-km transit to Site 1187 (new proposed Site OJ-14A) in 13.5 hr at an average speed of 10.2 kt. The vessel proceeded directly to the Global Positioning System coordinates for Site 1187, and, at 1112 hr on 29 October 2000, we deployed a beacon on site.

Hole 1187A

The depth objective in this hole was to core into basement until time expired or the bit failed as a result of excessive wear. We spudded Hole 1187A with the rotary core barrel (RCB) at 1920 hr on 29 October. The bit tagged the seafloor at 3803.6 m below sea level. We drilled ahead with a wash barrel in place to a depth of 365.5 m below seafloor, where progress became very slow because of a change in formation. From our interpretation of the seismic profile, we expected to encounter basement at ~410 mbsf. However, we encountered the sediment/basalt interface in the first RCB core (Core 192-1187A-2R) and inferred it to be at 372.5 mbsf, based upon the change in drilling parameters noted by the driller. We continued rotary coring in basement to a depth of 508.3 mbsf, where the bit expired after 65 rotating hours. The failure was manifested by high, erratic torque, indicating that one or more cones

F4. SCS reflection profile, p. 18.

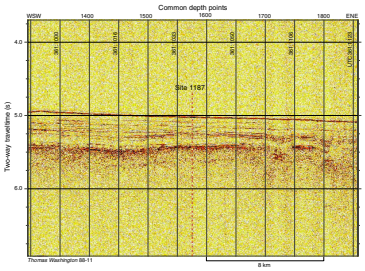

F5. SCS reflection profile, p. 19.

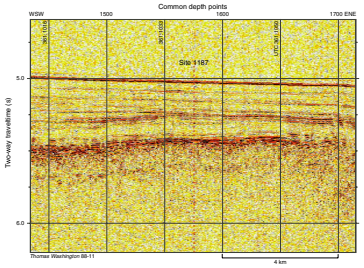

F6. SCS reflection profile, p. 20.

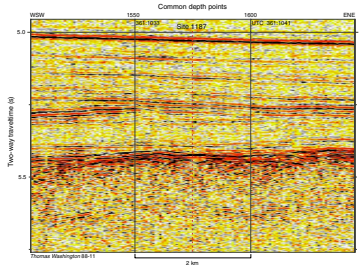

had fallen off the bit. The average recovery in basement was 74.3%, and the average penetration rate was 2.4 m/hr. Total penetration into basaltic basement was 135.8 m. Core depths and recovery are given in Tables T1 and T2.

After retrieving the drill string and bottom-hole assembly (BHA), we found that the bit was missing two cones and one cone shank. The two remaining cones had chipped and missing teeth in all rows. After retracting the hydrophones and thrusters and securing the drilling equipment, the crew put the vessel under way to Guam at 0330 hr on 3 November 2000. The 2337-km transit to Guam was completed in 4.5 days at an average speed of 11.6 kt. Leg 192 officially ended at 1700 hr on 7 September 2000, with the first line ashore in Apra Harbor, Guam.

T1. Coring summary, p. 52.

T2. Expanded coring summary, p. 53.

LITHOSTRATIGRAPHY

Overview

Site 1187 is located in 3804 m of water on the eastern edge of the main Ontong Java Plateau. Drilling was focused on the igneous basement and very little sediment was cored (Fig. F7). Coring began at 365.5 mbsf, and basalt was encountered at 372.5 mbsf (366.97 mbsf curated depth; see "Operations," p. 2). The sediment recovered is composed of 1.47 m of dark brown, ferruginous claystone that grades downward from burrow mottled to laminated and overlies a 2-cm-thick chalk layer. The chalk contains Aptian microfossils (see "Biostratigraphy," p. 5). Rare interbeds of recrystallized limestone are present within the basalt.

The 1.28 m of chalk, limestone, and chert recovered in a wash core (Core 192-1187A-1W) suggests that lithologies in the 365.5-m interval not cored include facies similar to Neogene and Paleogene pelagic sediments elsewhere on the plateau.

F7. Lithostratigraphic summary, p. 21.

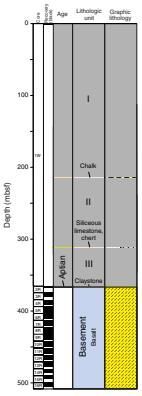

Unit Descriptions

Within the cored interval we recognize two lithologic units: an upper unit composed dominantly of claystone and a lower unit composed of basalt with rare recrystallized limestone between flows (see "Igneous Petrology," p. 6). To maintain consistency with other sites, we have designated the claystone as Unit III. Pieces of Oligocene foraminifer nannofossil chalk and Eocene siliceous limestone with chert in Core 192-1187A-1W confirm that rocks typical of Units I and II are present in the washed interval (see "Biostratigraphy," p. 21, and "Lithostratigraphy," p. 4, in the "Site 1183" chapter, "Biostratigraphy," p. 7, and "Lithostratigraphy," p. 5, in the "Site 1185" chapter, and "Biostratigraphy," p. 12, and "Lithostratigraphy," p. 4, in the "Site 1186" chapter).

Unit III

Interval: 192-1187A-2R-1, 0 cm, to 2R-2, 30 cm
Depth: 365.5–372.5 mbsf (366.97 mbsf curated depth)
Age: Aptian
Lithology: claystone, claystone with zeolite, chalk

The top of the unit was not recovered, and the base is placed at the contact with basalt (Section 192-1187A-2R-2, 30 cm; curated depth 366.97 mbsf). The lowest 2 cm of Unit III is white nannofossil chalk of Aptian age (see "Biostratigraphy," p. 5) that was used completely for paleontological studies. The overlying 1.45 m of Unit III that was recovered is brown claystone containing abundant brown semiopaque grains and 5%–15% zeolite. Biogenic grains include fish debris and rare foraminifers. The upper portion of the claystone is brown (10YR 4/3) and burrow mottled (Fig. F8). The lower portion is very dark brown (10YR 2/2) and dominantly laminated (Fig. F9), although rare small burrows are present. The change in fabric and color is gradational.

F8. Burrow-mottled claystone, p. 22.

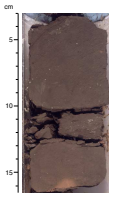

F9. Laminated claystone, p. 23.

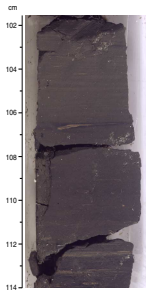

Basement

Interval: 192-1187A-2R-2, 30 cm, to 16R-5, 130 cm
Depth: 372.5 (366.97 mbsf curated depth) to 508.3 mbsf
Age: Cretaceous
Lithology: basalt flows with rare interbeds of limestone

The basement unit extends to the bottom of Hole 1187A and consists of basalt flows with rare, intercalated, thin limestone beds. A 5-cm-thick piece of light red, recrystallized limestone with greenish black glass clasts is at 375.2 mbsf curated depth (Sample 192-1187A-3R-1 [Piece 11, 69–74 cm]). A 3-cm-thick piece of light reddish brown recrystallized limestone with greenish black glass clasts is at 376.85 mbsf curated depth (Sample 192-1187A-3R-2 [Piece 4, 90–93 cm]). The basalt is described in "Igneous Petrology," p. 6, and "Alteration," p. 8.

Sedimentation History of Site 1187

Deposition at Site 1187 seems to match predictions based on results from other sites on the Ontong Java Plateau. However, because so little of the sedimentary record was cored, only very limited conclusions can be reached at this time.

A thin layer of chalk overlies the youngest basalt flow, but most of the 1.47 m of Aptian sedimentary rock recovered is noncalcareous. At shallower sites on the main Ontong Java Plateau, the Aptian is dominated by limestone. If the claystone at Site 1187 is representative of Aptian rocks at this paleodepth, then the record would suggest that the Aptian calcite compensation depth (CCD) was between Site 1187 and shallower sites. Alternatively, the apparent dominance of claystone might be a sampling artifact (carbonate-rich Aptian rocks might be common at Site 1187 above the level at which coring began). The transition between chalk and claystone is similarly difficult to interpret. Possible explanations include a change in the depth of the CCD relative to Site 1187 in the late Aptian, unusual depositional and early diagenetic conditions related to the subjacent basalt, or redeposition of shallower-water material.

Within the claystone there seems to be a progressive upward increase in the amount of bioturbation. Laminated claystone is present in other Leg 192 sites, but this is the only observation from Leg 192 of pervasively burrowed intervals in the same lithology. Comparisons of laminated and mottled intervals might be useful in testing paleoceanographic models (i.e., food supply vs. low oxygen) for the origin of the laminated fabric of the basal claystone (see "Lithostratigraphy," p. 4, in the "Site 1183" chapter and "Lithostratigraphy," p. 4, in the "Site 1186" chapter).

Finally, the post-Cretaceous history is probably similar (at a coarse resolution) to the history elsewhere on the main Ontong Java Plateau because lithologies typical of younger lithostratigraphic intervals are present in the wash core. The presence of upper Eocene pelagic limestone (see "Biostratigraphy," p. 5) indicates that the CCD was lower than the paleodepth of Site 1187 during the late Eocene.

BIOSTRATIGRAPHY

Overview

Approximately 1.47 m (Sections 192-1187A-2R-1 and 2R-2) of upper Aptian to (possibly) Albian chalk and claystone was recovered above basalt basement encountered in Section 2R-2 in Hole 1187A. A summary of the biostratigraphic indices identified in the rotary-cored portion of Hole 1187A is presented in Table T3.

In addition, the 1 m of limestone and pelagic ooze obtained from the wash core (Core 192-1187A-1W) was analyzed for foraminifers in order to better incorporate Site 1187 into a regional paleoceanographic model (see "Lithostratigraphy," p. 4, in the "Site 1183" chapter). Core 1W contains Oligocene pelagic ooze overlying middle to upper Eocene limestone.

T3. Planktonic foraminifer and calcareous nannofossil occurrences, p. 56.

Calcareous Nannofossils

The sediment recovered from the wash core (192-1187A-1W) was not examined for calcareous nannofossils.

Poorly preserved calcareous nannofossils are abundant in the white chalk (Sample 192-1187A-2R-2, 29 cm) directly above basement. The presence of *Eprolithus floralis* and *Hayesites irregularis* date this sample as late Aptian to late Albian; however, the absence of the Albian nannofossil taxa observed in mid-Cretaceous sections of cores recovered from Holes 1183A and 1186A favors a late Aptian age. The first occurrence of *Eprolithus floralis* also provided control on basal sediment ages at Sites 1183 and 1186.

Very rare and poorly preserved specimens of *Watznaueria barnesae,* which ranges throughout the Cretaceous, were recovered from two of eight samples taken from the brown claystone (see "Lithostratigraphy," p. 3).

Foraminifers

The upper portion of the sediment recovered in the wash core (Samples 192-1187A-1W, 4–9 cm, and 14–17 cm) is lower upper Oligocene ooze assigned to planktonic foraminifer Zone P21. An underlying limestone interval (Samples 192-1187A-1W, 94–96 cm, through 110–112 cm) was deposited below the foraminifer lysocline and is nearly barren of planktonic foraminifers. However, benthic foraminifers indicate a section comparable to the middle to upper Eocene section cored in Hole 1185 (Cores 192-1185A-2R through 8R). This correlation is further supported by a change in species composition that defines a global turnover in middle Eocene deep-water benthic foraminifers (see "Biostratigraphy," p. 7, in the "Site 1185" chapter). In addition, the occurrence of rare specimens of the dissolution-resistant planktonic

foraminifer species *Globigerina senni* confirms a middle Eocene age for Sample 192-1187A-1W, 110–112 cm.

Late Aptian planktonic foraminifers were recovered from both the brown claystone (interval 192-1187A-2R-1 to 2R-2) and the thin, white chalk (interval 2R-2, 28–30 cm) overlying basement (Table T3). Highly corroded specimens of *Globigerinelloides aptiensis,* which has been reported from the upper Aptian to middle Albian (Leckie, 1984), were recovered from the brown claystone (see "Lithostratigraphy," p. 3). A questionable specimen of the Albian taxon *Blefuscuiana albiana* was recovered from Sample 192-1187A-2R-1, 90–92 cm.

Paleoenvironment

Benthic foraminifers are common and moderately well preserved in the chalk immediately above basement (Sample 192-1187A-2R, 28–30 cm). This assemblage is dominated by *Gyroidinoides crassa, Gavelinella complanata,* and *Dorothia zedlerae,* which are indicative of the transition from upper to lower slope environments (Moullade, 1984).

Washed residues of the dark brown claystone (Sections 192-1187A-2R-1 and 2R-2) are composed almost entirely of abundant fish-bone debris and very small ferromanganese nodules. This composition is consistent with very slow deposition of clay in a lower slope to abyssal setting and indicates that the CCD rose above Site 1187 shortly after deposition of the upper Aptian limestone. Washed residues from relatively rare orange-brown claystone intervals (Sample 192-1187A-2R-1, 90–92 cm) differ by having much less ferromanganese nodule material and by yielding very rare, noncalcareous agglutinated benthic foraminifers (mainly species of *Ammodiscus* and *Glomospira*). Fish-bone debris remains dominant, however. Only in mottled claystone of the upper part of the section (Sample 192-1187A-2R, 17–20 cm) does the amount of fish-bone debris decrease.

The sediment recovered in Core 192-1187A-1W tentatively indicates that the CCD did not again drop below Site 1187 until middle Eocene time. However, calcareous sediment between the Eocene limestone and Albian–Aptian claystone was not recovered.

IGNEOUS PETROLOGY

Introduction

We reached basement at 372.5 mbsf (366.97 mbsf curated depth) and penetrated a further 135.8 m, recovering 74.3% of the rock cored (Cores 192-1187A-2R to 16R; Fig. F10). The age of the thin chalk layer directly above basement is late Aptian (~114–112 Ma; see "Biostratigraphy," p. 5). The basaltic basement was divided into 12 units ranging in thickness from 0.7 to 41.2 m. We assigned the unit boundaries on the presence of recrystallized limestone (Fig. F11), significant hyaloclastite intervals (Fig. F12), or downcore changes in character from massive to pillowed (see "Igneous Petrology," p. 12, in the "Explanatory Notes" chapter). A summary of the individual unit and unit boundary characteristics is given in Table T4. The units are composed of pillow lavas, except Units 6 and 7, which have massive bases with overlying pillows. The pillows, which we define as small cooling units with visible upper and lower chilled margins, range in thickness from several centimeters to 2.5 m (Fig. F10). Some of the cooling units interpreted as large pil-

F10. Cores, recovery, rock types, lithologic units, and cooling unit size, p. 24.

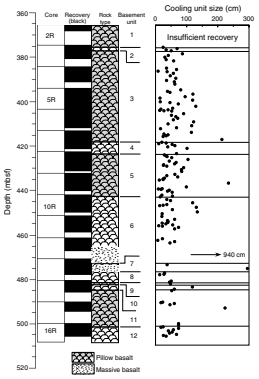

F11. Recrystallized limestone separating units, p. 25.

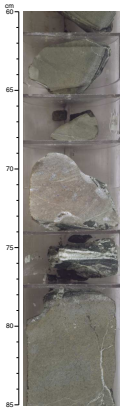

F12. Calcite-cemented hyaloclastite, p. 26.

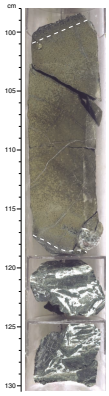

T4. Unit characteristics and boundary definitions, p. 57.

lows actually may be thin, massive flows, but the lack of three-dimensional information makes it impossible to distinguish between these alternatives.

Macroscopic Description

The recovered basalt units are aphyric to moderately olivine phyric (≤7% olivine; e.g., Section 192-1187A-13R-1 [Piece 9B]). Many complete vertical sections through individual pillows were recovered (Figs. F12, F13); one section along a pillow margin shows a breakout pillow (Fig. F14). From margin to interior, the pillows have the following features: a generally altered (but locally unaltered) glassy margin, an Fe oxyhydroxide–stained spherulitic zone (Figs. F12, F13), and an aphanitic central zone without spherulites. In the larger pillows, grain size coarsens gradually from aphanitic rims toward fine-grained interiors.

The fine-grained groundmass of both the pillowed and massive basalt is composed of plagioclase and clinopyroxene ± black oxides and generally has a poorly developed variolitic texture. Some basalt from the massive part of Unit 6 and the interior of the largest pillows has a mottled appearance produced by varying proportions of coarser grained and aphanitic patches.

Two plagioclase-rich xenoliths were found in Subunit 3B; one measures 15 mm × 25 mm (e.g., Section 192-1187A-3R-5 [Piece 7]). Rare, round to elongate and irregular vesicles (≤1.5 mm; e.g., in Section 192-1187A-16R-2 [Piece 1A]) are present adjacent to pillow margins and are filled with calcite and green clay. Rare to sparse irregular miarolitic cavities (as large as 10 mm × 20 mm) are most abundant in the fine-grained interiors of pillows and the massive portion of Unit 6. These cavities are filled with calcite, green and brown clay, Fe oxyhydroxide, and zeolites. Basalt in Hole 1187 is generally moderately to highly altered, although the fine-grained interiors of pillows and massive basalt (away from veins) and some of the glassy margins are only slightly altered (see "Alteration," p. 8). Olivine phenocrysts are generally replaced by Fe oxyhydroxide in spherulitic zones and by black or green clay near veins in the fine-grained intervals, although several intervals of fine-grained basalt contain unaltered olivine (e.g., Section 192-1187A-10R-7 [Piece 1B]).

Petrography

Olivine phenocrysts are commonly present as glomerocrysts and are generally replaced by Fe oxyhydroxide, brown clay, or calcite (Fig. F15). In the least altered areas (away from veins), the olivine crystals have unaltered interiors (Fig. F16) that occasionally contain glass inclusions (mostly devitrified). Euhedral to subhedral chrome spinel, typically associated with the olivine phenocrysts, is also present (Fig. F17).

The groundmass in the pillow margins is spherulitic and cryptocrystalline. Elongate, quenched, groundmass olivine is present, and spherulites contain radiating skeletal to feathery plagioclase (Fig. F15). A trace of skeletal to subhedral titanomagnetite is also present.

Fine-grained parts of the basalt have a variety of textures, including subophitic, variolitic, intergranular, and, less commonly, intrafasciculate (Fig. F18). In some thin sections from Unit 6, bimodal groundmass grain-size distributions are apparent (Fig. F19), giving the basalt the mottled appearance observed in hand specimen. Variolitic and intergranular textures are characteristic of the aphanitic basalt. Plagioclase

F13. Vertical section through a pillow, p. 27.

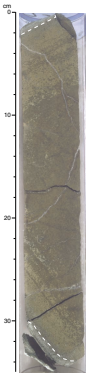

F14. Breakout pillow, p. 28.

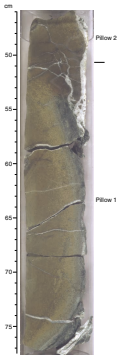

F15. Altered sperulites in quenched pillow margin, p. 29.

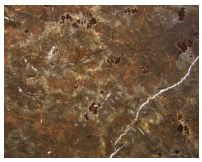

F16. Olivine phenocrysts partially altered to smectite, p. 30.

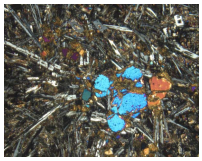

F17. Chrome spinel inclusions in unaltered olivine, p. 31.

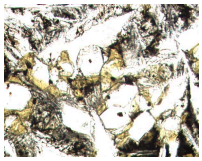

in these aphanitic zones is typically skeletal to feathery and, less commonly, subhedral to euhedral. Feathery, anhedral clinopyroxene is present between the plagioclase crystals. The coarser-grained patches of Unit 6 generally display subophitic and intrafasciculate textures. Titanomagnetite is present as small but ubiquitous crystals throughout the fine-grained basalt, and ranges from skeletal to euhedral. Blebs of sulfide (≤0.01 mm; too small for petrographic identification) are present within the mesostasis and as inclusions within the silicate minerals.

Geochemistry

Seven basalt samples from Hole 1187A were selected for whole-rock analysis by ICP-AES. All of the samples analyzed are olivine-normative tholeiitic basalts (Fig. F20; Table T5). Six are relatively primitive, having high Cr (464–501 ppm), Ni (171–196 ppm), and MgO (8.7–9.4 wt%) contents, Mg# of 0.65–0.66, and low TiO_2 (0.72–0.75 wt%) and Zr (36–41 ppm) contents. One sample (192-1187A-7R-6 [Piece 2, 66–70 cm]) taken from an aphanitic pillow margin has lower MgO content (but similar Cr, Ni, TiO_2, and Zr abundances) than the other samples (Table T5). Its elevated alkali contents, high weight loss on ignition, and apparent silica undersaturation (it is nepheline normative; Table T5) indicate that its composition has been affected by alteration processes; thus, it is excluded from Figures F20, F21, F22, and F23.

Comparison to Other Ontong Java Plateau Basalts

The basalt recovered from Hole 1187 is petrologically and chemically very similar to basalt of the upper group of units at Site 1185 (all units of Hole 1185A and Units 1–9 of Hole 1185B). Together, these basalts are the most Mg-rich yet found on the Ontong Java Plateau. The relatively primitive nature of the Site 1187 basalt and its similarity to that of the upper group at Site 1185 are clearly illustrated by immobile-element concentrations (Figs. F21, F22) and Mg# (Fig. F23). The basement units in Hole 1187 differ from the upper group at Site 1185 in having plagioclase-rich xenoliths. However, basalt flows from the two sites clearly represent a magma type hitherto unrecorded on the Ontong Java Plateau. Lavas of this type may be rather extensive in this region of the plateau's eastern flank, as they are >136 m thick in Hole 1187 and 125 m thick at Site 1185, 146 km to the south.

ALTERATION

The entire basaltic crustal section drilled at Hole 1187A exhibits the effects of pervasive halmyrolysis or submarine weathering, the low-temperature process of oceanic basalt alteration by bottom seawater. Alteration occurred under oxidizing conditions and with high water-rock ratios, resulting in the development of light to dark yellow-brown colors in the most exposed rocks (e.g., near the outer zones of cooling units) (Fig. F24). In contrast to the other Leg 192 sites, no black or dusky green halos were observed.

The basalt in Hole 1187 appears to have undergone the greatest overall alteration of basement of any Leg 192 site. This observation is consistent with the dominantly pillowed nature of the basalts recovered in this hole; massive basalt forms only a minor component and is present only in the lower parts of Units 6 and 7 (see "Igneous Petrology," p. 6).

F18. Variolitic to subophitic texture in pillow interior, p. 32.

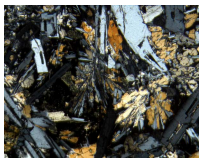

F19. Microcrystalline variolitic and coarser-grained patches in groundmass, p. 33.

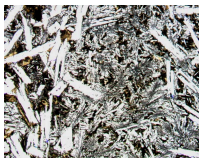

F20. Total alkalies vs. silica, p. 34.

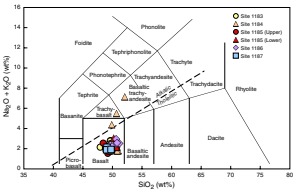

T5. Geochemical data for rock samples, Hole 1187A, p. 58.

F21. Cr vs. TiO_2, p. 35.

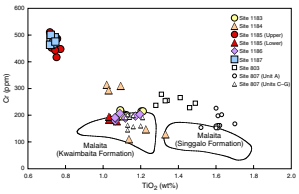

F22. Zr vs. TiO_2, p. 36.

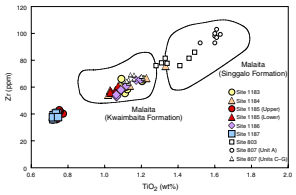

F23. TiO_2 vs. Mg#, p. 37.

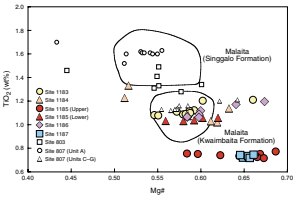

The light to dark yellow-brown colors in the outer portions of the pillow lavas result from the complete replacement of olivine (Fig. F25) and partial to complete alteration of groundmass by brown to tan smectite (probably an Fe-rich saponite) (Fig. F26) and Fe oxyhydroxide. Smectite, calcite, and minor goethite fill miarolitic cavities (Fig. F27, F28), which are surrounded by 2- to 10-mm-wide brown halos. The primary igneous minerals in these halos are totally replaced by brown smectite and minor calcite and goethite (Fig. F29).

Unaltered glass is more abundant at this site than at any other Leg 192 site, despite the pervasive alteration of pillow margins (Fig. F14). Away from pillow margins, the color grades into dark gray within several coarser-grained pillow interiors. Although olivine phenocrysts are generally completely replaced, unaltered or only incipiently altered olivine is present in several dark gray basalt intervals interpreted as either the interiors of large pillows or massive flows (Fig. F30). In this respect, Site 1187 is unique among the Leg 192 sites.

Veins throughout Hole 1187A are mostly filled with calcite, zeolites (identified in hand specimen; probably phillipsite with analcime), smectite, Fe oxyhydroxide, and rare celadonite, pyrite, and marcasite. No zeolites were observed in thin section. Abundant subhorizontal calcite veins are present in light to dark yellow-brown pillow margins, and calcite veins radiate from pillow interiors toward the margins in well-preserved pillows.

As noted above, dusky green and black halos that surround veins at the other basement sites are absent in basalt from Site 1187. Reduction fronts containing pyrite and/or marcasite are similarly absent. Two possible explanations are that (1) neither feature ever formed or (2) both may have formed but were overprinted by the later pervasive oxidative alteration that produced the various brown-colored halos. We prefer the second explanation because black and dusky green halos are ubiquitous and form quickly, within 1–2 m.y. of basalt emplacement (Honnorez, 1981; Böhlke et al., 1980; Laverne, 1987).

As with the upper alteration zone in basement at Site 1185, we again noticed a clear relationship between vein abundance and the color of host-rock alteration. The lighter yellow-brown colors in the basalts at both sites are generally associated with the parts of cores that display the most abundant horizontal and subhorizontal veins (Fig. F31). Because the degree of alteration is a function of permeability, the abundance of veins, pervasiveness of the alteration, and development of light and dark yellow-brown alteration colors indicate that basement in Hole 1187 was initially the most permeable of any drilled during Leg 192.

PALEOMAGNETISM

Introduction

Pass-through magnetometer measurements were taken on all split-core archive sections. Sediment cores were measured at 5-cm intervals. Coherent basalt pieces that could be oriented unambiguously with respect to the top were measured at 1-cm intervals. Pass-through magnetic susceptibility measurements were taken on all unsplit core sections at 4-cm intervals.

In order to isolate the characteristic remanent magnetization (ChRM), cores were subjected to alternating-field (AF) cleaning. The

F24. Yellow-brown alteration in basalt near pillow margin, p. 38.

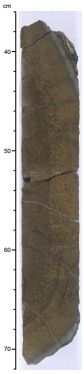

F25. Replacement of olivine phenocryst by smectite, p. 39.

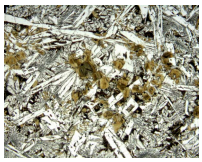

F26. Replacement of groundmass by smectite, p. 40.

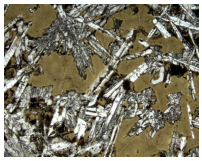

F27. Miarolitic cavities in basalt with alteration halos, p. 41.

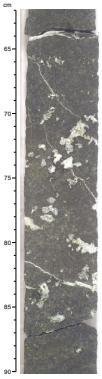

F28. Miarolitic cavity in basalt filled with smectite, calcite, and goethite, p. 42.

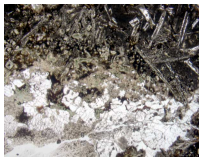

number of AF demagnetization steps and peak-field intensity varied depending on lithology, the natural remanent magnetization (NRM) intensity, and the amount of time available. On average, sediment half-cores were demagnetized using three AF steps in addition to the measurement of NRM. The basalt half-cores were demagnetized using a minimum of six AF steps. The maximum applied field ranged between 25 and 50 mT. We analyzed the results in Zijderveld and stereoplot diagrams; where possible, we calculated the ChRM direction using principal component analysis (Kirschvink, 1980). Examples of the AF demagnetization of sediment and basalt samples are shown in Figure F32.

Results from Sedimentary Units

We recovered 1.47 m of sediments, consisting of 1.45 m of dark brown ferruginous claystone overlying a 2-cm-thick chalk layer. The NRM intensity of the claystone is high for sediments and has a mean value of 4.3×10^{-2} A/m. The progressive downward increase in magnetic susceptibility of the claystone from 1×10^{-3} SI at 365.5 mbsf to 4×10^{-3} SI immediately above basement probably results from the decrease in bioturbation with depth observed in the core. The magnetization and susceptibility of the 2-cm chalk layer were not determined. AF demagnetization of the claystone with peak fields of 15 mT was effective in isolating the ChRM (Fig. F32A). Although the sediments were somewhat disturbed by drilling and the magnetic inclinations obtained were not very consistent, we were able to identify the polarity of the ChRM. At 365.7 mbsf we observed a downward transition from negative to positive (i.e., reversely magnetized) inclination values. The inclinations become negative again at 366.5 mbsf. Because the chalk layer underlying the claystone contains Aptian microfossils (see "Biostratigraphy," p. 5) and the basalts beneath the chalk are all normally magnetized, we have tentatively correlated this ~70-cm-thick reversely magnetized layer with the M″-1r″ (ISEA) Subchron within the Cretaceous Normal Superchron (Fig. F33). Because this subchron is thought to be short in duration and the claystone to have accumulated slowly, this correlation cannot be made with confidence. Accurate magnetic inclinations obtained from shore-based studies of discrete samples from this layer will enable us to document more carefully the presence or absence of this reversely magnetized interval.

Results from Basaltic Units

The basaltic basement recovered from Hole 1187 consists almost entirely of pillow lavas (Fig. F34). In the 100.9 m of basalt recovered (average recovery 74.3%), we distinguished a minimum of 147 pillows (see "Igneous Petrology," p. 6). As with other Leg 192 sites, the pillow lavas proved ideal for paleomagnetic studies, and ChRM directions could easily be defined using AF demagnetization and principal component analysis (Fig. F32B). The ChRM direction, NRM intensity, magnetic susceptibility, Koenigsberger ratio, and median destructive field (MDF) for all coherent basalt pieces longer than 15 cm for which a reliable ChRM direction could be defined are listed in Table T6. For coherent pieces longer than 50 cm, we list data for every ~25 cm.

The massive interiors of large pillows have slightly higher magnetic susceptibility than the more fine-grained pillow margins (see "Physical Properties," p. 11). These fine-scale variations are not apparent on the

F29. Halo surrounding miarolitic cavity, p. 43.

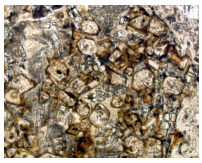

F30. Partially altered olivine crystals preserving incipient alteration to brown smectite, p. 44.

F31. Pervasively altered basalt grading in color toward pillow interior, p. 45.

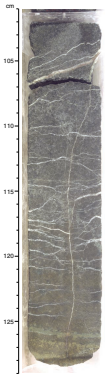

F32. Zijderveld diagrams, p. 46.

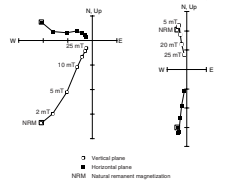

F33. Magnetic inclination variation with depth, p. 47.

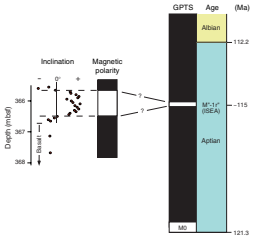

downhole plot of NRM intensity and MDF (Fig. F34), which displays more widely spaced depth intervals.

The magnetic inclination is negative for all 252 ChRM determinations (Table T6), indicating normal polarity for all basalt cores. The normal-polarity magnetization is consistent with the Aptian biostratigraphic age of the thin chalk layer immediately overlying basalt basement (see "Biostratigraphy," p. 5), indicating lava emplacement during the Cretaceous Normal Superchron sometime after M0 (~121 Ma) but before the M″-1r″ Subchron at ~115 Ma (Fig. F33). The downhole variation of ChRM inclinations is shown in Figure F34. Note that we do not observe any evidence for significant rotation (i.e., >30°) of pillows after they cooled below their magnetic blocking temperatures. We were unable to group the ChRM inclinations into paleomagnetic units at Site 1187 as we did at other Leg 192 sites (see "Paleomagnetism," p. 18, in the "Site 1185" chapter). The reason is that we had too few inclination values for each of the large number of cooling units to adequately define individual paleomagnetic units. Thus, we have used the statistics of Kono (1980) on the entire data set to obtain a mean inclination of –35.2° (N = 252, α_{95} = 0.9°, k = 107, and angular standard deviation [ASD] = 7.8°) and a corresponding paleolatitude of 19.4°S. Whereas we feel confident that the mean inclination value provides a reasonable estimate of the geomagnetic field during basalt emplacement, we note that the ASD is ~5° lower than that expected for the paleolatitude and age (McFadden et al., 1991). The lower than expected ASD value indicates that some of the measurements are not independent but sample the same paleosecular variation. Shore-based studies on discrete samples are necessary for a more precise definition of the paleomagnetic units and their mean inclination.

Because the basalt composition in Hole 1187 is very similar to that obtained for the upper igneous units at Site 1185 (see "Igneous Petrology," p. 6), we have compared the mean magnetic inclinations at both sites. The mean inclination at Site 1187 is essentially the same as that obtained from paleomagnetic units corresponding to the upper igneous units at Site 1185 (see Table T11, p. 120, in the "Site 1185" chapter).

F34. ChRM inclination, NRM intensity, and MDF, p. 48.

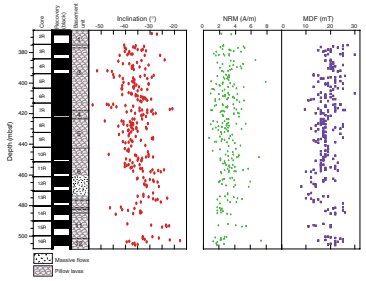

T6. ChRM direction, NRM, MDF, magnetic susceptibility, and Q-ratio, p. 59.

T7. Index properties data, p. 63.

F35. Index properties, p. 49.

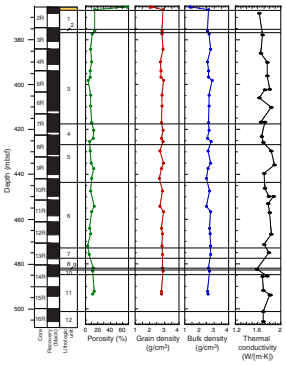

PHYSICAL PROPERTIES

Introduction

We measured index properties on discrete samples taken from most of the cores recovered from Hole 1187. Whole sections of these cores were also run through the multisensor track (MST) to measure magnetic susceptibility, gamma ray attenuation (GRA) bulk density, and natural gamma radiation (NGR). Sonic compressional (*P*-wave) velocities in basement units were measured on uncut split cores and minicores. We measured thermal conductivity on split rock samples from most of the cores.

Index Properties

We measured the wet mass, dry mass, and dry volume of each sample taken from the Hole 1187A cores and calculated wet and dry bulk density, water content, grain density, and porosity (Table T7; Fig. F35). As shown in Figure F35, porosity, grain density, and bulk density change abruptly at the boundary between sedimentary Unit III and basement

Unit 1. In basement, index properties remain fairly constant. Near the bottom of the hole, the grain and bulk density of the basalt from the lower part of Unit 11 both appear to decrease downhole (Fig. F35).

Multisensor Track Measurements

Magnetic Susceptibility

We determined magnetic susceptibility with the Bartington meter at 4-cm intervals along whole-core sections from most of the cores. Although values are generally <800 × 10^{-5} SI, higher magnetic susceptibility values (>1200 × 10^{-5} SI) in the basement units correlate with the presence of dense basalt (Fig. F36). We obtained similar results at Sites 1185 and 1186, where dense, massive basalt always exhibited higher magnetic susceptibility than more altered and heavily veined basalt. Magnetic susceptibility results are discussed further in "Paleomagnetism," p. 9, in conjunction with the NRM pass-through measurements.

Gamma Ray Attenuation Density

We estimated bulk densities from whole-core GRA measurements of the sections from Hole 1187A. In the Unit III claystone and chalk between 365.58 and 366.96 mbsf (curated depths), the average GRA density is 1.1 g/cm³ (Fig. F36). In basement, for the most part, only minor variations were observed in maximum GRA bulk densities (Fig. F36). Below 500 mbsf, however, in the lower part of Unit 11 and through Unit 12, mean GRA bulk densities decrease to <2.0 g/cm³. Although the diameter of the recovered core also decreased downhole in this interval, comparison of the GRA maximum bulk density profile with bulk density data obtained from discrete samples (up to the middle part of Unit 11) reveals similar trends in both sets of measurements, despite the consistently lower values of the GRA density data (Fig. F37).

Natural Gamma Radiation

NGR measurements of sediments from Unit III (Fig. F36) show high count rates (mean rate >6 counts per second [cps]). In basement, NGR measurements on unsplit sections of basalt cores generally show only minor fluctuations (usually below ~3 cps), but the downhole profile has a number of peaks >4 cps (Fig. F36). In Unit 3, for example, peaks of >4 cps at ~385, ~408, and ~415 mbsf appear to correspond to pillow basalt intervals in Cores 192-1187A-4R, 6R, and 8R, respectively, which are probably related to alteration and veining in the basalt. These observations are similar to those from Site 1186, where the highest NGR count (>5 cps) occurred in the pillow basalt.

P-Wave Velocity

We calculated *P*-wave velocity from discrete measurements on both split-core sections and cut samples (Table T8; Fig. F36). In the basement units, *P*-wave velocities are typically >5300 m/s in the relatively massive, unveined basalt sections of Units 3, 5, 6, and 7 and generally <5300 m/s in the more abundantly veined basalt sections of these units, as well as in the remaining basement units (Fig. F36). The high *P*-wave velocities (>5300 m/s) measured in the relatively unveined basalt also

F36. Velocity data and whole-core measurements, p. 50.

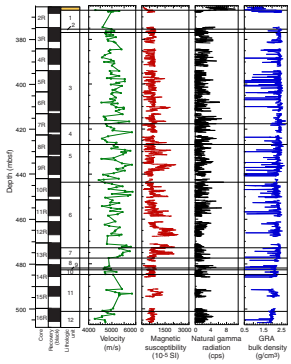

F37. Bulk density profiles comparison, p. 51.

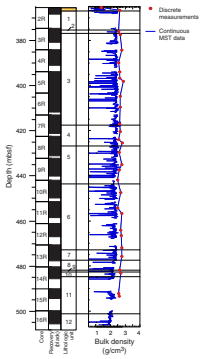

T8. *P*-wave velocity, p. 64.

correlate with the large magnetic susceptibility spikes observed in the same units (Fig. F36). Below 500 mbsf, in the lower part of Unit 11 and through Unit 12, *P*-wave velocities decrease significantly (<5300 m/s), in similar fashion to mean GRA bulk densities in this interval.

Thermal Conductivity

We determined thermal conductivity on selected samples of basalt (Table T9; Fig. F35). Thermal conductivity values varied from 1.6 to 1.9 W/(m·K), with higher values in the dense, massive basalt and lower values in the more altered and veined basalt. The average thermal conductivity of the basalt is 1.7 W/(m·K), similar to basalt from Hole 1186.

T9. Thermal conductivity values, p. 66.

REFERENCES

Böhlke, J.K., Honnorez, J., and Honnorez-Guerstein, B.M., 1980. Alteration of basalts from Site 396B, DSDP: petrographic and mineralogical studies. *Contrib. Mineral. Petrol.,* 73:341–364.

Honnorez, J., 1981. The aging of the oceanic crust at low temperature. *In* Emiliani, C. (Ed.), *The Sea* (Vol. 7): *The Oceanic Lithosphere:* New York (Wiley), 525–587.

International Hydrographic Organization/Intergovernmental Oceanographic Commission (IHO/IOC), 1997. *General Bathymetric Chart of the Ocean (GEBCO) Digital Atlas:* London (British Oceanographic Data Centre).

Kirschvink, J.L., 1980. The least-squares line and plane and the analysis of palaeomagnetic data. *Geophys. J. R. Astron. Soc.,* 62:699–718.

Kono, M., 1980. Statistics of paleomagnetic inclination data. *J. Geophys. Res.,* 85:3878–3882.

Kroenke, L.W., Berger, W.H., Janecek, T.R., et al., 1991. *Proc. ODP, Init. Repts.,* 130: College Station, TX (Ocean Drilling Program).

Laverne, C., 1987. Les altérations des basaltes en domaine océanique: minéralogie, pétrologie et géochimie d'un système hydrothermal: le puits 504B, Pacifique oriental [Thèse]. Univ. Aix-Marseille III.

Le Bas, M.J., Le Maitre, R.W., Streckeisen, A., and Zanettin, B., 1986. A chemical classification of volcanic rocks based on the total alkali-silica diagram. *J. Petrol.,* 27:745–750.

Leckie, R.M., 1984. Mid-Cretaceous planktonic foraminiferal biostratigraphy off Central Morocco, Deep Sea Drilling Project Leg 79, Sites 545 and 547. *In* Hinz, K., Winterer, E.L., et al., *Init. Repts. DSDP,* 79: Washington (U.S. Govt. Printing Office), 579–620.

Macdonald, G.A., and Katsura, T., 1964. Chemical composition of Hawaiian lavas. *J. Petrol.,* 5:82–133.

Mahoney, J.J., Storey, M., Duncan, R.A., Spencer, K.J., and Pringle, M.S., 1993. Geochemistry and age of the Ontong Java Plateau. *In* Pringle, M.S., Sager, W.W., Sliter, W.V., and Stein, S. (Eds.), *The Mesozoic Pacific: Geology, Tectonics, and Volcanism.* Geophys. Monogr., Am. Geophys. Union, 77:233–262.

McFadden, P.L., Merrill, R.T., McElhinny, M.W., and Lee, S., 1991. Reversals of the Earth's magnetic field and temporal variations of the dynamo families. *J. Geophys. Res.,* 96:3923–3933.

Moullade, M., 1984. Intérêt des petits foraminifères benthiques "profonds," pour la biostratigraphie et l'analyse des paléoenvironnements océaniques Mésozoïques. *In* Oertli, H.J. (Ed.), BENTHOS '83: Proc. 2nd Int. Symp. Benthic Foraminifera. *Bull. Cent. Rech. Expl.-Prod. Elf-Aquitaine,* 6:429-464.

Sandwell, D.T., and Smith, W.H.F., 1997. Marine gravity anomaly from Geosat and ERS-1 satellite altimetry. *J. Geophys. Res.,* 102:10039–10054.

Smith, W.H.F., and Sandwell, D.T., 1997. Global seafloor topography from satellite altimetry and ship depth soundings. *Science,* 277:1956–1962.

Tarduno, J.A., Sliter, W.V., Bralower, T.J., McWilliams, M., Premoli-Silva, I., and Ogg, J.G., 1989. M-sequence reversals recorded in DSDP sediment cores from the western Mid-Pacific Mountains and Magellan Rise. *Geol. Soc. Am. Bull.,* 101:1306–1316.

Tejada, M.L.G., Mahoney, J.J., Neal, C.R., Duncan, R.A., and Petterson, M.G., in press. Basement geochemistry and geochronology of central Malaita, Solomon Islands, with implications for the origin and evolution of the Ontong Java Plateau. *J. Petrol.*

VandenBerg, J., Klootwijk, C.T., and Wonders, A.A.H., 1978. Late Mesozoic and Cenozoic movements of the Italian peninsula: further paleomagnetic data from the Umbrian sequence: *Geol. Soc. Am. Bull.,* 89:133–150.

Figure F1. Predicted bathymetry (after Smith and Sandwell, 1997) of the Ontong Java Plateau showing the locations of Site 1187 and other Leg 192 sites (stars). The plateau is outlined. Black dots = previous Ocean Drilling Program and Deep Sea Drilling Project drill sites that reached basement; white dots = Site 288, which did not reach basement but bottomed in Aptian limestone, and Site OJ-7, which was proposed for Leg 192 but not drilled. The bathymetric contour interval is 1000 m (IHO/IOC, 1997).

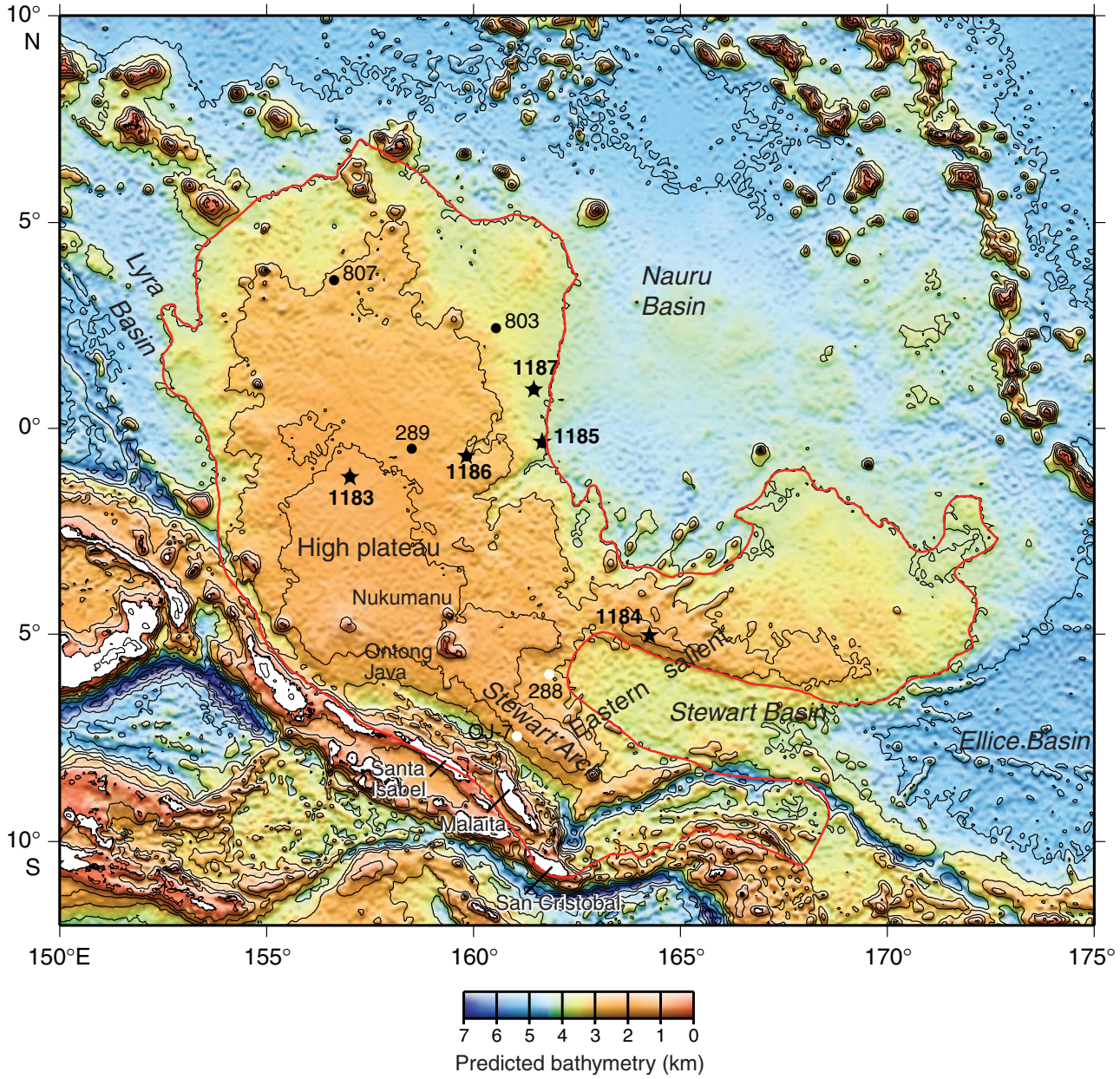

Figure F2. Satellite-derived free-air gravity map of the Ontong Java Plateau region (after Sandwell and Smith, 1997). The plateau is outlined. Stars show locations of Site 1187 and other Leg 192 sites. Black dots = previous ODP and DSDP drill sites that reached basement; white dots = Site 288, which did not reach basement but bottomed in Aptian limestone, and Site OJ-7, which was proposed for Leg 192 but not drilled. Black lines = surveys providing multichannel seismic control: *Hakuho Maru* KH98-1 Leg 2 (1998) and *Maurice Ewing* EW95-11 (1995). White lines = surveys providing single-channel seismic control: *Glomar Challenger* Leg 7 GC07 (1969), *Glomar Challenger* Leg 30 GC30 (1973), *Glomar Challenger* Leg 89 GC89 (1982), *Thomas Washington* TW-11 (1988), and *JOIDES Resolution* Leg 130 JR130 (1990). The bathymetric contour interval is 1000 m (IHO/IOC, 1997).

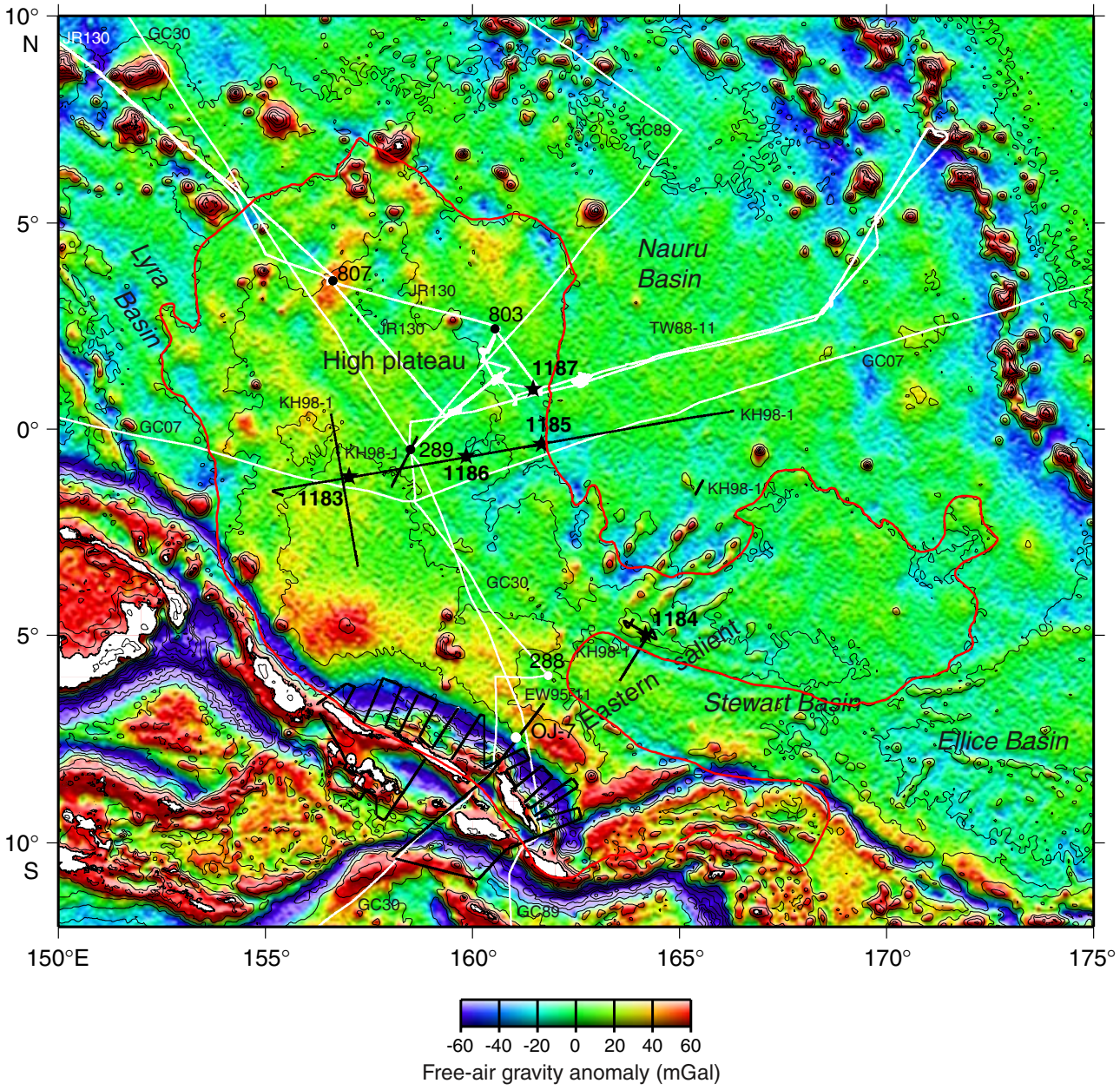

Figure F3. Location of Site 1187 (and 804) and site-survey data on satellite-derived free-air gravity map (after Sandwell and Smith, 1997). Navigation for *Thomas Washington* cruise 88-11 is shown in Julian-day time. Water depths in the survey area are between 3000 and 4500 m (IHO/IOC, 1997).

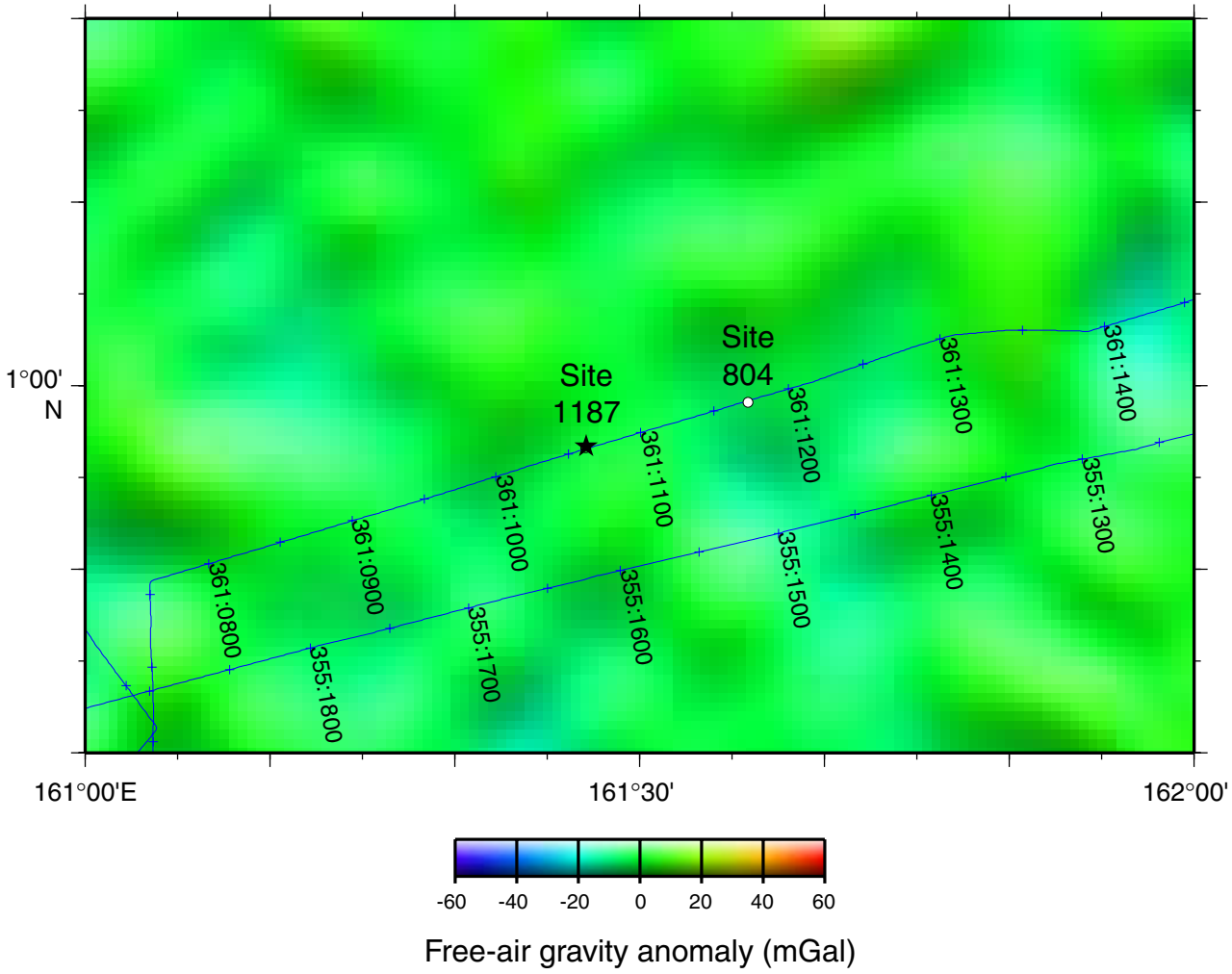

Figure F4. Single-channel seismic reflection profile across Site 1187 (see Fig. F3, p. 17, for location). Vertical exaggeration is ~6.67 at seafloor. UTC = Universal Time Coordinated.

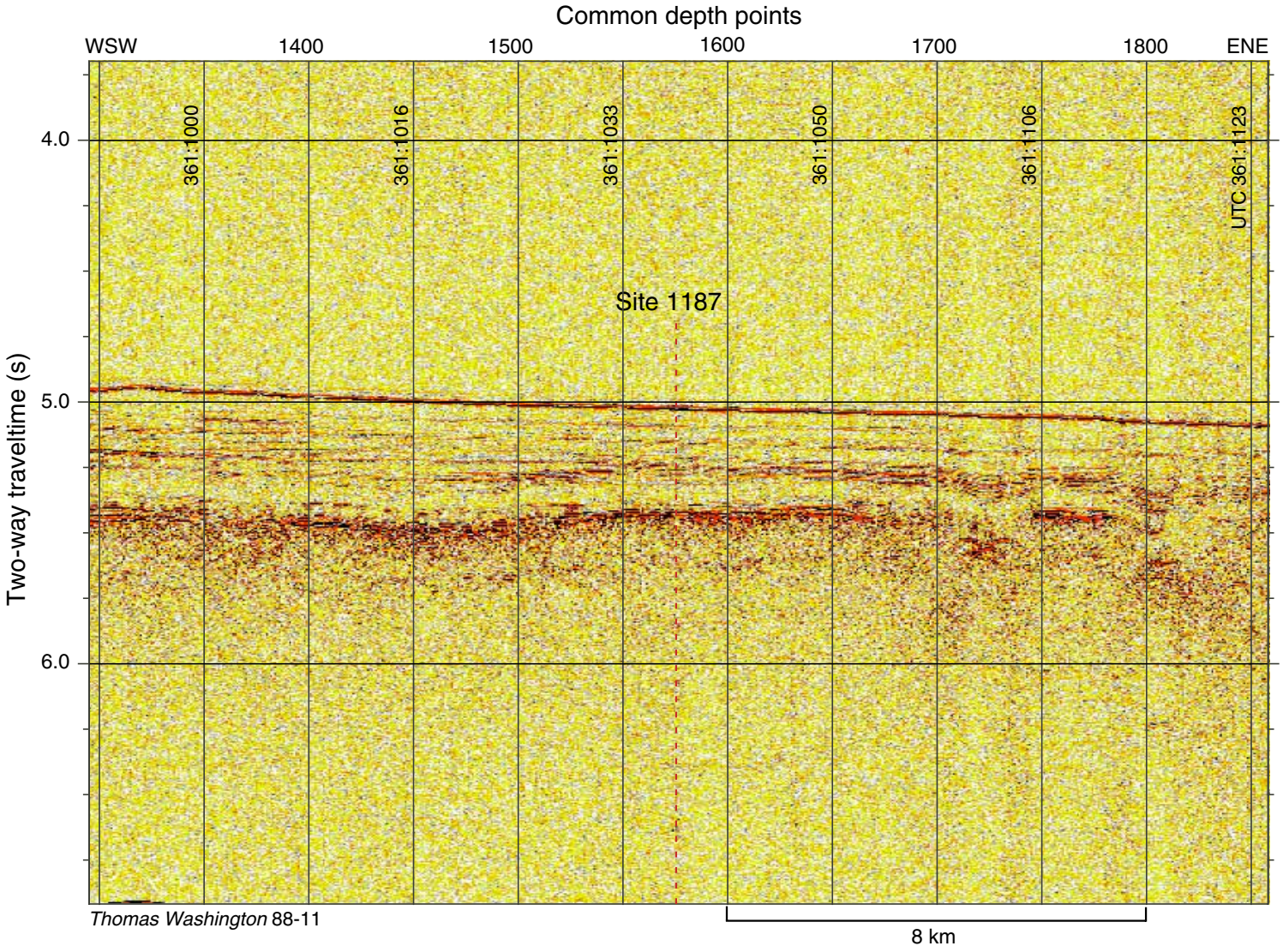

Figure F5. Single-channel seismic reflection profile across Site 1187 (see Fig. F3, p. 17, for location). Vertical exaggeration is ~6.67 at seafloor. UTC = Universal Time Coordinated.

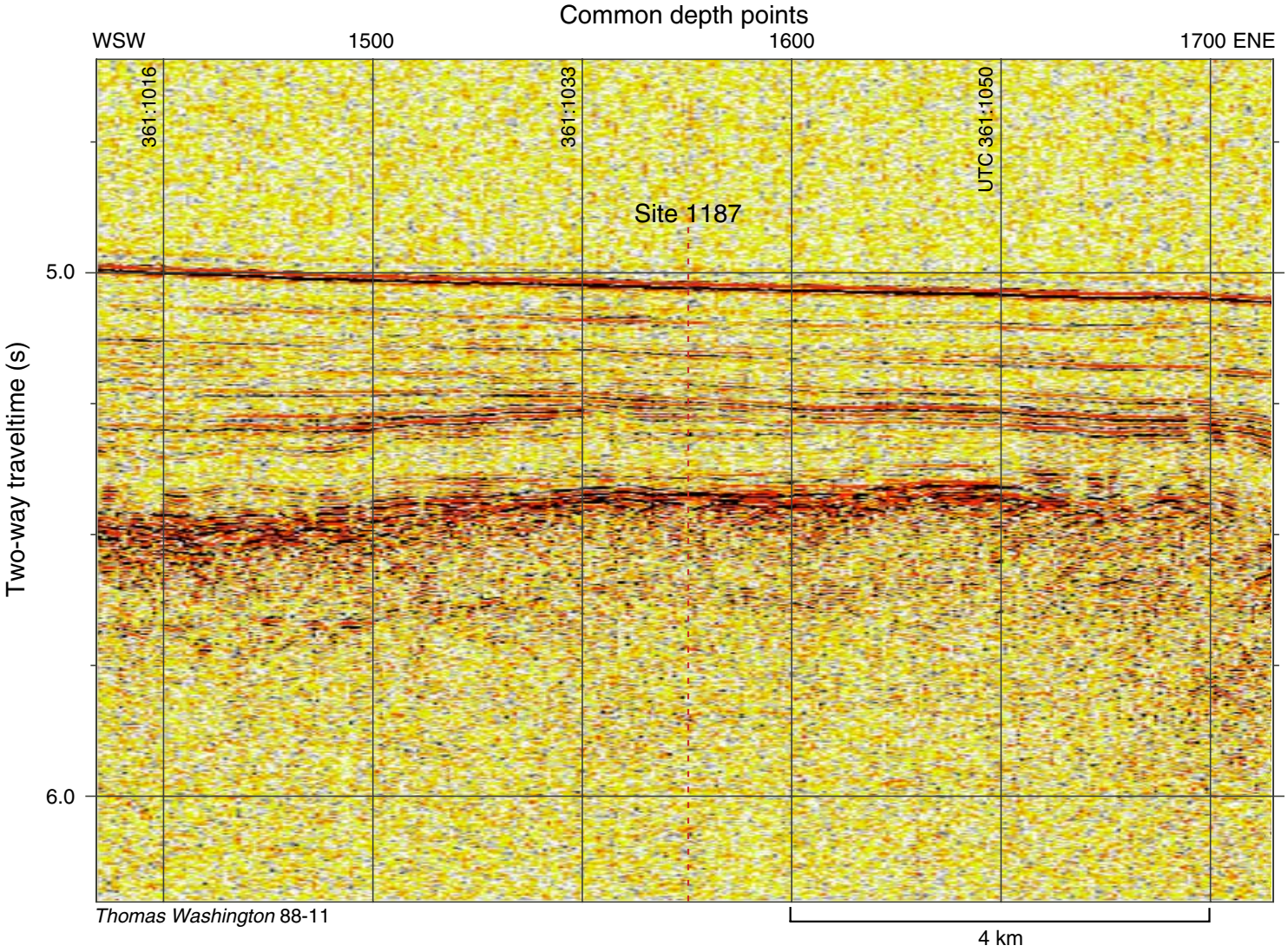

Figure F6. Single-channel seismic reflection profile across Site 1187 (see Fig. F3, p. 17, for location). Vertical exaggeration is ~6.67 at seafloor. UTC = Universal Time Coordinated.

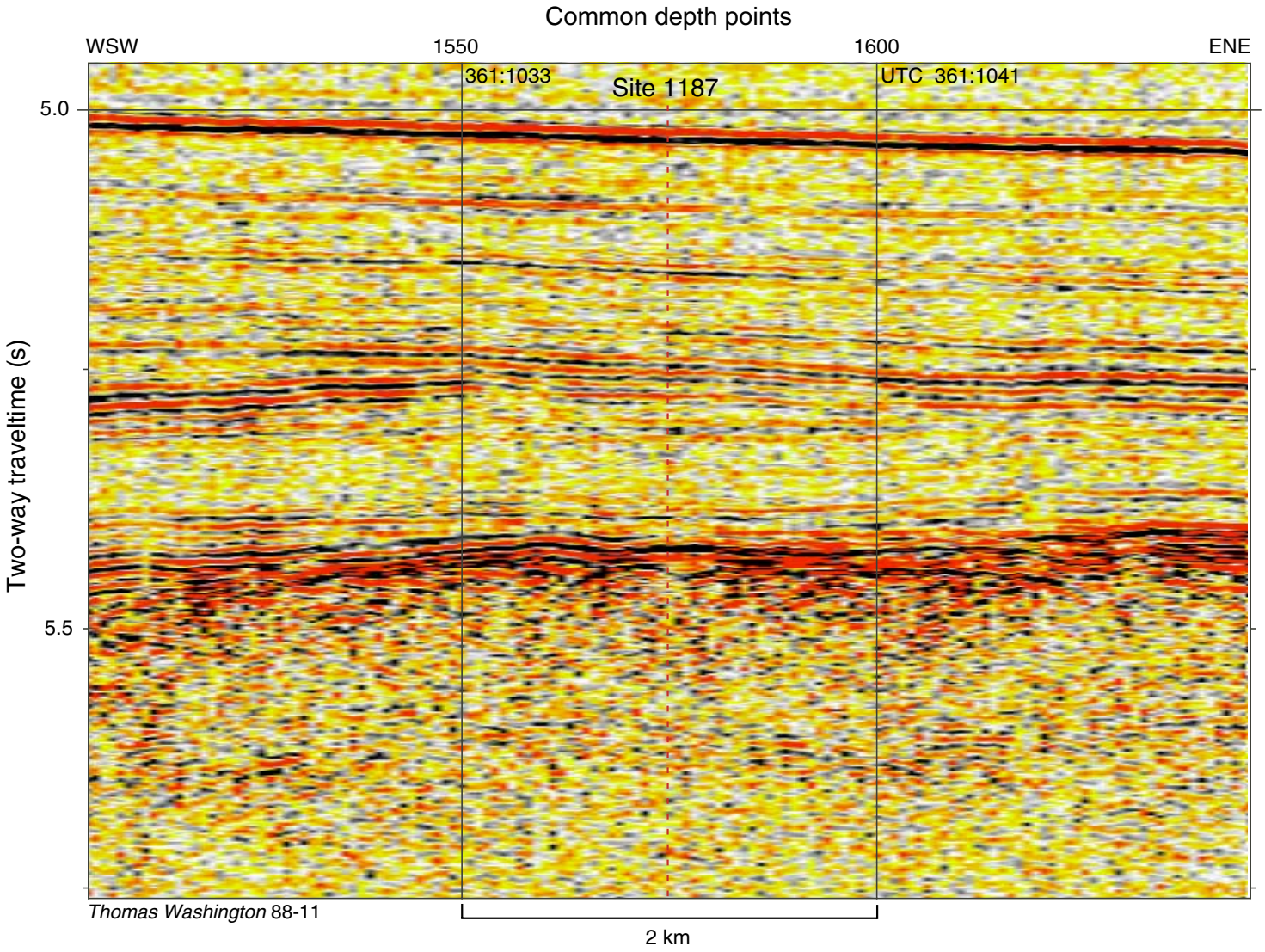

Figure F7. Core recovery (in black), observed and inferred lithostratigraphic divisions, and graphic lithology from Hole 1187A. Material in the wash core (Core 192-1187A-1W) is placed in an approximately appropriate position by comparison to the succession at other sites on the main Ontong Java Plateau but could have come from anywhere within the washed interval. The vertical extent of the dark gray boxes illustrates the proportion of the stratigraphic record not sampled.

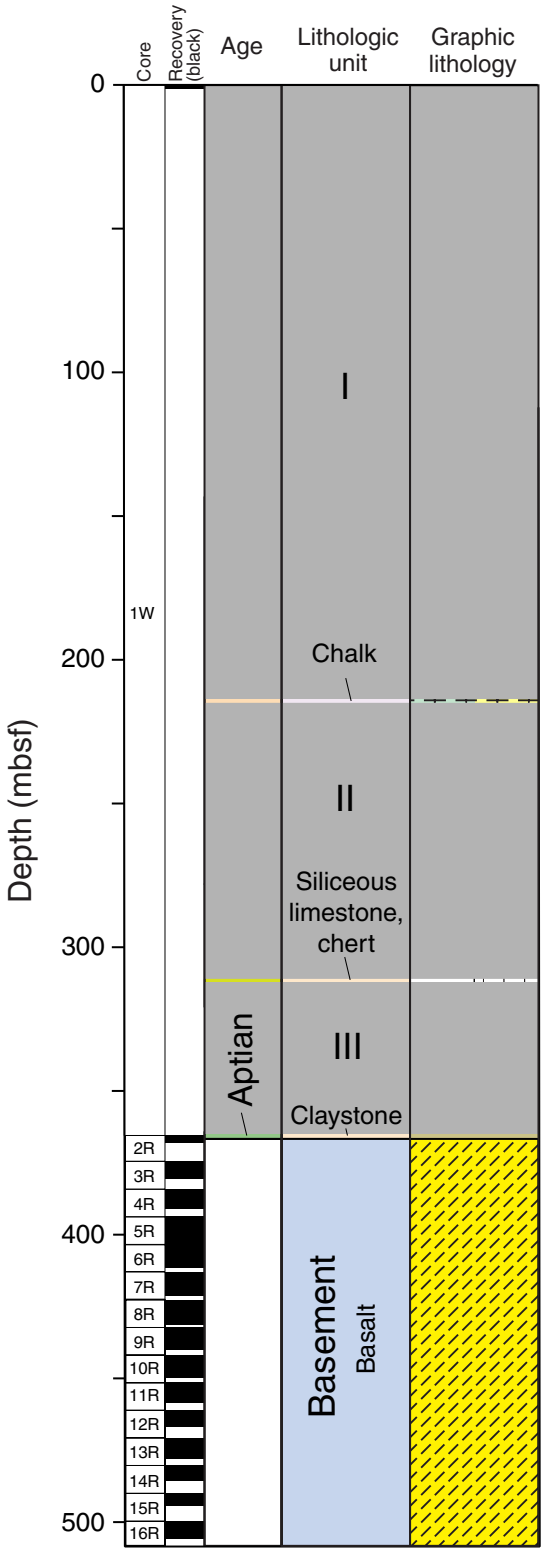

Figure F8. Burrow-mottled claystone of Unit III (interval 192-1187A-2R-1, 3–16 cm; Aptian).

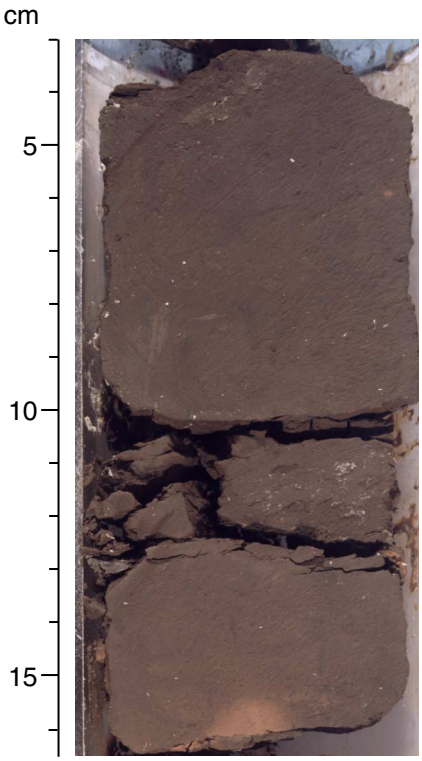

Figure F9. Laminated claystone of Unit III (interval 192-1187A-2R-1, 102–114 cm; Aptian).

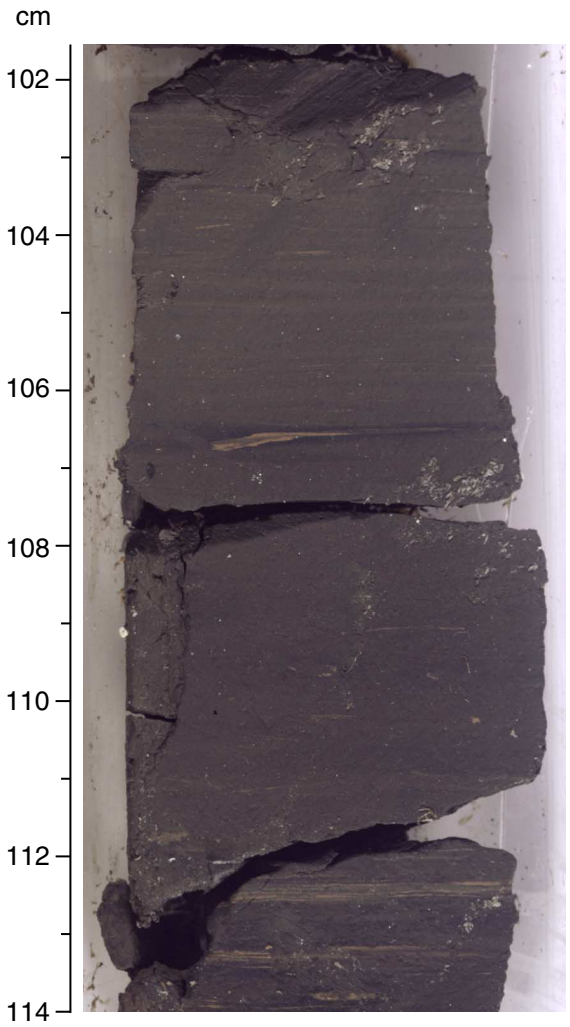

Figure F10. Log of cores, recovery, rock types, basement units, and cooling unit size at Site 1187.

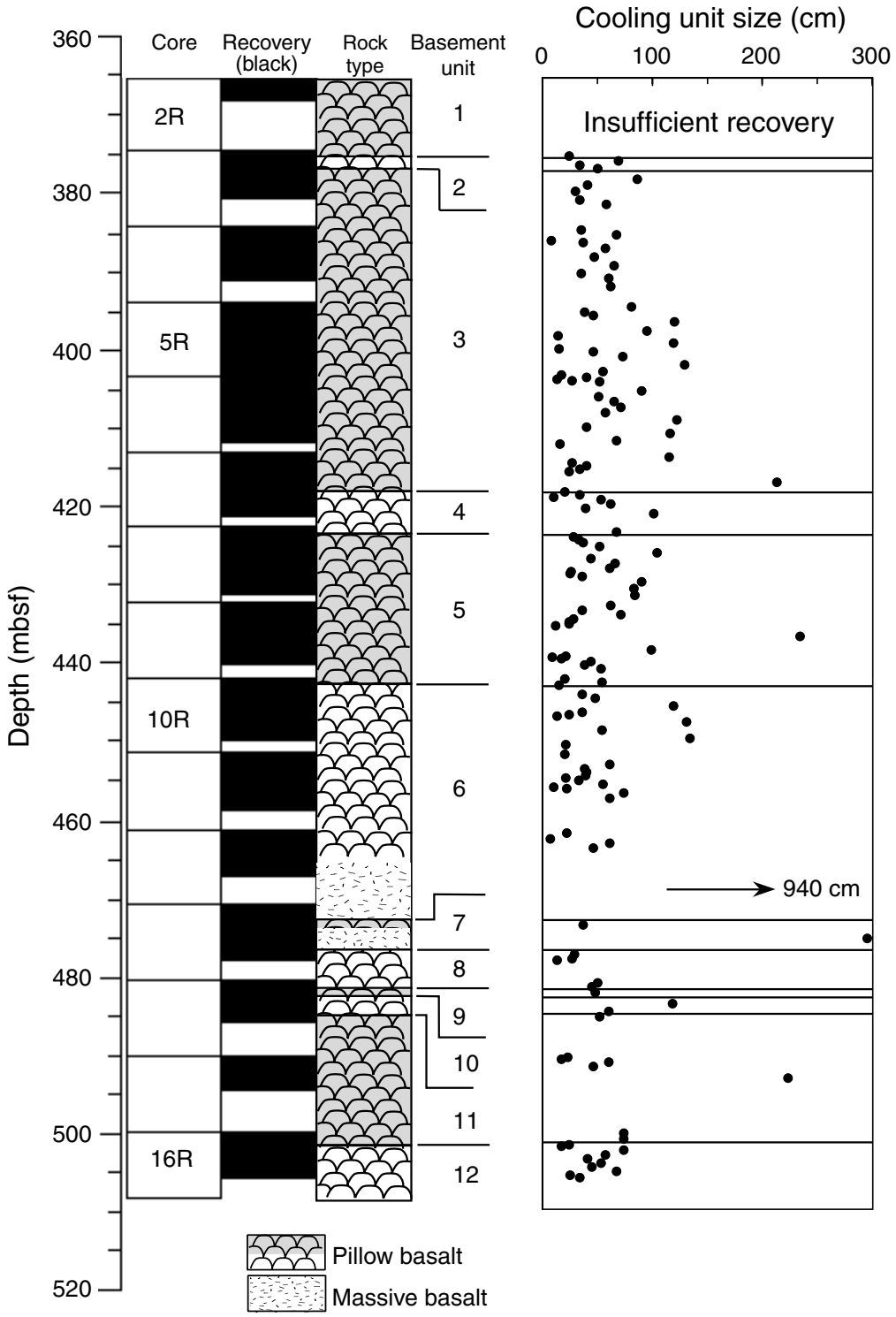

Figure F11. Interval 192-1187A-3R-1, 60–85 cm, showing the recrystallized limestone (Subunit 2A; 69–74 cm) that separates Unit 1 from Subunit 2B. Also visible are the glassy margin of a pillow in Unit 1 and the upper glassy margin of a pillow in Subunit 2B.

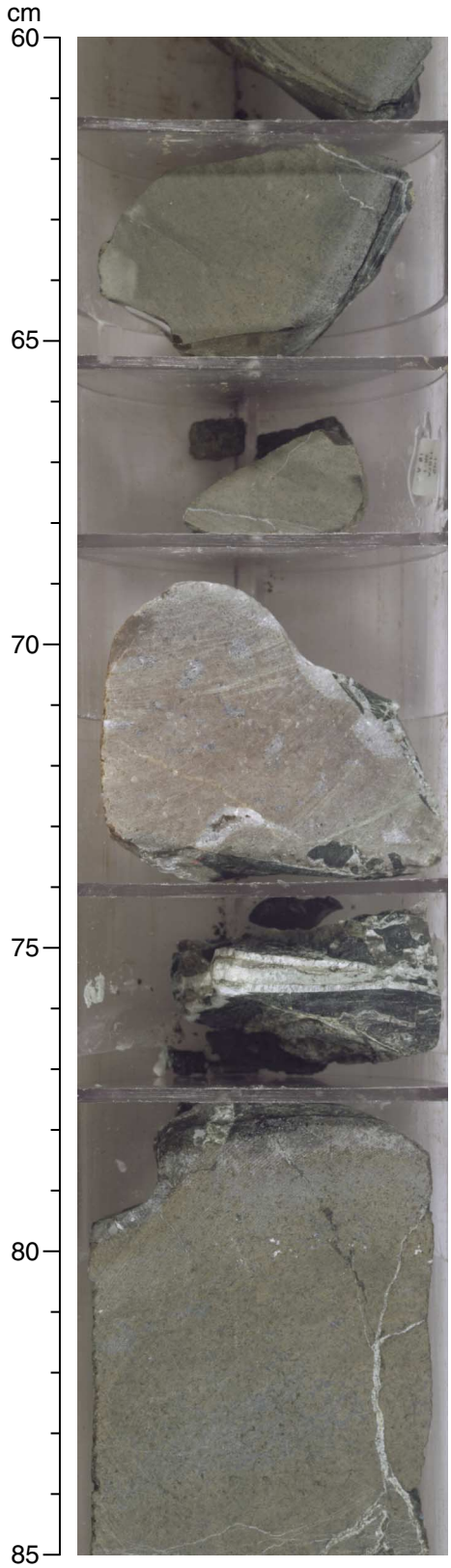

Figure F12. Interval 192-1187A-7R-4, 98–130 cm, showing the calcite-cemented hyaloclastite that defines the boundary between Subunit 3B and Unit 4. Also visible is a complete vertical section through the lowermost pillow of Subunit 3B, including its upper and lower glassy margins (highlighted), and the aphanitic interior containing an Fe oxyhydroxide–stained spherulitic zone (parallel to the pillow margin).

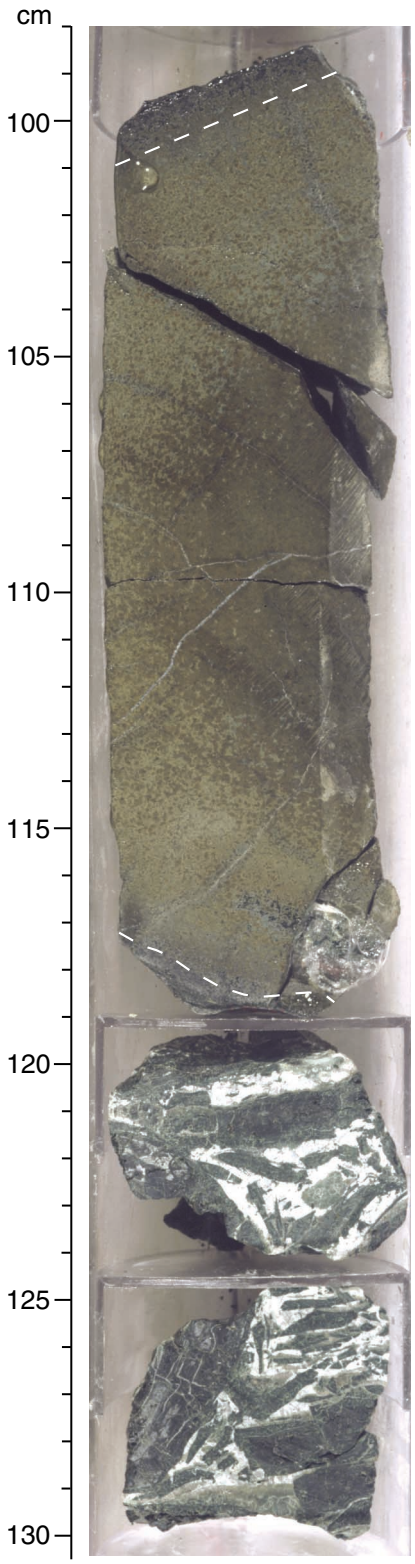

Figure F13. Interval 192-1187A-8R-2, 0–35 cm, showing a complete vertical section through a pillow from Unit 5, including its upper and lower glassy margins (highlighted), and the aphanitic interior containing an Fe oxyhydroxide–stained spherulitic region (parallel to the pillow margin).

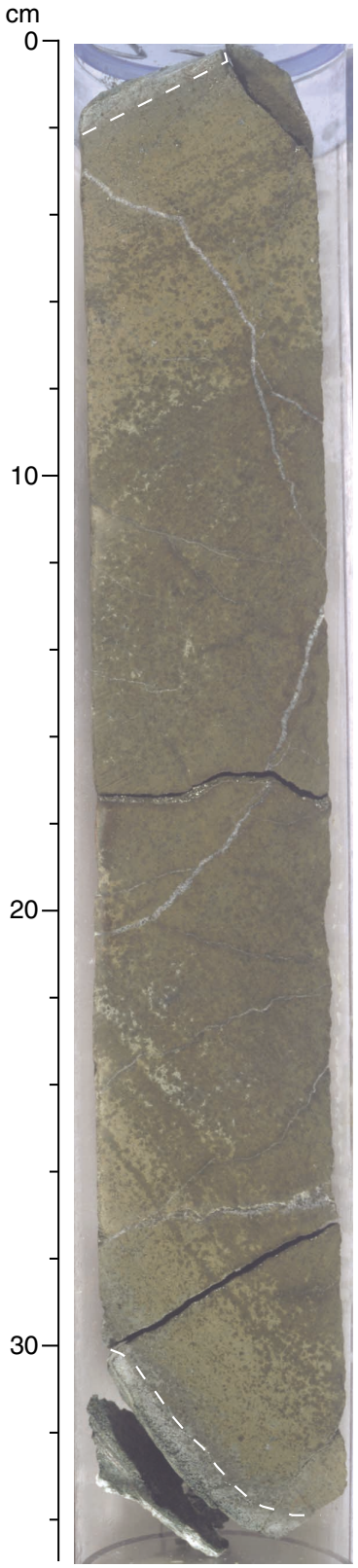

Figure F14. Interval 192-1187A-11R-1, 46–77 cm (Unit 6), showing a breakout pillow (pillow 2) and the Fe oxyhydroxide–stained spherulitic region parallel and adjacent to the glassy margin of pillow 1.

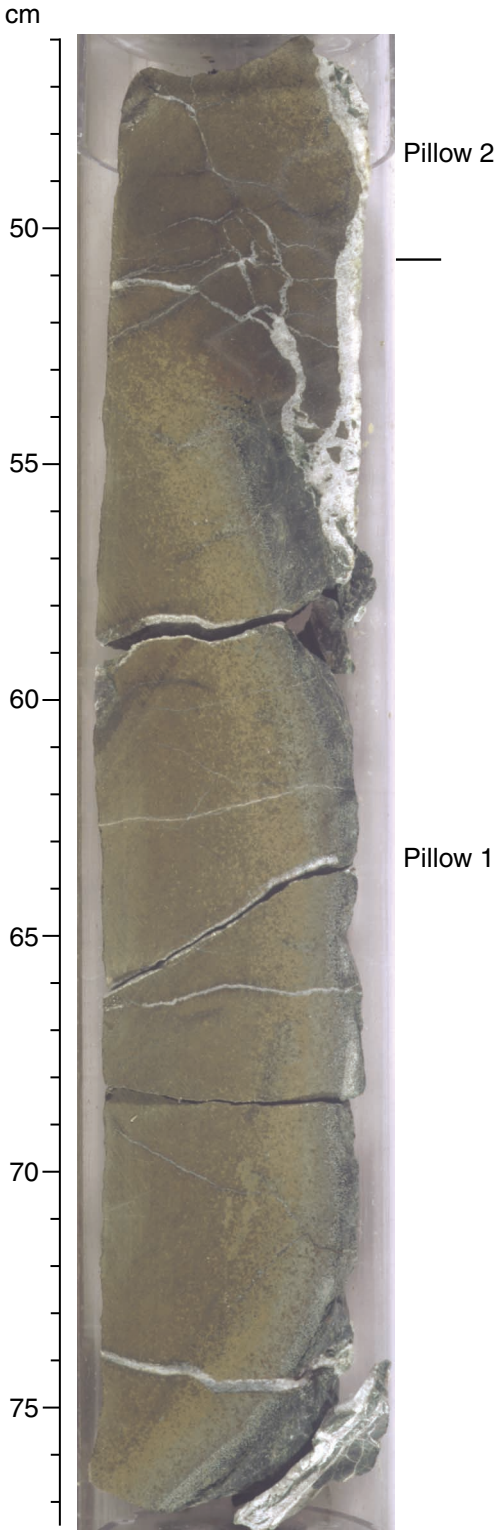

Figure F15. Quenched pillow margin containing spherulites that have been highlighted by alteration in Sample **192-1187A-7R-6 (Piece 2, 66–70 cm).** Elongate groundmass olivine, acicular plagioclase (white, elongate parts of the spherulites), and glomerocrysts of euhedral olivine are present (field of view = 5.5 mm; plane-polarized light; photomicrograph ID# 1187A_244).

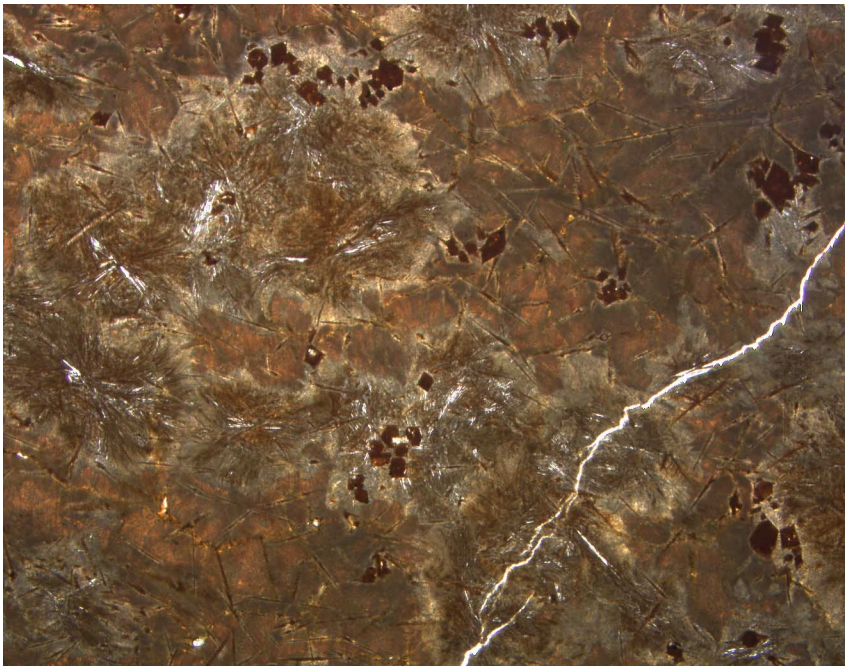

Figure F16. Olivine phenocrysts partially altered to brown smectite but with unaltered interiors in Sample 192-1187A-6R-6 (Piece 2C, 105–107 cm). The groundmass consists of radiating elongate plagioclase laths and small interstitial crystals of clinopyroxene. This thin section was taken from the center of a pillow (field of view = 2.8 mm; crossed polars; photomicrograph ID# 1187A_240).

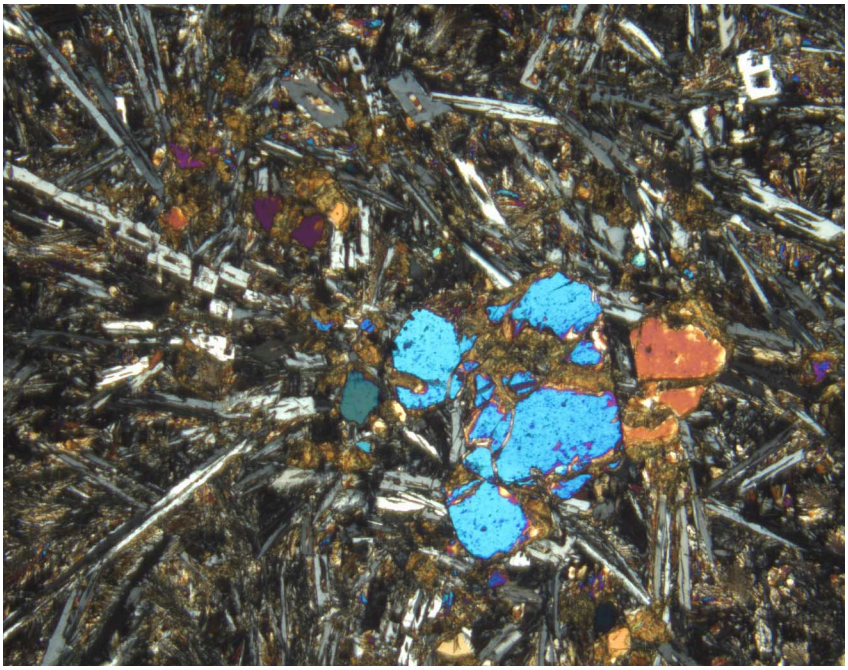

Figure F17. Chrome spinel inclusions in unaltered olivine in Sample **192-1187A-15R-4 (Piece 1B, 42–44 cm)** (field of view = 0.7 mm; plane-polarized light; photomicrograph ID# 1187A_254).

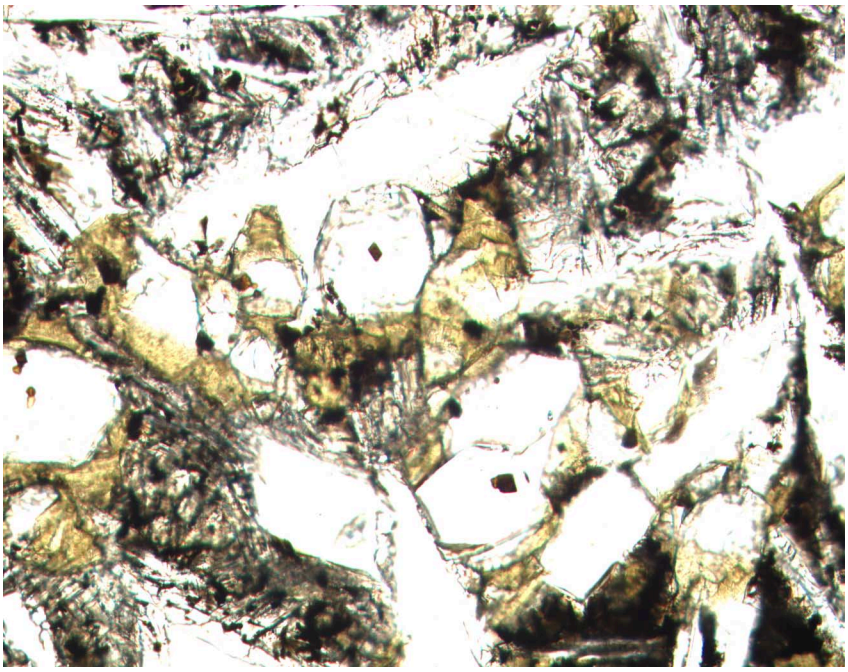

Figure F18. Variolitic to subophitic texture in a pillow interior in Sample **192-1187A-9R-4 (Piece 2C, 56–58 cm).** An intrafasciculate texture, in which hollow plagioclase laths contain elongate crystals of clinopyroxene, is also visible (field of view = 1.4 mm; crossed polars; photomicrograph ID# 1187A_243).

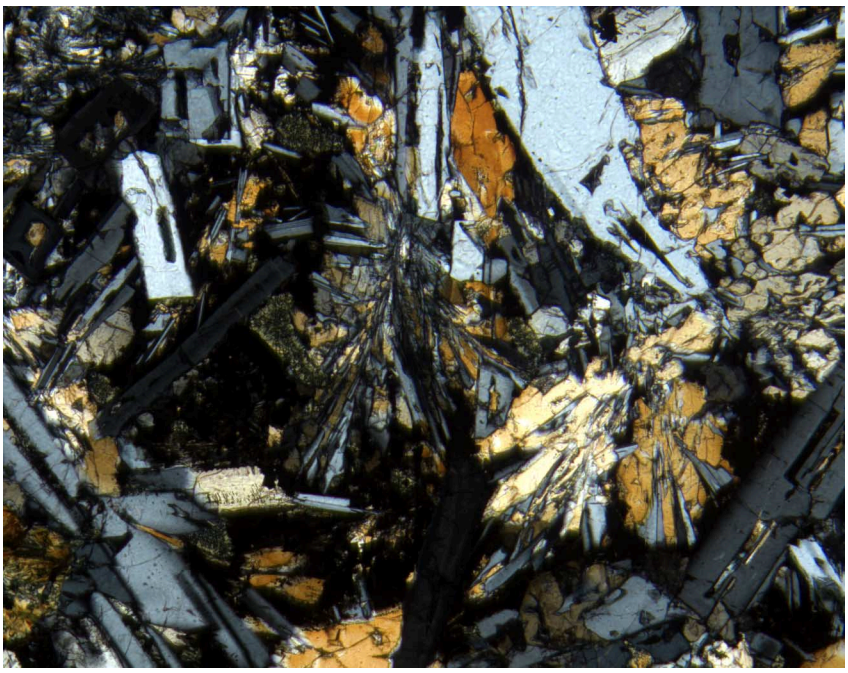

Figure F19. Microcrystalline variolitic and coarser grained patches coexisting in the groundmass of the interior of the massive basal part of Unit 6 in Sample **192-1187A-12R-5 (Piece 2A, 90–93 cm).** In hand specimen, the rock has a mottled appearance (field of view = 2.5 mm; plane-polarized light; photomicrograph ID# 1187A_255).

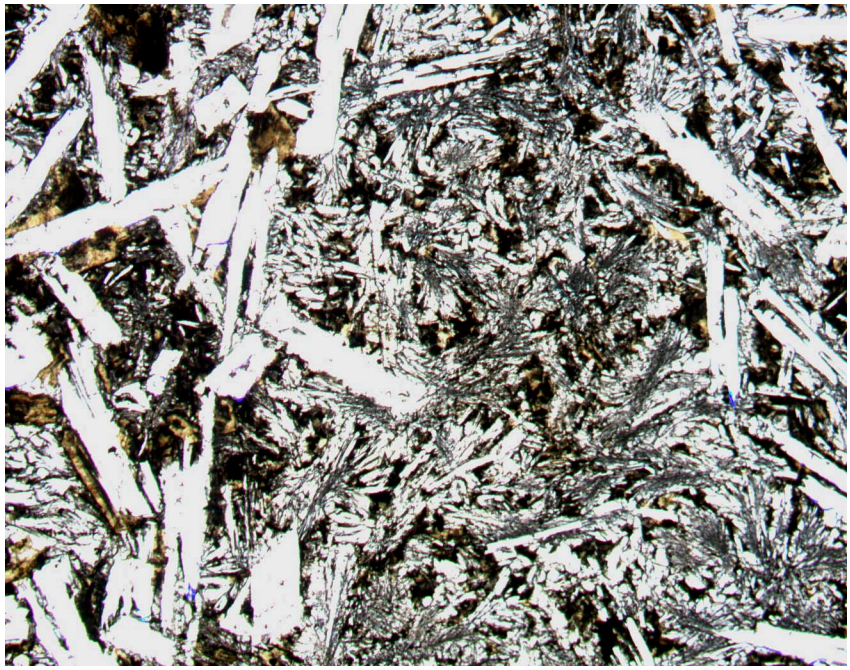

Figure F20. Total alkalies vs. silica diagram (after Le Bas et al., 1986) showing data for Leg 192 basalt and volcaniclastic rocks. Data for the Site 1187 basalt plot in the tholeiitic basalt field. The dashed line separates Hawaiian tholeiitic and alkalic basalts (Macdonald and Katsura, 1964).

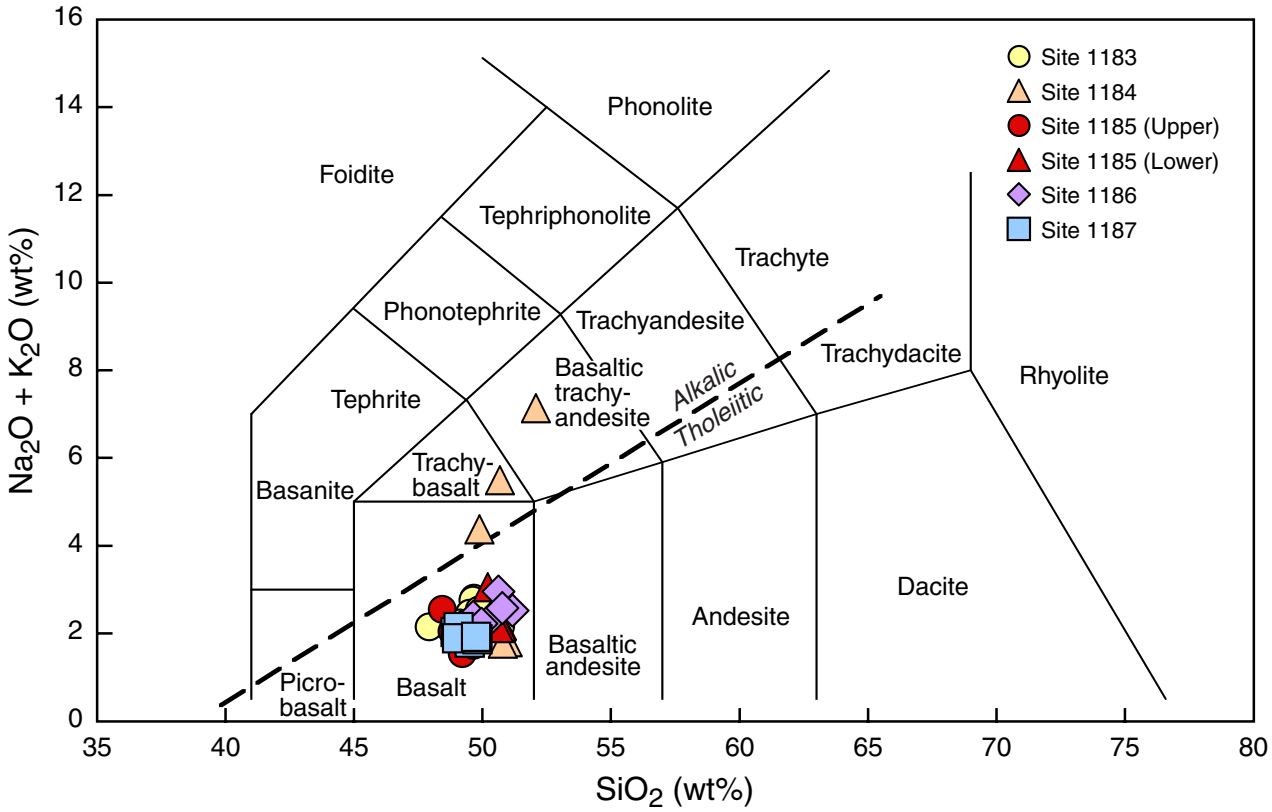

Figure F21. Cr vs. TiO_2 diagram for basalt and volcaniclastic rocks. Basalt from Site 1187 is distinct from that of the Kwaimbaita and Singgalo Formations of Malaita (Tejada et al., in press) and from that recovered during Leg 130 at Sites 803 and 807 (Mahoney et al., 1993). The high Cr contents of the Site 1187 basalt show its relatively primitive nature and demonstrate the compositional similarity to the upper group of basalt at Site 1185.

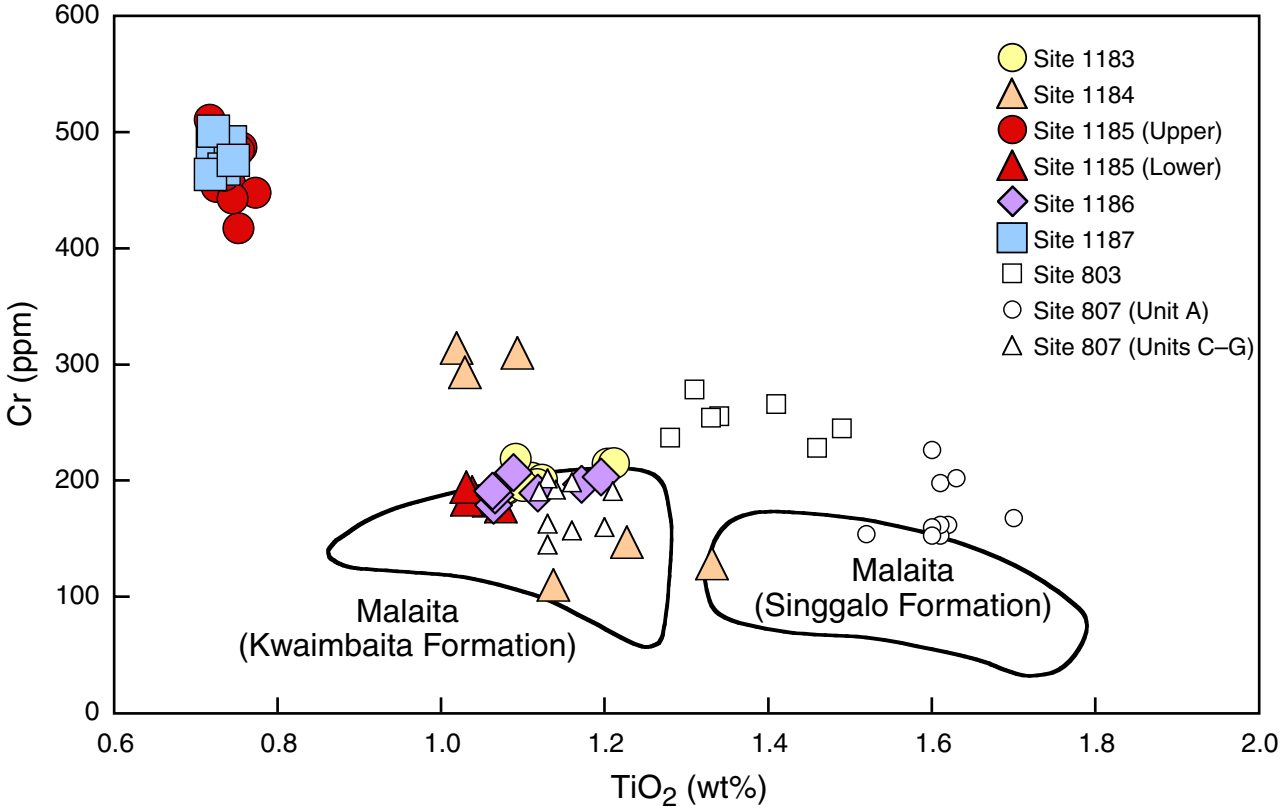

Figure F22. Zr vs. TiO_2 diagram for basalt and volcaniclastic rocks. Basalt from Site 1187 is clearly distinct from that of the Kwaimbaita and Singgalo Formations of Malaita (Tejada et al., in press) and from that recovered during Leg 130 at Sites 803 and 807 (Mahoney et al., 1993). The low Zr and TiO_2 contents of the Site 1187 basalt units illustrate their compositional similarity to the upper group of basalt at Site 1185.

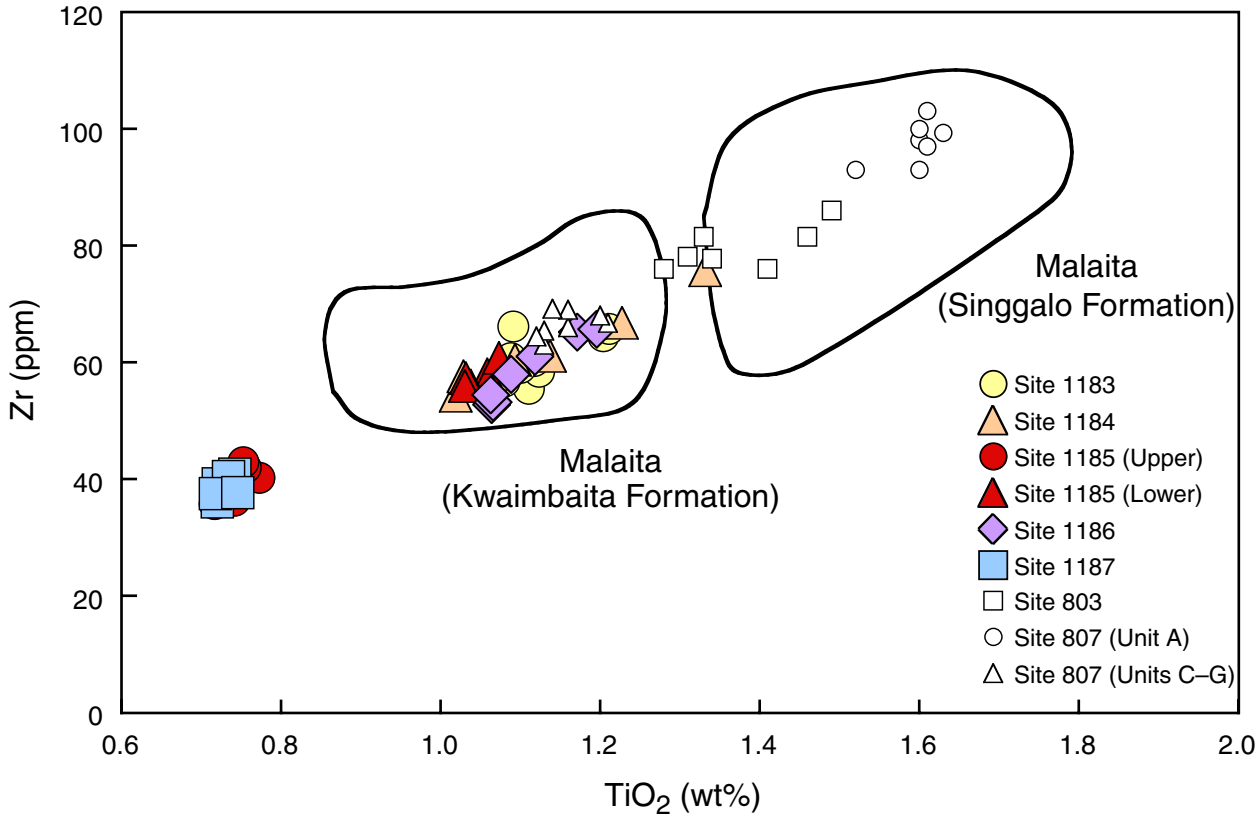

Figure F23. TiO_2 vs. Mg# diagram for basalt and volcaniclastic rocks. Basalt from Site 1187 is distinct from that of the Kwaimbaita and Singgalo Formations of Malaita (Tejada et al., in press) and from that recovered during Leg 130 at Sites 803 and 807 (Mahoney et al., 1993). The high Mg# and low TiO_2 contents of the Site 1187 basalt units show their relatively primitive nature and demonstrate the compositional similarity to the upper group of basaltic units at Site 1185. Mg# is calculated assuming that 12% of the iron is Fe^{3+}, which is equivalent to $Fe_2O_3/(Fe_2O_3+FeO) = 0.13$, or $Fe_2O_3/FeO = 0.15$.

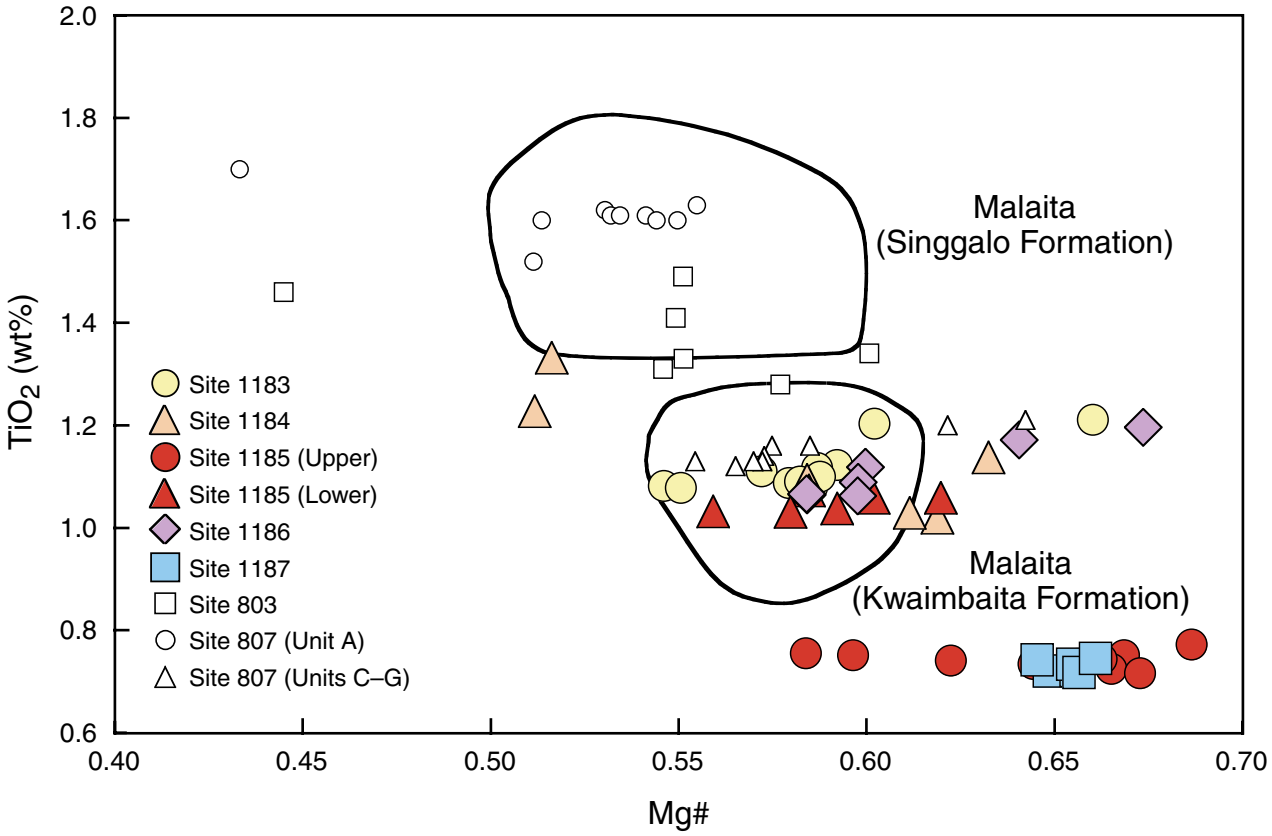

Figure F24. Interval 192-1187A-8R-2, 36–72 cm, showing well-developed light and dark yellow-brown alteration in basalt near a pillow margin. A small amount of dark, partially altered glass is visible (top right and bottom right). Note that the alteration bands follow the curvature of the pillow rim.

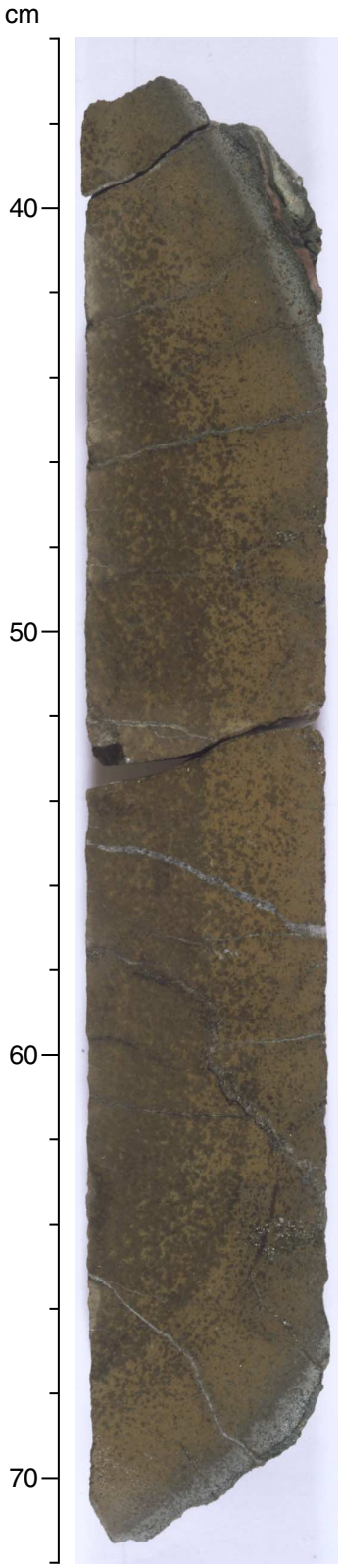

Figure F25. Basalt showing total replacement of olivine phenocrysts by brown to tan smectite in Sample 192-1187A-10R-7 (Piece 1B, 30–32 cm). Plagioclase and clinopyroxene are unaltered (field of view = 2.8 mm; plane-polarized light; photomicrograph ID# 1187A_261).

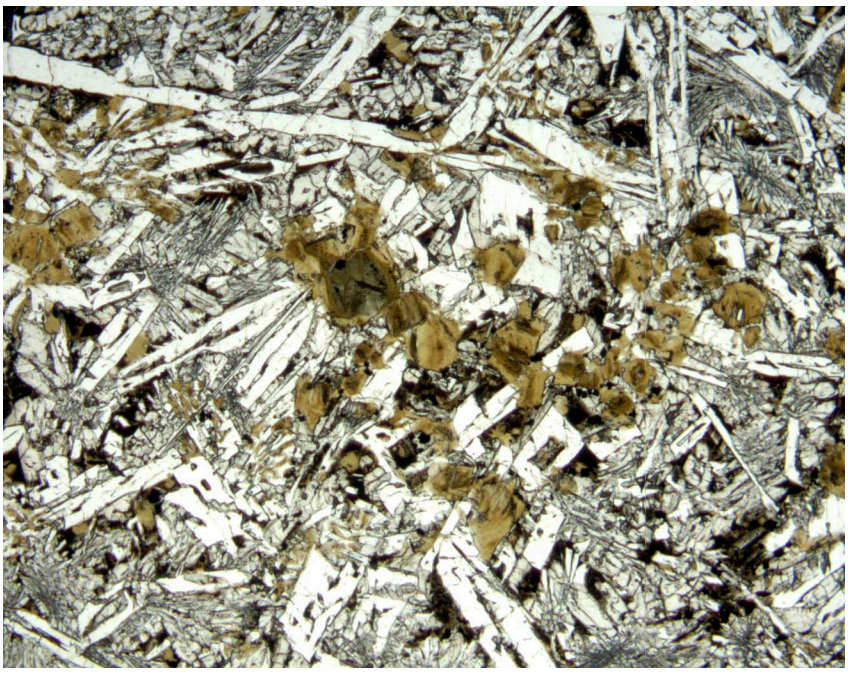

Figure F26. Basalt showing almost complete replacement of the groundmass by brown to tan smectite in Sample **192-1187A-12R-5 (Piece 2A, 90–93 cm).** Plagioclase and clinopyroxene are unaltered (field of view = 2.8 mm; plane-polarized light; photomicrograph ID# 1187A_253).

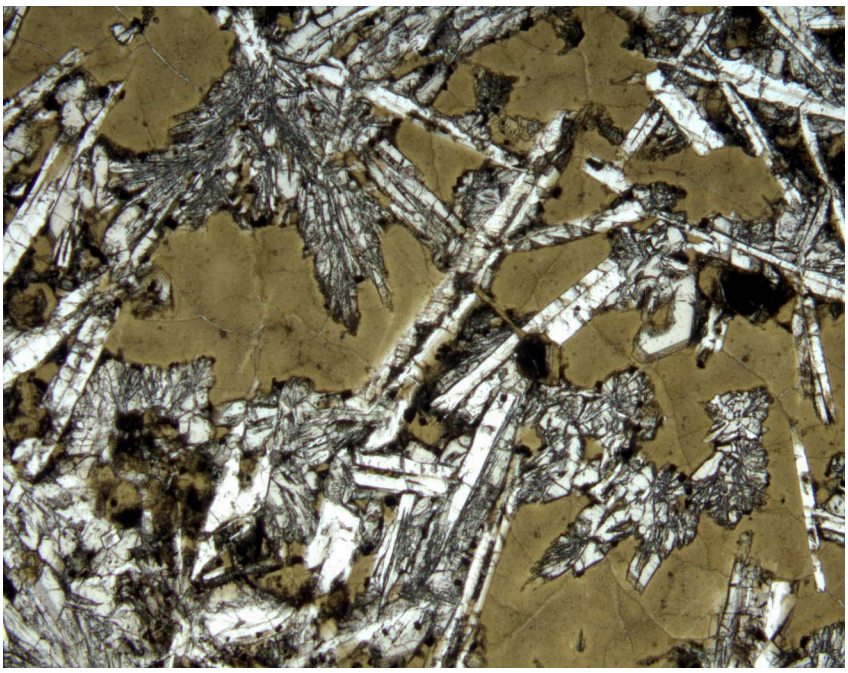

Figure F27. Interval 192-1187A-7R-7, 62–90 cm, showing miarolitic cavities in basalt with brown alteration halos. The cavities are filled with calcite, brown to tan smectite, and minor goethite.

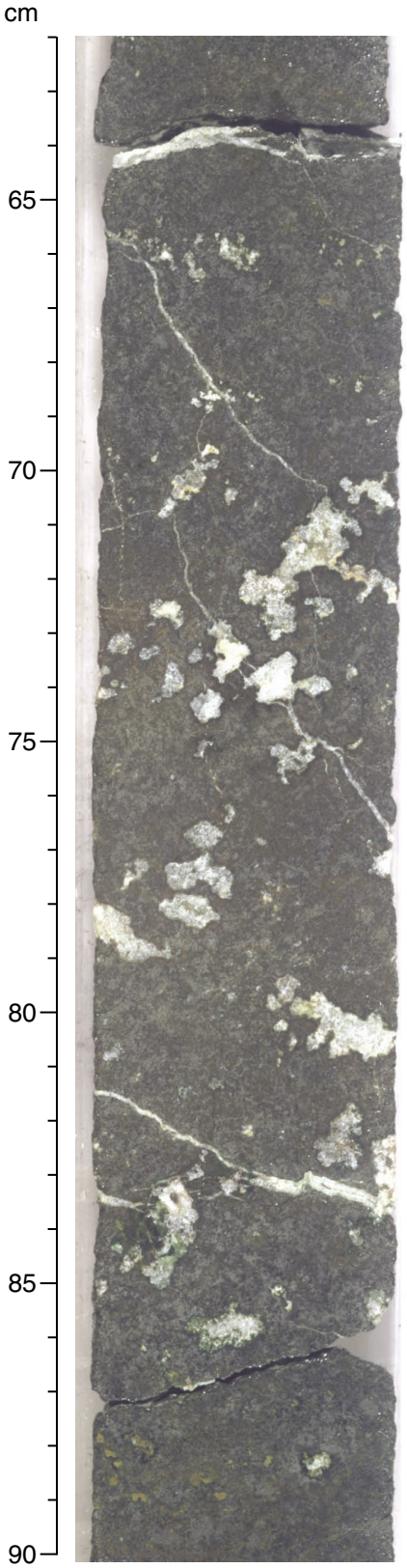

Figure F28. Miarolitic cavity in basalt filled with brown smectite (brown to tan), calcite (white with two cleavages), and minor goethite (dark brown to black) in Sample 192-1187A-5R-4 (Piece 5, 91–94 cm). The wall rock around the miarolitic cavity is pervasively replaced by brown smectite. Plagioclase outside the alteration halo is only partially altered (field of view = 5.5 mm; plane-polarized light; photomicrograph ID# 1187A_259).

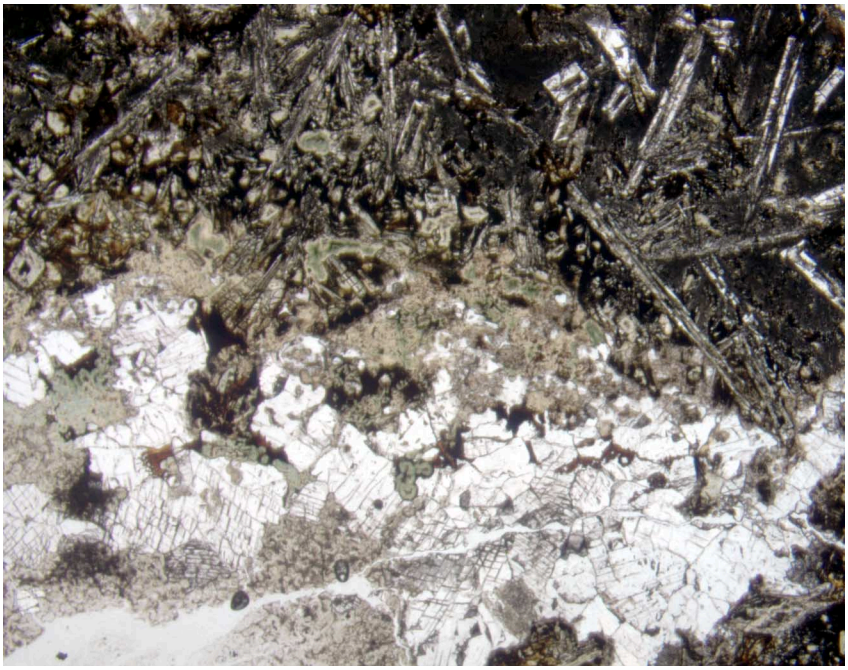

Figure F29. In the brown halos surrounding miarolitic cavities, the wall-rock basalt is completely replaced by smectite (brown to tan), calcite (white), and minor goethite (black) in Sample 192-1187A-5R-4 (Piece 5, 91–94 cm) (field of view = 1.4 mm; plane-polarized light; photomicrograph ID# 1187A_260).

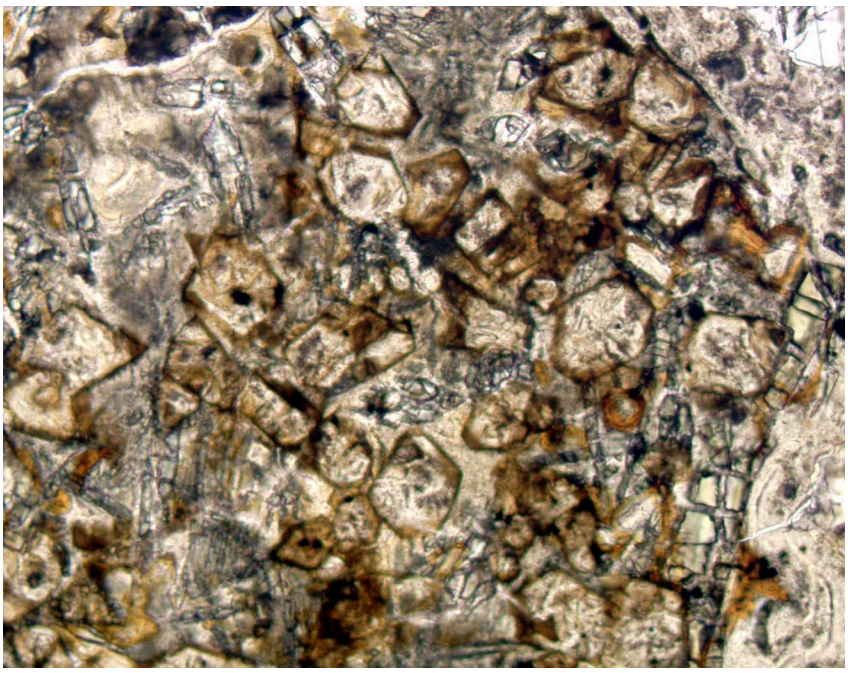

Figure F30. Partially altered olivine phenocrysts preserving incipient alteration to brown smectite in Sample **192-1187A-15R-4 (Piece 1B, 42–44 cm).** Plagioclase is unaltered (field of view = 2.8 mm; plane-polarized light; photomicrograph ID# 1187A_252).

Figure F31. Interval 192-1187A-5R-6 (Piece 4, 102–128 cm) showing pervasively altered basalt grading from light and dark yellow-brown (right) to dark brown toward a pillow interior (left). The sample contains several thin horizontal calcite veins connected by a thin, nearly vertical calcite vein.

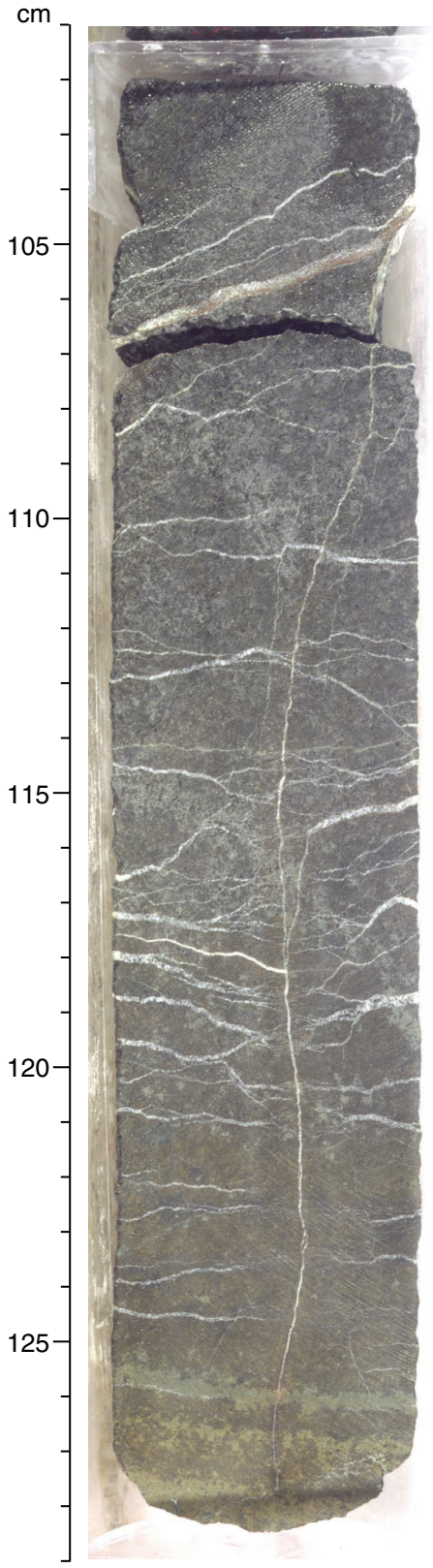

Figure F32. Examples of good-quality Zijderveld diagrams for archive-half core measurements of (**A**) a sediment sample from Section 192-1187A-2R-1, 90 cm, and (**B**) basalt Piece 4 from Section 192-1187A-10R-4, 107 cm.

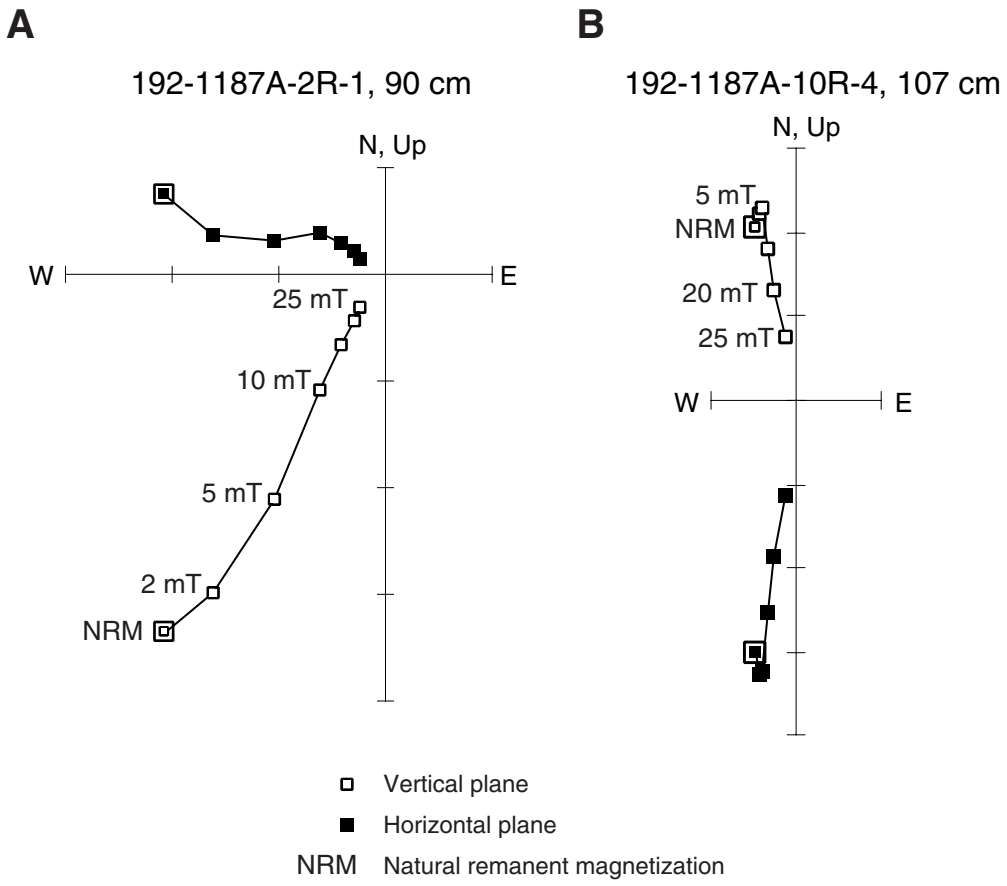

Figure F33. Variation in magnetic inclination with depth for the brown claystone in Core 192-1187A-2R and suggested correlation of the interpreted magnetic polarities with the geomagnetic polarity timescale (GPTS). ISEA is alternative name of reversed interval M″-1r″ (e.g., Tarduno et al., 1989) from the site code (Italy, *Sentino stream,* Site A) used by VandenBerg et al. (1978) in the initial recognition of this subchron.

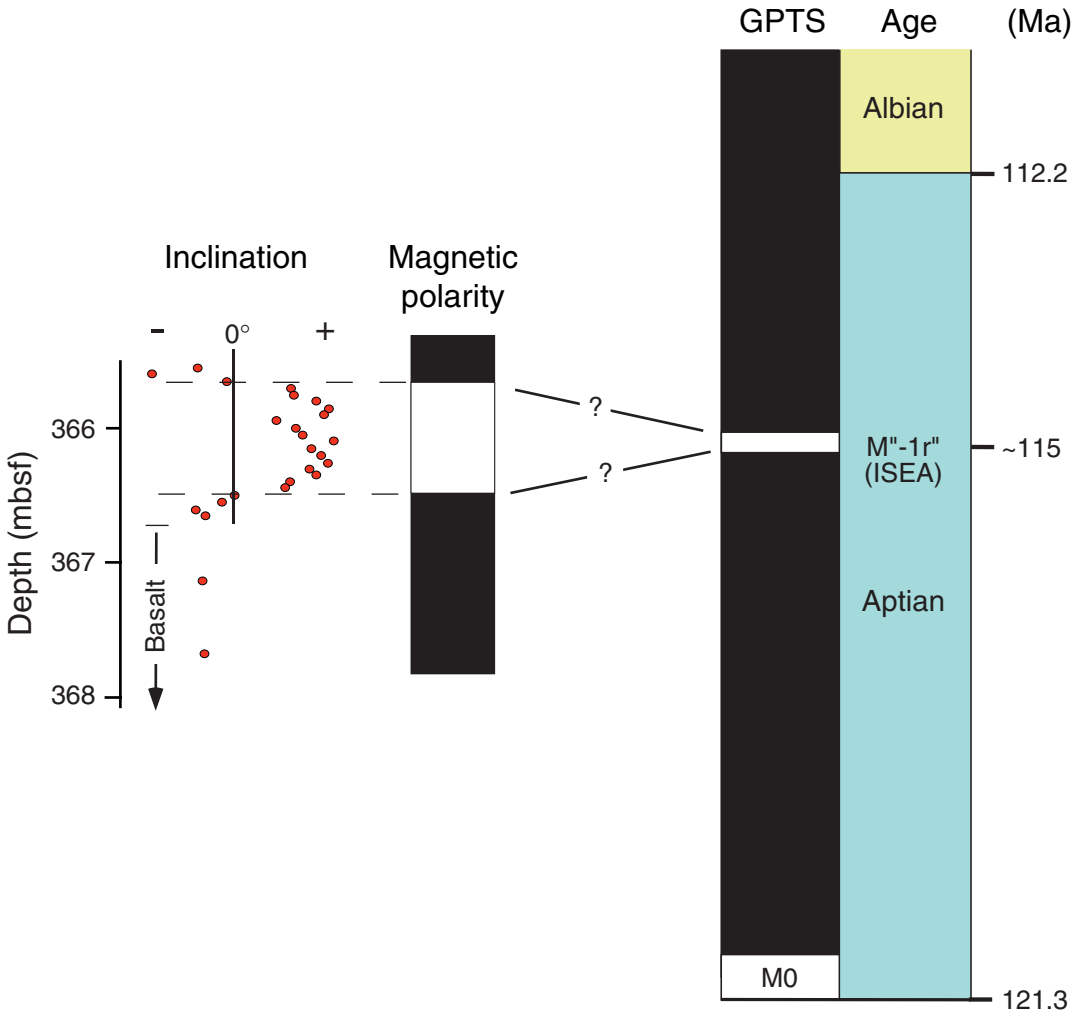

Figure F34. Downhole variation in characteristic remanent magnetization inclination, natural remanent magnetization (NRM) intensity, and median destructive field (MDF).

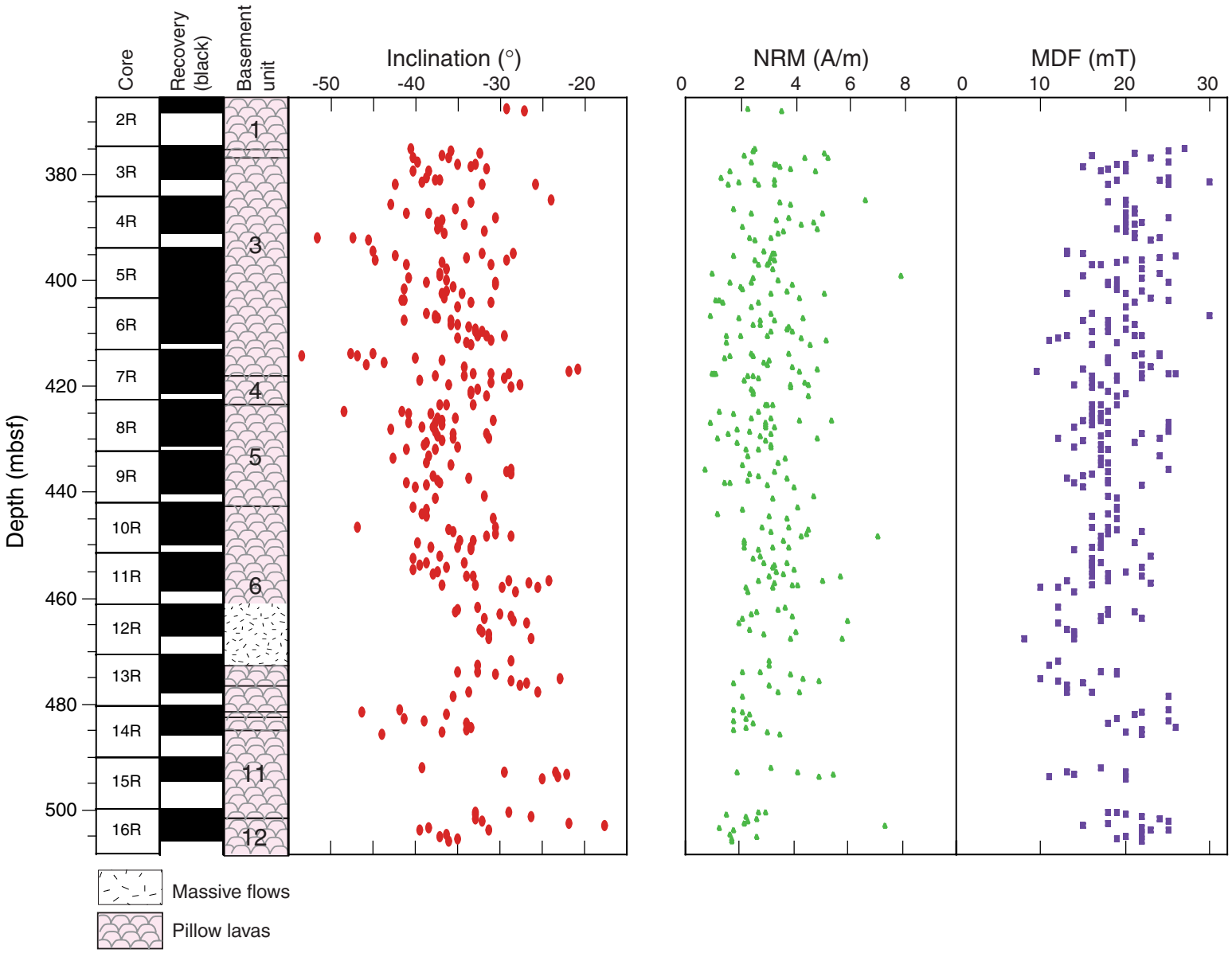

Figure F35. Index properties and thermal conductivity vs. depth for Hole 1187A. Sedimentary Unit III is shaded in the "Lithologic units" column; basement units are unshaded. No discrete samples were taken for index properties measurements from the lower part of Unit 11 or from Unit 12.

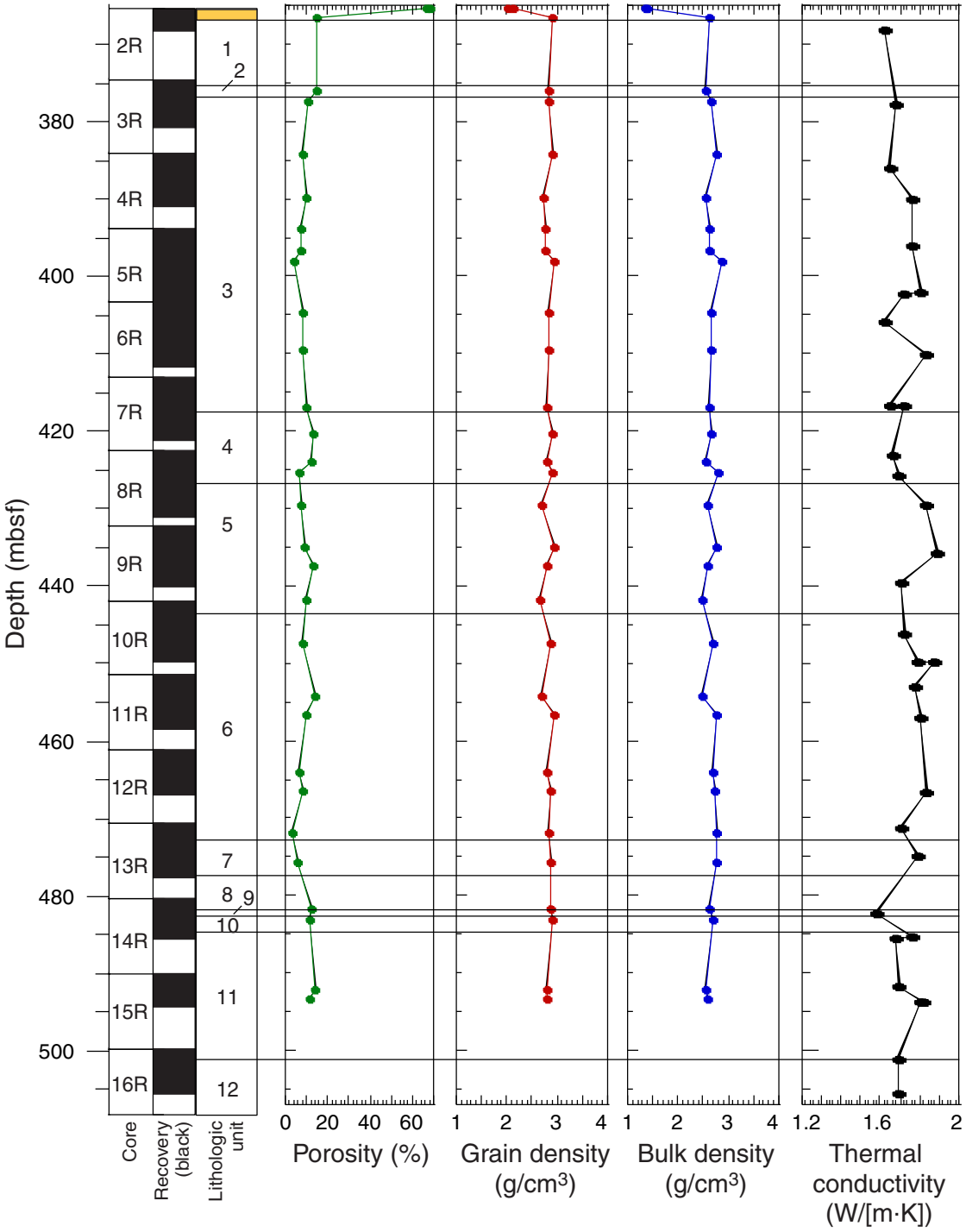

Figure F36. Velocity data and whole-core measurements of magnetic susceptibility, natural gamma radiation, and GRA bulk density vs. depth for Hole 1187A. Sedimentary Unit III is shaded in the "Lithologic units" column; basement units are unshaded.

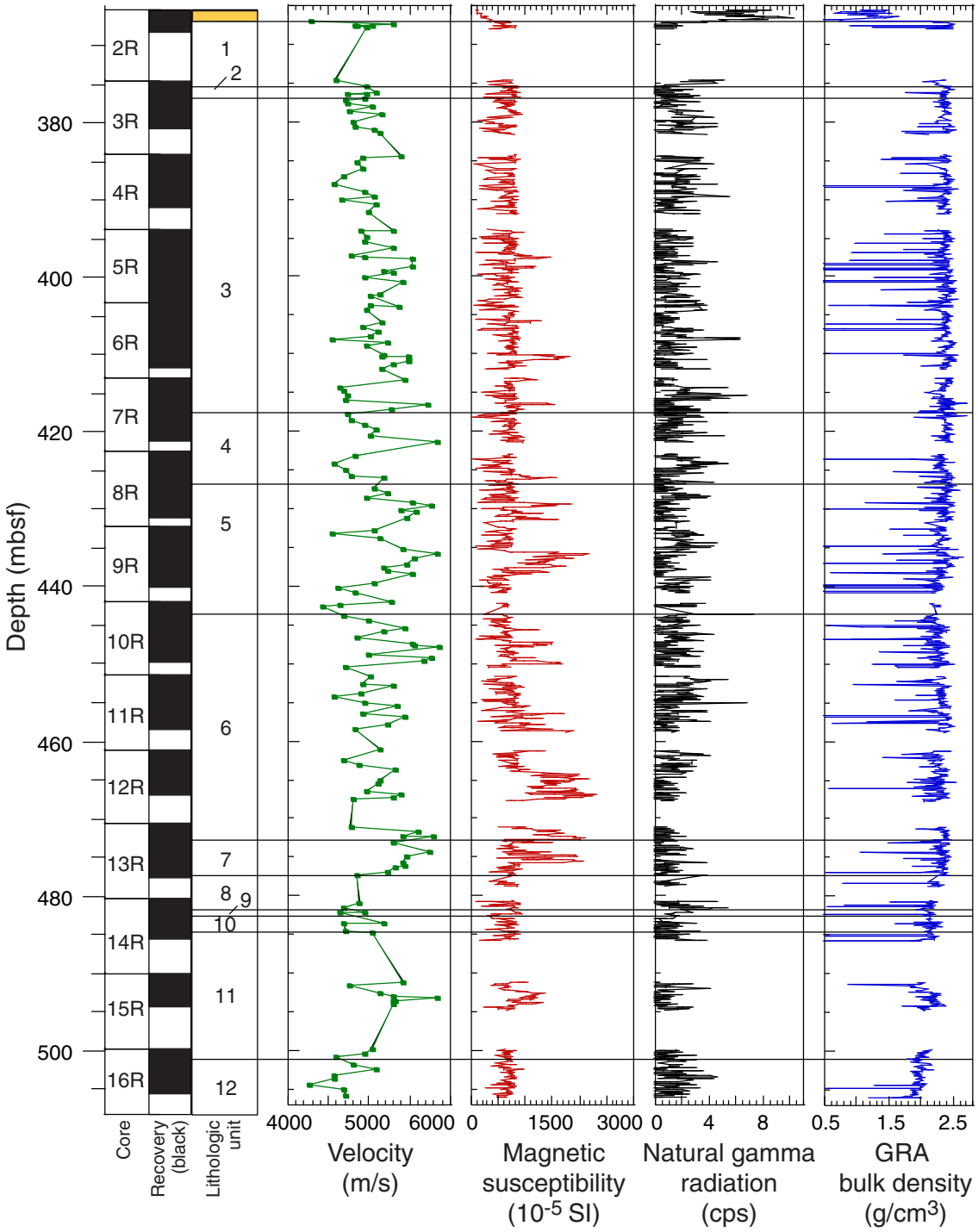

Figure F37. Comparison of the bulk density profiles for Hole 1187A obtained from whole-core sections using the multisensor track (MST) and from measurements of discrete samples using a pycnometer. In general, the two sets of data show the same trends, despite the consistently lower values of the gamma ray attenuation (GRA) density data. Sedimentary Unit III is shaded in the "Lithologic units" column; basement units are unshaded.

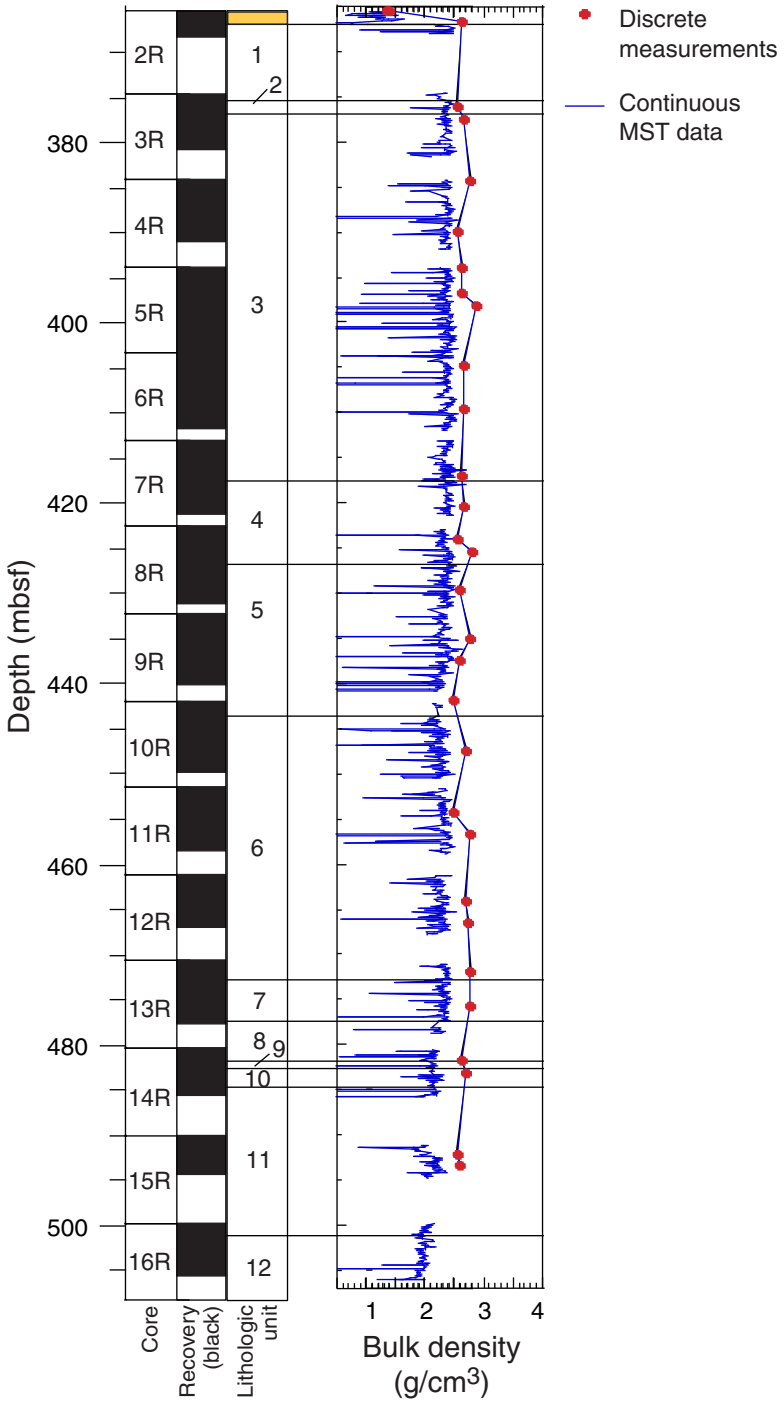

Table T1. Coring summary, Hole 1187A.

Core	Date (2000)	Time (local)	Depth (mbsf) Top	Depth (mbsf) Bottom	Length (m) Cored	Length (m) Recovered	Recovery (%)
192-1187A-							
1W	30 Oct	0540	0.0	365.5	0.0	1.28*	NA
2R	30 Oct	0935	365.5	374.5	9.0	2.67	29.7
3R	30 Oct	1410	374.5	384.2	9.7	6.19	63.8
4R	30 Oct	1910	384.2	393.8	9.6	6.86	71.5
5R	31 Oct	0140	393.8	403.4	9.6	9.76	101.7
6R	31 Oct	0830	403.4	413.0	9.6	8.30	86.5
7R	31 Oct	1340	413.0	422.6	9.6	8.12	84.6
8R	31 Oct	1930	422.6	432.3	9.7	8.63	89.0
9R	1 Nov	0050	432.3	441.9	9.6	7.94	82.7
10R	1 Nov	0645	441.9	451.5	9.6	7.88	82.1
11R	1 Nov	1220	451.5	461.1	9.6	7.00	72.9
12R	1 Nov	1625	461.1	470.7	9.6	5.88	61.3
13R	1 Nov	2115	470.7	480.3	9.6	7.22	75.2
14R	2 Nov	0340	480.3	490.0	9.7	5.43	56.0
15R	2 Nov	1020	490.0	499.7	9.7	4.47	46.1
16R	2 Nov	1500	499.7	508.3	8.6	5.99	69.7
				Cored:	142.8	102.34	71.7
				Drilled:	365.5		
				Total:	508.3		

Notes: * = not included in recovered core and recovery percent columns. NA = not applicable. This table is also available in **ASCII format.**

Table T2. Expanded coring summary, Hole 1187A. (See table notes. Continued on next two pages.)

Core	Date (2000)	Time (local)	Core depth (mbsf) Top	Core depth (mbsf) Bottom	Length (m) Cored	Length (m) Recovered	Recovery (%)	Section	Length (m) Liner	Length (m) Curated	Section depth (mbsf) Top	Section depth (mbsf) Bottom	Catwalk samples
192-1187A-													
1W	30 Oct	540	0.0	365.5	0.0	1.28	NA						
								1	1.28	1.28	0.00	1.28	PAL, PAL, PAL, PAL
									1.28	1.28			
2R	30 Oct	935	365.5	374.5	9	2.67	29.7						
								1	1.18	1.18	365.50	366.68	PAL, PAL, PAL
								2	0.94	1.46	366.68	368.14	PAL, PAL, PAL
								3	0.55	0.10	368.14	368.24	
								Totals:	2.67	2.74			
3R	30 Oct	1410	374.5	384.2	9.7	6.19	63.8						
								1	0.20	1.46	374.5	375.96	
								2	1.45	1.48	375.96	377.44	
								3	1.39	1.45	377.44	378.89	
								4	1.42	1.49	378.89	380.38	BANC
								5	1.48	1.25	380.38	381.63	
								6	0.25	0.00			
								Totals:	6.19	7.13			
4R	30 Oct	1910	384.2	393.8	9.6	6.86	71.5						
								1	0.67	1.49	384.20	385.69	
								2	1.50	1.50	385.69	387.19	BANC
								3	1.50	1.50	387.19	388.69	
								4	1.43	1.17	388.69	389.86	
								5	1.46	1.50	389.86	391.36	
								6	0.30	0.63	391.36	391.99	
								CC(w/CC)	0.00	0.00			
								Totals:	6.86	7.79			
5R	31 Oct	140	393.8	403.4	9.6	9.76	101.7						
								1	1.30	1.38	393.80	395.18	
								2	1.47	1.50	395.18	396.68	
								3	1.50	1.43	396.68	398.11	
								4	1.50	1.50	398.11	399.61	
								5	1.07	1.50	399.61	401.11	
								6	1.42	1.29	401.11	402.40	
								7	1.50	1.19	402.40	403.59	BANC
								8	0.00	0.41	403.59	404.00	
								Totals:	9.76	10.20			
6R	31 Oct	830	403.4	413.0	9.6	8.30	86.5						
								1	0.74	1.23	403.40	404.63	BANC
								2	1.34	1.50	404.63	406.13	
								3	1.50	1.45	406.13	407.58	
								4	1.21	0.59	407.58	408.17	
								5	1.47	1.36	408.17	409.53	
								6	1.50	1.31	409.53	410.84	
								7	0.54	1.15	410.84	411.99	
								Totals:	8.30	8.59			
7R	31 Oct	1340	413.0	422.6	9.6	8.12	84.6						
								1	0.92	1.47	413.00	414.47	
								2	1.34	1.26	414.47	415.73	
								3	1.50	1.19	415.73	416.92	

Table T2 (continued).

Core	Date (2000)	Time (local)	Core depth (mbsf) Top	Core depth (mbsf) Bottom	Length (m) Cored	Length (m) Recovered	Recovery (%)	Section	Length (m) Liner	Length (m) Curated	Section depth (mbsf) Top	Section depth (mbsf) Bottom	Catwalk samples
								4	1.50	1.30	416.92	418.22	BANC
								5	1.50	1.08	418.22	419.30	
								6	1.36	1.03	419.30	420.33	
								7	0.00	1.02	420.33	421.35	
								Totals:	8.12	8.35			
8R	31 Oct	1930	422.6	432.3	9.7	8.63	89.0						
								1	0.95	1.39	422.60	423.99	
								2	1.47	1.35	423.99	425.34	BANC
								3	1.50	1.49	425.34	426.83	
								4	1.50	1.31	426.83	428.14	
								5	1.50	1.36	428.14	429.50	
								6	1.42	1.37	429.50	430.87	
								7	0.29	0.86	430.87	431.73	
								Totals:	8.63	9.13			
9R	1 Nov	0050	432.3	441.9	9.6	7.94	82.7						
								1	0.22	1.38	432.30	433.68	
								2	1.50	1.41	433.68	435.09	
								3	1.44	1.01	435.09	436.10	BANC
								4	0.36	1.41	436.10	437.51	
								5	1.29	1.46	437.51	438.97	
								6	1.28	1.46	438.97	440.43	
								7	1.46	0.54	440.43	440.97	
								8	0.39	0.00			
								Totals:	7.94	8.67			
10R	1 Nov	645	441.9	451.5	9.6	7.88	82.1						
								1	0.00	1.50	441.90	443.40	BANC
								2	1.48	1.50	443.40	444.90	
								3	1.51	1.22	444.90	446.12	
								4	1.39	1.29	446.12	447.41	
								5	1.38	0.91	447.41	448.32	
								6	1.51	1.27	448.32	449.59	
								7	0.61	0.94	449.59	450.53	
								Totals:	7.88	8.63			
11R	1 Nov	1220	451.5	461.1	9.6	7.00	72.9						
								1	1.08	1.20	451.50	452.70	
								2	1.48	1.50	452.70	454.20	
								3	1.50	1.00	454.20	455.20	
								4	1.30	1.40	455.20	456.60	BANC
								5	1.42	1.44	456.60	458.04	
								6	0.22	0.80	458.04	458.84	
								Totals:	7.00	7.34			
12R	1 Nov	1625	461.1	470.7	9.6	5.88	61.3						
								1	1.26	1.48	461.10	462.58	
								2	1.48	1.46	462.58	464.04	
								3	1.47	1.35	464.04	465.39	
								4	1.50	1.16	465.39	466.55	
								5	0.17	1.25	466.55	467.80	
								Totals:	5.88	6.70			

Table T2 (continued).

Core	Date (2000)	Time (local)	Core depth (mbsf) Top	Core depth (mbsf) Bottom	Length (m) Cored	Length (m) Recovered	Recovery (%)	Section	Length (m) Liner	Length (m) Curated	Section depth (mbsf) Top	Section depth (mbsf) Bottom	Catwalk samples
13R	1 Nov	2115	470.7	480.3	9.6	7.22	75.2						
								1	1.13	1.29	470.70	471.99	
								2	1.46	1.39	471.99	473.38	
								3	1.48	1.29	473.38	474.67	
								4	1.47	1.00	474.67	475.67	
								5	1.50	1.50	475.67	477.17	
								6	0.18	1.37	477.17	478.54	BANC
								7	0.00	0.17	478.54	478.71	
								Totals:	7.22	8.01			
14R	2 Nov	0340	480.3	490.0	9.7	5.43	56.0						
								1	0.94	1.50	480.30	481.80	
								2	1.41	1.38	481.80	483.18	BANC
								3	1.48	1.50	483.18	484.68	
								4	1.46	1.50	484.68	486.18	
								5	0.14	0.34	486.18	486.52	
								Totals:	5.43	6.22			
15R	2 Nov	1020	490.0	499.7	9.7	4.47	46.1						
								1	1.14	0.85	490.00	490.85	
								2	1.33	1.27	490.85	492.12	
								3	1.46	1.35	492.12	493.47	
								4	0.54	1.5	493.47	494.97	
								Totals:	4.47	4.97			
16R	2 Nov	1500	499.7	508.3	8.6	5.99	69.7						
								1	1.49	0.94	499.70	500.64	
								2	1.40	1.39	500.64	502.03	BANC
								3	1.45	1.33	502.03	503.36	
								4	1.44	1.46	503.36	504.82	
								5	0.21	1.30	504.82	506.12	
								Totals:	5.99	6.42			
			Coring totals:		142.8	102.34	71.7						

Notes: NA = not applicable. CC = core catcher, PAL = paleontology, BANC = microbiological study. This table is also available in **ASCII format.**

Table T3. List of planktonic foraminifer and calcareous nannofossil occurrences and age assignments in sediments, Site 1187.

Core, section, interval (cm)	Event	Species	Zone/Subzone	Depth (mbsf)	Stage
192-1187A-					
2R-1, 1		Highest sample		365.53	late Aptian-Albian
2R-1, 90-92	LO	*B. albianus*?		366.40	
2R-1, 90-92	LO	*G. aptiensis*		366.40	
2R-2, 28-30	HO	*G. ferreolensis*	Cheniourensis-bejaouensis	366.96	late Aptian
2R-2, 28-30	HO	*G. barri*	Cheniourensis-bejaouensis	366.96	
2R-2, 28-30	HO	*B. praetrochoidea*	Cheniourensis-bejaouensis	366.96	
2R-2, 28-30	HO	*H. irregularis*	NC9B	366.96	
2R-2, 28-30	LO	*E. floralis*	NC7A	366.96	

Notes: HO = highest occurrence, LO = lowest occurrence. Shaded = planktonic foraminifers, unshaded = calcareous nannofossils. This table is also available in **ASCII format.**

Table T4. Basement unit thicknesses and general characteristics and criteria used for defining unit boundaries, Hole 1187A.

Unit/ Subunit	Thickness (m)	Characteristics	Unit top defined by
192-1187A:			
1	8.22	Pillowed	First appearance of basalt (below white chalk and brown claystone)
2A, 2B	0.05 + 1.61	Pillowed	Recrystallized limestone containing altered glass clasts (5-cm piece: Subunit 2A)
3A, 3B	0.04 + 41.23	Pillowed	Recrystallized limestone with minor hyaloclastite (3-cm piece: Subunit 3A)
4	5.41	Pillowed	Hyaloclastite (11-cm interval)
5	19.4	Pillowed; contains one cooling unit that is 2.43 m thick	Hyaloclastite (13-cm interval)
6	29.99	Pillowed (upper ~19.5 m) and massive (lower ~9 m)	Interval dominated by hyaloclastite (57 cm) with minor aphanitic basalt pieces
7	3.86	Small-scale pillowed cooling units (upper 0.9 m) overlying a 3-m-thick cooling unit	Downward change from massive cooling unit to pillowed cooling units
8	5.02	Pillowed	Downward change from large-scale (massive?) cooling unit to small-scale pillowed cooling units
9	0.7	Pillowed; only one pillow present	Hyaloclastite (22-cm interval)
10	2.48	Pillowed	Hyaloclastite (15-cm interval)
11	16.46	Pillowed; contains one cooling unit that is 2.23 m thick	Hyaloclastite (11-cm interval)
12	>6.86	Pillowed	Hyaloclastite (17-cm interval)

Table T5. Whole-rock compositions of basalt samples, Hole 1187A.

	192-1187A-						
Core, section:	3R-3	4R-2	6R-6	7R-6	9R-4	10R-7	12R-5
Piece:	3B	13B	2C	2	2C	1B	2A
Interval (cm):	68-70	122-124	105-107	66-70*	56-58	30-32	90-93
Unit/Subunit:	3B	3B	3B	4	5	6	6
Depth (mbsf):	378.12	386.91	410.58	419.96	436.66	449.89	467.45
Major element (wt%):							
SiO_2	49.00	49.00	49.50	48.10	49.00	49.80	49.80
TiO_2	0.72	0.74	0.72	0.78	0.73	0.72	0.75
Al_2O_3	15.30	15.30	14.90	16.50	15.20	15.30	15.80
Fe_2O_3T	10.70	10.80	10.80	11.90	11.10	10.40	10.10
MnO	0.20	0.19	0.18	0.19	0.19	0.17	0.17
MgO	8.79	8.70	9.15	6.87	9.39	8.85	8.78
CaO	12.40	12.60	12.30	13.20	12.50	12.20	12.70
Na_2O	1.82	1.83	1.74	2.05	1.78	1.83	1.85
K_2O	0.22	0.32	0.04	0.97	0.11	0.03	0.07
P_2O_5	0.04	0.03	0.04	0.06	0.04	0.04	0.04
Total	99.19	99.51	99.37	100.62	100.04	99.34	100.06
Mg#	0.65	0.65	0.66	0.57	0.66	0.66	0.66
LOI	1.79	2.46	0.86	3.48	1.03	1.20	0.98
CIPW norms:							
Q	0.0	0.0	0.0	0.0	0.0	0.0	0.0
Or	1.3	1.9	0.3	5.8	0.6	0.2	0.4
Ab	15.6	15.7	15.0	16.0	15.1	15.7	15.8
An	33.5	33.0	33.3	33.1	33.4	34.1	34.8
Ne	0.0	0.0	0.0	0.8	0.0	0.0	0.0
Di	23.4	24.5	22.9	26.4	23.5	22.0	23.1
Hy	17.0	14.9	22.6	0.0	16.2	23.4	19.3
Ol	5.7	6.6	2.5	14.2	7.4	1.2	3.2
Il	1.4	1.4	1.4	1.5	1.4	1.4	1.4
Mt	1.9	1.9	1.9	2.1	2.0	1.8	1.8
Ap	0.1	0.1	0.1	0.1	0.1	0.1	0.1
Trace element (ppm):							
Ni	176	185	196	157	171	195	184
Cr	490	492	501	506	467	464	476
V	243	244	242	289	246	235	245
Zr	36	41	39	41	40	38	38
Sc	44	43	43	46	43	43	43
Y	17	19	17	19	18	18	19
Sr	91	89	84	121	89	85	95
Ba	6	5	7	18	6	5	6

Notes: * = highly altered basalt, excluded from Figures **F20,** p. 34, **F21,** p. 35, **F22,** p. 36, and **F23,** p. 37. Fe_2O_3T = total Fe expressed as Fe_2O_3. For Mg# (= atomic $Mg/[Mg + Fe^{2+}]$) and CIPW norms, 12% of total iron is assumed to be Fe^{3+}, which is equivalent to $Fe_2O_3/(Fe_2O_3 + FeO) = 0.13$, or $Fe_2O_3/FeO = 0.15$. LOI = percent weight loss on ignition at 1100°C. All analyses were conducted on ignited samples. This table is also available in **ASCII format.**

Table T6. Characteristic remanent magnetization direction, natural remanent magnetization intensity, median destructive field, magnetic susceptibility, and Koenigsberger ratio for selected basalt pieces. (See table notes. Continued on next three pages.)

Core, section, piece	Depth (mbsf)	Basement unit	Dec (°)	Inc (°)	NRM (A/m)	MDF (mT)	κ (10^{-3} SI)	Q-ratio
192-1187A-								
2R-2 (Piece 2)	367.14	1	153.1	–29.1	2.30		6.84	11.2
2R-2 (Piece 9)	367.68	1	239.3	–27.1	3.53		8.18	14.4
3R-1 (Piece 1)	374.58	1	241.4	–40.4	2.59	27	7.82	11.0
3R-1 (Piece 5)	374.91	1	168.5	–35.8	2.50	25	7.17	11.6
3R-1 (Piece 13)	375.50	2	313.0	–32.4	5.13	21	7.56	22.6
3R-1 (Piece 14)	375.89	2	149.6	–36.9	2.20	16	7.23	10.1
3R-2 (Piece 2)	376.20	2	29.7	–36.0	4.40	23	8.12	18.1
3R-2 (Piece 3)	376.55	2	324.2	–40.3	5.29	23	7.87	22.4
3R-2 (Piece 11)	377.37	3	77.9	–39.8	2.47	25	7.95	10.4
3R-3 (Piece 2)	377.59	3	94.5	–35.1	3.36	20	7.64	14.7
3R-3 (Piece 3)	377.81	3	55.3	–33.0	3.26	19	7.87	13.8
3R-3 (Piece 3)	378.01	3	57.0	–33.4	3.52	15	6.96	16.9
3R-3 (Piece 4)	378.31	3	274.6	–31.5	3.87	18	5.79	22.3
3R-3 (Piece 8)	378.77	3	334.5	–40.3	4.82	17	8.27	19.4
3R-4 (Piece 1)	378.98	3	211.7	–38.4	1.65	20	8.48	6.5
3R-4 (Piece 22)	380.31	3	130.9	–38.7	1.35	25	5.44	8.3
3R-5 (Piece 1)	380.55	3	325.7	–37.2	3.30	19	7.97	13.8
3R-5 (Piece 2)	380.72	3	221.3	–37.7	2.57	24	6.60	13.0
3R-5 (Piece 4)	381.19	3	225.9	–39.3	2.00	30	4.91	13.6
3R-5 (Piece 8)	381.28	3	185.7	–42.4	1.57	35	3.10	16.9
3R-5 (Piece 9)	381.44	3	204.5	–32.2	2.67	25	6.13	14.5
3R-5 (Piece 11)	381.58	3	299.5	–25.8	3.30	18	7.95	13.8
4R-1 (Piece 3)	384.32	3	181.1	–24.0	6.65	20	7.85	28.2
4R-1 (Piece 6)	384.81	3	320.2	–33.4	3.52	18	8.99	13.1
4R-1 (Piece 7)	385.01	3	311.3	–42.8	3.90	20	7.50	17.3
4R-2 (Piece 6)	386.01	3	251.0	–35.2	1.77	21	7.60	7.8
4R-2 (Piece 13)	386.72	3	188.6	–38.3	5.09	21	7.26	23.4
4R-2 (Piece 13)	386.98	3	174.9	–41.0	2.41	20	7.04	11.4
4R-3 (Piece 6)	387.60	3	19.3	–30.4	3.82	25	7.85	16.2
4R-3 (Piece 8)	387.97	3	125.6	–36.7	3.38	20	7.69	14.7
4R-3 (Piece 13)	388.49	3	321.0	–37.4	4.77	22	7.96	20.0
4R-4 (Piece 3)	389.03	3	319.2	–34.3	4.26	21	8.44	16.8
4R-4 (Piece 4)	389.30	3	106.5	–37.1	2.12	20	7.30	9.7
4R-5 (Piece 1)	390.02	3	239.2	–37.4	4.89	19	8.51	19.2
4R-5 (Piece 4)	390.39	3	348.9	–31.8	3.65	20	7.25	16.8
4R-5 (Piece 5)	390.77	3	334.9	–36.5	3.44	21	7.63	15.0
4R-6 (Piece 1)	391.54	3	238.2	–51.5	2.37	21	8.02	9.9
4R-6 (Piece 1)	391.66	3	232.5	–47.4	3.16	24	7.84	13.4
4R-6 (Piece 1)	391.75	3	237.0	–45.4	2.60	23	8.00	10.8
5R-1 (Piece 3)	394.14	3	281.1	–44.9	2.88	13	6.76	14.2
5R-1 (Piece 3)	394.30	3	290.0	–32.1	3.22	15	9.48	11.3
5R-1 (Piece 4)	394.54	3	30.6	–28.3	3.30	13	7.07	15.6
5R-1 (Piece 6)	394.98	3	242.5	–42.3	1.75	26	6.82	8.6
5R-2 (Piece 1)	395.27	3	352.4	–33.9	3.13	24	7.63	13.7
5R-2 (Piece 1)	395.55	3	348.6	–29.1	3.32	22	8.28	13.4
5R-2 (Piece 2)	395.91	3	146.6	–44.8	2.57	20	8.34	10.3
5R-2 (Piece 2)	396.24	3	144.4	–36.8	3.09	19	8.14	12.7
5R-2 (Piece 2)	396.44	3	140.4	–41.0	2.72	16	7.69	11.8
5R-3 (Piece 1)	396.73	3	223.6	–31.0	3.04	17	7.00	14.5
5R-3 (Piece 4)	397.36	3	208.2	–36.4	3.21	22	9.23	11.6
5R-3 (Piece 5)	398.04	3	152.6	–37.1	1.02	24	5.61	6.1
5R-4 (Piece 4)	398.73	3	337.6	–37.0	7.95	15	10.70	24.8
5R-4 (Piece 4)	398.90	3	343.3	–40.7	2.53	22	8.60	9.8
5R-4 (Piece 6)	399.51	3	301.2	–36.2	3.43	19	7.14	16.0
5R-5 (Piece 2)	399.74	3	22.0	–30.4	1.62	25	2.95	18.3
5R-5 (Piece 4)	399.98	3	330.5	–38.7	2.44	18	6.86	11.9
5R-5 (Piece 5)	400.20	3	299.8	–30.5	3.97	18	7.01	18.9
5R-5 (Piece 9)	400.70	3	174.3	–35.6	2.06	19	7.77	8.8
5R-6 (Piece 1)	401.28	3	139.7	–41.3	2.10	19	7.46	9.4
5R-6 (Piece 1)	401.43	3	137.5	–36.2	3.76	22	7.72	16.2
5R-6 (Piece 3)	401.93	3	229.1	–36.9	5.12	20	8.40	20.3
5R-6 (Piece 4)	402.18	3	20.7	–34.5	3.14	13	7.04	14.9
5R-7 (Piece 1)	402.68	3	193.8	–36.6	4.19	23	8.80	15.9
5R-7 (Piece 4)	403.29	3	189.7	–41.6	1.13	25	5.04	7.5

Table T6 (continued).

Core, section, piece	Depth (mbsf)	Basement unit	Dec (°)	Inc (°)	NRM (A/m)	MDF (mT)	κ (10^{-3} SI)	Q-ratio
5R-7 (Piece 4)	403.39	3	52.1	–41.3	1.27	25	4.98	8.5
5R-8 (Piece 2)	403.90	3	23.4	–31.1	2.72	21	6.61	13.7
6R-1 (Piece 5)	403.75	3	264.1	–33.5	1.37	21		
6R-1 (Piece 14)	404.48	3	13.2	–35.0	2.45	20	8.17	10.0
6R-2 (Piece 2)	405.86	3	241.2	–38.8	3.16	16	10.83	9.7
6R-3 (Piece 2)	406.20	3	119.9	–37.6	0.94	30	3.86	8.1
6R-3 (Piece 2)	406.45	3	123.7	–37.6	4.37	20	8.33	17.5
6R-3 (Piece 3)	406.72	3	101.4	–37.4	1.97	20	8.35	7.9
6R-3 (Piece 5)	407.01	3	335.4	–41.3	2.75	15	7.70	11.9
6R-3 (Piece 5)	407.25	3	333.7	–35.9	3.32	18	8.58	12.9
6R-4 (Piece 1)	407.82	3	58.7	–35.1	2.51	21	8.63	9.7
6R-4 (Piece 1)	408.04	3	48.3	–35.8	2.79	21	8.77	10.6
6R-5 (Piece 1)	408.47	3	43.7	–33.6	3.84	18	7.70	16.6
6R-5 (Piece 1)	408.71	3	44.7	–32.9	3.78	20	7.97	15.8
6R-5 (Piece 1)	409.03	3	40.7	–32.9	3.92	16	6.79	19.2
6R-5 (Piece 1)	409.27	3	41.3	–32.1	3.19	18	7.91	13.4
6R-6 (Piece 1)	409.86	3	223.2	–32.7	1.53	21	8.10	6.3
6R-6 (Piece 2)	409.99	3	26.1	–29.5	2.07	22	5.40	12.8
6R-6 (Piece 2)	410.09	3	17.5	–31.5	3.01	13	8.05	12.5
6R-6 (Piece 2)	410.38	3	26.3	–35.0	4.30	12	17.93	8.0
6R-7 (Piece 1)	410.89	3	33.1	–31.0	5.18	11	8.33	20.7
6R-7 (Piece 2)	411.17	3	312.7	–33.9	1.50	19	6.38	7.8
6R-7 (Piece 2)	411.51	3	317.4	–33.3	4.61	16	9.78	15.7
7R-1 (Piece 3)	413.26	3	222.4	–47.6	2.45	24	10.80	7.6
7R-1 (Piece 4)	413.45	3	185.8	–44.9	3.83	22	10.09	12.7
7R-1 (Piece 4)	413.64	3	176.8	–53.4	2.50	24	6.44	12.9
7R-1 (Piece 4)	413.97	3	182.2	–46.9	1.66	21	7.25	7.6
7R-1 (Piece 5)	414.34	3	108.0	–39.9	1.44	18	7.48	6.4
7R-2 (Piece 1)	414.71	3	111.6	–36.9	3.11	18	7.24	14.3
7R-2 (Piece 4)	415.18	3	218.1	–43.8	2.87	18	8.20	11.7
7R-2 (Piece 5)	415.44	3	242.6	–45.7	3.02	22	7.91	12.7
7R-3 (Piece 1)	416.01	3	176.9	–34.3	3.98	23	6.97	19.0
7R-3 (Piece 2)	416.52	3	12.3	–20.8	4.88	15	13.70	11.9
7R-3 (Piece 2)	416.81	3	13.7	–21.7	4.24	9.5	9.01	15.7
7R-4 (Piece 1)	417.09	3	203.9	–28.9	1.15	25	8.65	4.4
7R-4 (Piece 1)	417.25	3	212.1	–33.1	1.07	22	8.76	4.1
7R-4 (Piece 1)	417.34	3	225.1	–31.1	0.99	26	7.60	4.3
7R-4 (Piece 2)	417.48	3	113.9	–34.2	2.30	16	6.78	11.3
7R-4 (Piece 2)	417.75	3	151.9	–37.5	2.48	19	7.83	10.6
7R-4 (Piece 4)	418.01	3	44.0	–29.4	2.71	22	6.64	13.6
7R-5 (Piece 1)	418.44	4	121.3	–39.5	2.17	19	8.00	9.0
7R-5 (Piece 4)	418.98	4	359.4	–31.0	4.39	16	7.93	18.5
7R-5 (Piece 4)	419.11	4	2.9	–27.7	4.51	17	8.18	18.4
7R-6 (Piece 1)	419.46	4	10.7	–36.1	3.90	14	7.19	18.1
7R-6 (Piece 1)	419.76	4	352.4	–28.8	3.91	16	7.44	17.5
7R-6 (Piece 5)	420.23	4	133.8	–32.7	2.46	35	8.01	10.2
7R-7 (Piece 1)	420.65	4	149.2	–33.3	2.53	18	9.00	9.4
7R-7 (Piece 2)	421.01	4	181.7	–33.3	2.49	20	7.46	11.1
7R-7 (Piece 2)	421.26	4	176.0	–31.5	4.53	19	9.64	15.7
8R-1 (Piece 7)	422.96	4	132.4	–36.4	2.97	19	7.37	13.4
8R-1 (Piece 7)	423.05	4	128.8	–37.2	3.24	17	7.05	15.3
8R-1 (Piece 7)	423.23	4	120.8	–33.2	3.00	16	6.14	16.3
8R-2 (Piece 1)	424.12	5	246.4	–48.3	2.71	16	6.71	13.5
8R-2 (Piece 2)	424.43	5	249.1	–41.6	1.25	18	4.09	10.2
8R-2 (Piece 3)	424.63	5	269.5	–40.7	1.77	17	5.28	11.2
8R-2 (Piece 5)	424.94	5	133.6	–38.2	1.77	17	7.20	8.2
8R-3 (Piece 1)	425.51	5	295.4	–37.3	2.43	16	7.26	11.2
8R-3 (Piece 1)	425.77	5	280.9	–35.3	3.15	17	10.45	10.0
8R-3 (Piece 1)	425.94	5	274.2	–30.9	5.39	15	12.35	14.5
8R-3 (Piece 1)	426.13	5	267.3	–36.8	4.21	17	8.45	16.6
8R-3 (Piece 1)	426.27	5	291.2	–37.6	2.98	18	6.86	14.5
8R-3 (Piece 2)	426.51	5	317.3	–40.8	0.91	25	4.50	6.8
8R-3 (Piece 2)	426.70	5	317.9	–36.9	2.94	16	7.94	12.3
8R-4 (Piece 2)	427.06	5	304.6	–39.2	3.28	14	7.00	15.6
8R-4 (Piece 2)	427.20	5	284.0	–38.0	2.95	14	7.79	12.6
8R-4 (Piece 3)	427.68	5	154.0	–42.8	1.88	25	7.49	8.4
8R-4 (Piece 3)	427.97	5	150.8	–37.6	2.35	25	7.96	9.8
8R-5 (Piece 1)	428.32	5	279.7	–35.5	1.56	22	6.84	7.6
8R-5 (Piece 2)	428.59	5	14.5	–31.5	3.14	18	8.52	12.3

Table T6 (continued).

Core, section, piece	Depth (mbsf)	Basement unit	Dec (°)	Inc (°)	NRM (A/m)	MDF (mT)	κ (10^{-3} SI)	Q-ratio
8R-5 (Piece 3)	428.87	5	309.7	–37.4	2.75	17	7.11	12.9
8R-5 (Piece 5)	429.19	5	210.7	–35.4	1.20	24	6.20	6.5
8R-5 (Piece 6)	429.38	5	52.9	–31.2	4.85	12	17.92	9.0
8R-6 (Piece 1)	429.84	5	271.9	–36.7	2.98	15	6.30	15.8
8R-6 (Piece 2)	430.23	5	123.4	–38.6	1.91	21	7.57	8.4
8R-6 (Piece 3)	430.55	5	140.0	–38.9	3.17	17	11.10	9.5
8R-7 (Piece 1)	431.06	5	305.2	–35.1	3.16	14	9.85	10.7
8R-7 (Piece 2)	431.31	5	194.7	–37.5	2.26	18	15.60	4.8
8R-7 (Piece 2)	431.47	5	200.6	–41.1	2.67	17	7.84	11.4
9R-1 (Piece 1)	432.55	5	80.1	–38.3	2.30	24	7.25	10.6
9R-1 (Piece 3)	433.18	5	260.8	–42.7	3.67	17	6.80	18.0
9R-2 (Piece 1)	433.99	5	279.3	–38.6	3.42	18	7.18	15.9
9R-2 (Piece 4)	434.45	5	284.3	–35.8	2.09	17	7.31	9.5
9R-3 (Piece 2)	435.20	5	247.6	–28.7	0.75	25	2.71	9.2
9R-3 (Piece 4)	435.55	5	144.2	–29.3	3.26	18	7.03	15.5
9R-3 (Piece 5)	436.03	5	137.9	–28.7	2.34	16	16.65	4.7
9R-4 (Piece 2)	436.66	5	46.4	–37.8	2.71	15	14.47	6.2
9R-4 (Piece 2)	436.88	5	35.5	–33.7	3.75	13	13.30	9.4
9R-4 (Piece 3)	437.34	5	111.0	–37.4	2.29	18	15.40	5.0
9R-5 (Piece 1)	437.67	5	212.6	–37.0	1.62	14	6.34	8.5
9R-5 (Piece 3)	437.94	5	174.5	–41.0	1.47	18	5.72	8.6
9R-5 (Piece 3)	438.14	5	187.9	–38.8	3.05	22	13.70	7.4
9R-5 (Piece 4)	438.46	5	201.7	–39.9	4.04	15	10.00	13.5
9R-6 (Piece 12)	440.28	5	319.6	–31.9	4.76	18	7.09	22.4
9R-7 (Piece 3)	440.65	5	78.9	–37.6	3.24	19	6.12	17.6
10R-1 (Piece 6)	442.54	5	98.1	–40.3	4.16	19	6.84	20.3
10R-2 (Piece 4)	443.75	6	289.4	–39.3	1.22	18	5.64	7.2
10R-2 (Piece 6)	443.88	6	80.5	–38.7	3.09	16	5.86	17.6
10R-2 (Piece 9)	444.59	6	9.1	–30.9	3.76	19	6.72	18.6
10R-3 (Piece 4)	446.02	6	75.6	–30.6	2.81	16	5.72	16.4
10R-4 (Piece 1)	446.33	6	147.7	–46.8	3.83	18	6.83	18.7
10R-4 (Piece 2)	446.64	6	96.6	–36.0	4.54	19	7.59	19.9
10R-4 (Piece 4)	447.19	6	188.0	–35.4	3.17	22	7.94	13.3
10R-5 (Piece 1)	447.59	6	247.8	–30.6	4.45	18	12.53	11.8
10R-5 (Piece 2)	447.74	6	331.4	–28.6	7.11	17	8.73	27.2
10R-5 (Piece 2)	448.04	6	0.8	–31.5	4.26	17	6.86	20.7
10R-6 (Piece 1)	448.58	6	104.0	–34.8	3.62	17	8.27	14.6
10R-6 (Piece 1)	448.81	6	109.6	–33.1	2.17	17	6.33	11.4
10R-6 (Piece 4)	449.26	6	228.6	–39.7	2.16	21	11.52	6.3
10R-7 (Piece 1)	449.80	6	159.3	–38.1	3.80	17	15.44	8.2
10R-7 (Piece 1)	449.97	6	150.9	–33.3	3.23	16	16.48	6.5
10R-7 (Piece 1)	450.14	6	142.0	–35.0	2.17	17	5.90	12.3
10R-7 (Piece 2)	450.44	6	116.6	–33.4	2.68	14	5.93	15.1
11R-1 (Piece 4)	451.67	6	201.1	–37.1	2.75	23	6.82	13.4
11R-1 (Piece 8)	452.17	6	314.5	–40.2	2.48	16	4.77	17.3
11R-2 (Piece 1)	452.78	6	106.8	–34.3	2.93	17	7.29	13.4
11R-2 (Piece 1)	452.97	6	101.0	–38.6	3.78	16	9.39	13.4
11R-2 (Piece 1)	453.17	6	106.5	–39.5	3.30	16	5.84	18.8
11R-2 (Piece 2)	453.61	6	80.0	–36.2	3.25	22	7.32	14.8
11R-2 (Piece 4)	454.01	6	0.9	–40.2	4.01	16	7.07	18.9
11R-3 (Piece 1)	454.44	6	178.1	–37.3	3.37	20	8.18	13.7
11R-3 (Piece 3)	455.02	6	84.1	–38.0	3.60	18	8.01	15.0
11R-4 (Piece 1)	455.32	6	214.6	–34.0	3.10	16	8.12	12.7
11R-4 (Piece 1)	455.65	6	209.8	–33.1	5.71	22	8.46	22.5
11R-4 (Piece 5)	456.14	6	5.4	–24.3	2.67	18	9.46	9.4
11R-4 (Piece 6)	456.42	6	106.3	–29.0	5.07	13	14.76	11.5
11R-5 (Piece 1)	456.73	6	111.1	–26.5	3.28	23	9.72	11.3
11R-5 (Piece 2)	457.10	6	231.1	–36.8	4.18	16	13.16	10.6
11R-5 (Piece 2)	457.30	6	220.9	–32.8	3.96	16	6.20	21.3
11R-5 (Piece 4)	457.50	6	9.7	–25.5	3.24	12	6.30	17.2
11R-5 (Piece 5)	457.66	6	72.1	–29.8	2.27	10	8.93	8.5
11R-6 (Piece 3)	458.39	6	127.8	–28.1	2.32	14	13.54	5.7
12R-1 (Piece 4)	461.35	6	342.1	–32.5	3.66	12	12.20	10.0
12R-1 (Piece 12)	461.81	6	350.1	–35.1	3.45	18	8.49	13.5
12R-1 (Piece 14)	462.17	6	250.3	–35.2	2.63	21	7.23	12.1
12R-1 (Piece 17)	462.44	6	322.0	–30.1	2.45	18	8.50	9.6
12R-2 (Piece 7)	463.07	6	298.9	–28.7	3.92	17	8.57	15.2
12R-2 (Piece 8)	463.30	6	117.5	–31.7	2.09	22	9.29	7.5
12R-2 (Piece 11)	463.70	6	288.1	–28.3	5.98	17	10.58	18.8

Table T6 (continued).

Core, section, piece	Depth (mbsf)	Basement unit	Dec (°)	Inc (°)	NRM (A/m)	MDF (mT)	κ (10^{-3} SI)	Q-ratio
12R-3 (Piece 2)	464.24	6	127.2	–26.8	1.96	12	19.81	3.3
12R-4 (Piece 1)	465.51	6	164.1	–32.4	2.39	13	14.23	5.6
12R-4 (Piece 1)	465.83	6	173.4	–32.2	4.11	14	12.70	10.8
12R-4 (Piece 2)	466.30	6	308.7	–31.3	2.89	14	18.61	5.2
12R-5 (Piece 1)	467.13	6	344.7	–26.4	3.86	14	22.17	5.8
12R-5 (Piece 2)	467.38	6	27.2	–31.4	5.80	8	17.62	11.0
13R-1 (Piece 8)	471.35	6	18.1	–28.7	3.08	12	10.36	9.9
13R-2 (Piece 1)	472.19	6	266.9	–32.6	3.09	11	13.46	7.7
13R-3 (Piece 1)	473.50	7	98.1	–32.7	2.77	17	7.51	12.3
13R-3 (Piece 2)	473.63	7	192.7	–35.1	2.09	19	7.72	9.0
13R-3 (Piece 5)	474.10	7	263.2	–30.5	3.86	19	9.45	13.6
13R-4 (Piece 1)	474.90	7	342.6	–22.8	4.37	10	18.34	7.9
13R-4 (Piece 4)	475.38	7	292.8	–28.7	4.91	12	18.57	8.8
13R-5 (Piece 1)	475.76	7	295.4	–26.7	1.80	15	6.96	8.6
13R-5 (Piece 1)	476.17	7	289.2	–27.6	3.08	13	7.45	13.8
13R-5 (Piece 6)	477.11	8	317.0	–25.4	3.42	16	7.02	16.2
13R-6 (Piece 1)	477.23	8	303.7	–33.7	4.23	13	7.54	18.7
13R-6 (Piece 16)	478.29	8	231.7	–35.5	2.14	25	7.79	9.2
14R-1 (Piece 8)	480.61	8	195.6	–41.8	1.76	25	7.35	8.0
14R-1 (Piece 10)	481.02	8	306.9	–46.2	2.08	22	8.64	8.0
14R-1 (Piece 14)	481.44	8	255.6	–36.2	2.35	21	8.10	9.7
14R-2 (Piece 9)	482.24	9	11.6	–41.3	2.22	19	9.13	8.1
14R-2 (Piece 18)	482.96	10	267.3	–38.9	1.77	25	7.77	7.6
14R-3 (Piece 1)	483.32	10	353.4	–34.0	2.53	18	7.98	10.6
14R-3 (Piece 4)	484.17	10	247.9	–33.5	2.21	26	7.72	9.5
14R-3 (Piece 7)	484.64	10	157.8	–34.0	1.81	22	8.39	7.2
14R-4 (Piece 1)	484.79	10	110.5	–36.8	3.04	20	7.30	13.9
14R-4 (Piece 5)	485.35	11	312.9	–44.0	3.50	22	6.78	17.2
15R-2 (Piece 2)	491.65	11	342.7	–39.2	3.14	17	6.69	15.6
15R-3 (Piece 1)	492.25	11	255.6	–23.4	1.92	20	10.17	6.3
15R-3 (Piece 3)	492.59	11	301.6	–29.5	4.16	13	12.44	11.1
15R-3 (Piece 3)	492.82	11	303.1	–22.1	5.49	14	11.59	15.8
15R-3 (Piece 3)	493.18	11	300.6	–23.1	4.93	11	11.92	13.8
15R-4 (Piece 1)	493.63	11	252.0	–25.1	10.20	20	8.64	39.4
16R-1 (Piece 4)	500.00	11	13.4	–28.9	2.71	18	7.99	11.3
16R-1 (Piece 5)	500.19	11	127.5	–32.9	2.97	19	7.33	13.5
16R-1 (Piece 5)	500.43	11	123.4	–32.9	1.51	20	6.38	7.9
16R-2 (Piece 1)	500.78	11	17.4	–26.3	2.26	22	7.43	10.1
16R-2 (Piece 1)	501.28	11	11.9	–33.0	2.66	24	7.17	12.4
16R-2 (Piece 7)	501.78	12	295.4	–32.0	2.28	25	8.19	9.3
16R-3 (Piece 1)	502.14	12	83.1	–21.7	2.15	18	6.72	10.7
16R-3 (Piece 3)	502.41	12	53.3	–17.6	7.40	15	9.63	25.6
16R-3 (Piece 4)	503.04	12	108.6	–38.5	1.24	22	7.46	5.5
16R-3 (Piece 4)	503.28	12	113.1	–31.4	1.76	25	7.41	7.9
16R-4 (Piece 1)	503.54	12	104.6	–39.4	1.80	23	7.37	8.1
16R-4 (Piece 7)	504.43	12	232.5	–36.4	1.68	22	7.69	7.3
16R-4 (Piece 7)	504.62	12	215.4	–37.0	2.61	20	7.54	11.5
16R-5 (Piece 2)	505.21	12	292.2	–35.0	1.72	19	6.78	8.5
16R-5 (Piece 3)	505.63	12	167.2	–36.0	1.72	22	7.38	7.8

Notes: Dec = declination, Inc = inclination, NRM = natural remanent magnetization, MDF = median destructive field, κ = magnetic susceptibility, Q-ratio = Koenigsberger ratio. A present-day field of 30 A/m was used for Koenigsberger ratio calculations. This table is also available in **ASCII format.**

Table T7. Index properties data, Hole 1187A.

Core, section, interval (cm)	Depth (mbsf)	Water content (%)		Density (g/cm^3)			Porosity (%)	Void ratio
		Bulk	Dry	Bulk	Dry	Grain		
192-1187A-								
2R-1, 6-8	365.57	52.296	109.626	1.340	0.639	2.025	68.430	2.168
2R-1, 22-24	365.73	49.180	96.771	1.395	0.709	2.148	66.994	2.030
2R-2, 86-88	367.54	5.859	6.223	2.630	2.476	2.914	15.047	0.177
3R-2, 54-56	376.50	5.976	6.356	2.565	2.412	2.836	14.968	0.176
3R-3, 64-66	378.08	3.993	4.159	2.657	2.551	2.845	10.359	0.116
4R-1, 25-27	384.45	2.938	3.027	2.761	2.680	2.911	7.922	0.086
4R-5, 65-67	390.51	3.836	3.989	2.552	2.454	2.714	9.559	0.106
5R-1, 23-25	394.03	2.957	3.048	2.624	2.547	2.756	7.580	0.082
5R-3, 90-92	397.58	2.737	2.814	2.640	2.568	2.763	7.057	0.076
5R-4, 121-123	399.32	1.615	1.642	2.869	2.823	2.957	4.527	0.047
6R-2, 108-110	405.71	3.287	3.398	2.667	2.579	2.820	8.559	0.094
6R-6, 56-58	410.09	3.190	3.295	2.672	2.587	2.822	8.325	0.091
7R-4, 32-34	417.24	3.832	3.984	2.626	2.525	2.800	9.825	0.109
7R-7, 98-100	421.31	5.172	5.454	2.653	2.516	2.905	13.400	0.155
8R-2, 64-66	424.63	4.879	5.129	2.569	2.444	2.785	12.242	0.139
8R-3, 59-61	425.93	2.277	2.330	2.802	2.738	2.920	6.231	0.066
8R-6, 72-74	430.22	2.800	2.881	2.590	2.518	2.710	7.083	0.076
9R-3, 91-93	436.00	3.468	3.592	2.764	2.668	2.944	9.361	0.103
9R-5, 6-8	437.57	5.107	5.382	2.582	2.450	2.812	12.878	0.148
10R-1, 12-14	442.02	4.215	4.401	2.493	2.388	2.662	10.264	0.114
10R-5, 40-42	447.81	3.187	3.292	2.708	2.621	2.863	8.428	0.092
11R-3, 2-4	454.22	5.691	6.035	2.472	2.331	2.702	13.736	0.159
11R-5, 31-33	456.91	3.666	3.806	2.759	2.658	2.950	9.880	0.110
12R-3, 46-48	464.50	2.538	2.604	2.685	2.617	2.804	6.655	0.071
12R-5, 79-81	467.34	3.021	3.116	2.738	2.655	2.889	8.079	0.088
13R-2, 31-33	472.30	1.306	1.324	2.771	2.735	2.835	3.535	0.037
13R-5, 61-63	476.28	2.258	2.310	2.771	2.709	2.885	6.111	0.065
14R-2, 36-38	482.16	4.865	5.114	2.630	2.502	2.859	12.494	0.143
14R-3, 28-30	483.46	4.386	4.587	2.699	2.580	2.917	11.559	0.131
15R-3, 88-90	493.00	5.448	5.762	2.563	2.424	2.807	13.639	0.158
15R-4, 20-22	493.67	4.612	4.835	2.584	2.465	2.789	11.637	0.132

Note: This table is also available in **ASCII format.**

Table T8. *P*-wave velocity measured using the contact probe system, Hole 1187A. (**See table notes.** Continued on next page.)

Core, section, interval (cm)	Depth (mbsf)	Direction	Velocity (m/s)
192-1187A-			
2R-1, 13-15	365.64	Cz	1562.4
2R-1, 13-15	365.64	Cy	1654.6
2R-2, 39-41	367.08	_x	4273.7
2R-2, 79-81	367.48	_x	5295.2
2R-2, 84-86	367.53	_x	4820.3
2R-2, 85-87	367.54	Mx	5039.6
2R-2, 97-99	367.66	_x	4852.9
2R-2, 117-119	367.86	_x	4956.9
3R-1, 6-8	374.57	_x	4585.3
3R-1, 83-85	375.34	_x	4959.9
3R-2, 34-36	376.31	_x	5091.1
3R-2, 53-55	376.50	Mx	4741.4
3R-2, 54-56	376.51	_x	4957.9
3R-2, 104-106	377.01	_x	4945.4
3R-2, 129-131	377.26	_x	4697.5
3R-3, 11-13	377.56	_x	4736.6
3R-3, 63-65	378.08	Mx	5043.0
3R-3, 64-66	378.09	_x	5041.0
3R-3, 117-119	378.62	_x	4753.5
3R-4, 12-14	379.02	_x	5143.4
3R-4, 119-121	380.09	_x	4798.2
3R-5, 34-36	380.73	_x	4813.5
3R-5, 64-66	381.03	_x	5056.4
3R-5, 104-106	381.43	_x	5129.4
4R-1, 25-27	384.46	Mx	5396.8
4R-1, 36-38	384.57	_x	4918.9
4R-1, 99-101	385.20	_x	4841.1
4R-2, 39-41	386.09	_x	4925.5
4R-2, 129-131	386.99	_x	4686.3
4R-3, 95-97	388.15	_x	4561.1
4R-4, 43-45	389.13	_x	4936.8
4R-4, 103-105	389.73	_x	5060.7
4R-5, 26-28	390.13	_x	4662.1
4R-5, 87-89	390.74	_x	5081.3
4R-6, 29-31	391.66	_x	5000.9
5R-1, 24-26	394.05	_x	5293.2
5R-1, 24-26	394.05	Mx	4894.8
5R-1, 114-116	394.95	_x	4973.4
5R-2, 32-34	395.51	_x	4948.8
5R-2, 109-111	396.28	_x	5296.0
5R-3, 58-60	397.27	_x	4780.9
5R-3, 90-92	397.59	Mx	4931.4
5R-3, 109-111	397.78	_x	5526.7
5R-4, 59-61	398.71	_x	5530.6
5R-4, 121-123	399.33	Mx	5175.8
5R-4, 134-136	399.46	_x	5305.9
5R-5, 52-54	400.14	_x	4932.7
5R-5, 99-101	400.61	_x	5407.4
5R-6, 114-116	402.26	_x	5126.0
5R-7, 15-17	402.56	_x	5013.6
5R-8, 35-37	403.95	_x	5370.0
6R-1, 34-36	403.75	_x	5006.0
6R-1, 101-103	404.42	_x	4959.9
6R-2, 119-121	405.83	_x	5163.4
6R-3, 44-46	406.58	_x	4911.0
6R-3, 99-101	407.13	_x	5106.6
6R-4, 19-21	407.78	_x	5015.7
6R-4, 49-51	408.08	_x	4541.2
6R-5, 29-31	408.47	_x	5228.0
6R-5, 69-71	408.87	_x	4972.7
6R-6, 64-66	410.18	_x	5173.5
6R-6, 86-88	410.40	_x	5150.0
6R-6, 89-91	410.43	_x	5488.7
6R-6, 124-126	410.78	_x	5483.8
6R-7, 4-6	410.89	_x	5485.8
6R-7, 51-53	411.36	_x	5304.8
6R-7, 109-111	411.94	_x	5146.7
7R-1, 34-36	413.35	_x	5434.8
7R-1, 139-141	414.40	_x	4647.3
7R-2, 29-31	414.77	_x	4694.8
7R-2, 79-81	415.27	_x	4723.7
7R-3, 15-17	415.89	_x	4714.0
7R-3, 74-76	416.48	_x	5708.6
7R-4, 31-33	417.24	Mx	5278.2
7R-4, 79-81	417.72	_x	4732.5
7R-5, 24-26	418.47	_x	4781.4
7R-5, 89-91	419.12	_x	4950.5
7R-6, 37-39	419.68	_x	5082.2
7R-7, 22-24	420.56	_x	5006.5
7R-7, 97-99	421.31	Mx	5831.4
8R-1, 65-67	423.26	_x	4836.0
8R-2, 19-21	424.19	_x	4561.5
8R-2, 99-101	424.99	_x	4709.6
8R-3, 42-44	425.77	_x	4772.6
8R-3, 59-61	425.94	Mx	5180.8
8R-4, 55-57	427.39	_x	5059.4
8R-4, 105-107	427.89	_x	5231.8
8R-5, 39-41	428.54	_x	4973.1
8R-5, 107-109	429.22	_x	5536.1
8R-6, 16-18	429.67	_x	5768.1
8R-6, 72-74	430.23	Mx	5392.5
8R-6, 89-91	430.40	_x	5585.1
8R-7, 34-36	431.22	_x	5464.7
9R-1, 44-46	432.75	_x	5052.0
9R-1, 89-91	433.20	_x	4550.9
9R-2, 13-15	433.82	_x	5131.5
9R-3, 14-16	435.24	_x	5416.3
9R-3, 69-71	435.79	_x	5826.0
9R-4, 24-26	436.35	_x	5542.5
9R-4, 109-111	437.20	_x	5450.1
9R-5, 5-7	437.57	Mx	5175.9
9R-5, 59-61	438.11	_x	5224.5
9R-5, 87-89	438.39	_x	5537.9
9R-6, 64-66	439.62	_x	5050.4
9R-6, 119-121	440.17	_x	4617.3
9R-7, 33-35	440.77	_x	4831.9
10R-1, 11-13	442.02	Mx	5271.2
10R-1, 44-46	442.35	_x	4637.0
10R-1, 69-71	442.60	_x	4435.9
10R-2, 47-49	443.88	_x	4690.6
10R-2, 106-108	444.47	_x	4987.1
10R-3, 49-51	445.40	_x	5432.8
10R-3, 97-99	445.88	_x	5172.8
10R-4, 49-51	446.62	_x	4839.4
10R-4, 122-124	447.35	_x	5521.5
10R-5, 17-19	447.59	_x	5563.0
10R-5, 39-41	447.81	Mx	5870.1
10R-6, 47-49	448.80	_x	4997.0
10R-6, 92-94	449.25	_x	5759.2
10R-7, 6-8	449.66	_x	5681.9
10R-7, 86-88	450.46	_x	4718.1
11R-1, 17-19	451.68	_x	5002.3
11R-1, 107-109	452.58	_x	4907.8
11R-2, 22-24	452.93	_x	5285.0
11R-2, 113-115	453.84	_x	4904.7
11R-3, 1-3	454.22	Mx	4561.7
11R-3, 94-96	455.15	_x	4938.8
11R-4, 32-34	455.53	_x	5330.8
11R-4, 134-136	456.55	_x	4913.7
11R-5, 30-32	456.91	Mx	5439.1
11R-5, 119-121	457.80	_x	5223.2
11R-6, 34-36	458.39	_x	4826.7
12R-1, 7-9	461.18	_x	5132.2
12R-1, 131-133	462.42	_x	4687.0
12R-2, 45-47	463.04	_x	4870.5

Table T8 (continued).

Core, section, interval (cm)	Depth (mbsf)	Direction	Velocity (m/s)
12R-2, 109-111	463.68	_x	5324.0
12R-3, 99-101	465.04	_x	5133.7
12R-4, 3-5	465.43	_x	5106.4
12R-4, 103-105	466.43	_x	4962.4
12R-5, 41-43	466.97	_x	5393.8
12R-5, 79-81	467.35	Mx	5292.6
12R-5, 97-99	467.53	_x	4790.4
13R-1, 43-45	471.14	_x	4776.9
13R-1, 104-106	471.75	_x	5594.3
13R-2, 29-31	472.29	_x	5415.2
13R-2, 31-33	472.31	Mx	5779.6
13R-2, 107-109	473.07	_x	5295.0
13R-3, 89-91	474.28	_x	5743.4
13R-4, 14-16	474.82	_x	5468.9
13R-4, 95-97	475.63	_x	5416.1
13R-5, 49-51	476.17	_x	5447.6
13R-5, 61-63	476.29	Mx	5323.1
13R-5, 129-131	476.97	_x	5224.2
13R-6, 23-25	477.41	_x	4840.2
14R-1, 64-66	480.95	_x	4871.1
14R-1, 119-121	481.50	_x	4690.1
14R-2, 35-37	482.16	Mx	4949.0
14R-2, 39-41	482.20	_x	4644.0
14R-3, 27-29	483.46	Mx	5175.2
14R-3, 33-35	483.52	_x	4677.6
14R-3, 138-140	484.57	_x	4716.5
14R-4, 7-8	484.76	_x	5028.3
15R-2, 39-41	491.25	_x	5423.4
15R-2, 75-77	491.61	_x	4751.6
15R-3, 41-43	492.54	_x	5139.8
15R-3, 87-89	493.00	Mx	5300.2
15R-3, 104-106	493.17	_x	5828.7
15R-4, 9-10	493.57	_x	5308.4
15R-4, 19-21	493.67	Mx	5298.0
15R-4, 59-61	494.07	_x	5302.8
16R-1, 7-8	499.78	_x	5030.9
16R-1, 69-71	500.40	_x	4931.9
16R-2, 19-21	500.84	_x	4588.6
16R-2, 113-115	501.78	_x	4799.1
16R-3, 44-46	502.48	_x	5090.6
16R-3, 115-117	503.19	_x	4566.6
16R-4, 15-17	503.52	_x	4559.9
16R-4, 105-107	504.42	_x	4268.8
16R-5, 27-29	505.10	_x	4687.1
16R-5, 89-91	505.72	_x	4705.9

Notes: C = cut sample, _ = uncut split core, M = minicore. z = along the core, y = across the core face, x = into the core. This table is also available in **ASCII format.**

Table T9. Thermal conductivity values, Hole 1187A.

Core, section, interval (cm)	Depth (mbsf)	Thermal conductivity (W/[m·K])
192-1187A-		
2R-3, 5-7	368.19	1.621
3R-3, 35-37	377.79	1.680
4R-2, 44-46	386.13	1.656
4R-5, 30-32	390.16	1.759
5R-2, 100-102	396.18	1.756
5R-6, 110-112	402.21	1.810
5R-6, 111-113	402.22	1.724
6R-2, 125-127	405.88	1.623
6R-6, 65-67	410.18	1.827
7R-3, 105-107	416.78	1.649
7R-3, 106-108	416.79	1.725
8R-1, 66-68	423.26	1.666
8R-3, 43-45	425.77	1.685
8R-6, 16-18	429.66	1.830
9R-3, 70-72	435.79	1.882
9R-6, 70-72	439.67	1.704
10R-4, 20-22	446.32	1.726
10R-7, 22-24	449.81	1.790
10R-7, 23-25	449.82	1.868
11R-2, 30-32	453.00	1.770
11R-5, 50-52	457.10	1.802
12R-5, 35349	466.65	1.838
13R-1, 60-62	471.30	1.706
13R-4, 25-27	474.92	1.790
14R-2, 45-47	482.25	1.581
14R-4, 76-78	485.44	1.769
14R-4, 77-79	485.45	1.674
15R-2, 88-90	491.73	1.691
15R-4, 35-37	493.82	1.812
15R-4, 36-38	493.83	1.801
16R-2, 55-57	501.19	1.693
16R-5, 80-82	505.62	1.698

Note: This table is also available in **ASCII format.**